INVESTIGATION OF ROCKFALL AROUND ANKARA CITADEL

A THESIS SUBMITTED TO
THE GRADUATE SCHOOL OF NATURAL AND APPLIED SCIENCES
OF
THE MIDDLE EAST TECHNICAL UNIVERSITY

BY

NYEIN EI SAN

IN PARTIAL FULFILLMENT OF THE REQUIREMENTS
FOR
THE DEGREE OF MASTER OF SCIENCE
IN
GEOLOGICAL ENGINEERING

JUNE 2017

Approval of the thesis:

INVESTIGATION OF ROCKFALL AROUND ANKARA CITADEL

submitted by **NYEIN EI SAN** in partial fulfillment of the requirements for the degree of **Master of Sceinces in Geological Engineering Department, Middle East Technical University** by,

Prof. Dr. Gülbin Dural Ünver _____
Dean, Graduate School of **Natural and Applied Sciences**

Prof. Dr. Erdin Bozkurt _____
Head of Department, **Geological Engineering**

Prof. Dr. Tamer Topal _____
Supervisor, **Geological Engineering Dept., METU**

Assist. Prof. Dr. Müge K. Akın _____
Co-Supervisor, **Civil Engineering Dept., Abdullah Gül Univerisity**

Examining Committee Members:

Prof. Dr. Nurkan Karahanoğlu _____
Geological Engineering Dept., METU

Prof. Dr. Tamer Topal _____
Geological Engineering Dept., METU

Prof. Dr. Erdal Çokça _____
Civil Engineering Dept., METU

Prof. Dr. Murat Ercanoğlu _____
Geological Engineering Dept., Hacettepe University

Assist. Prof. Dr. Müge K. Akın _____
Civil Engineering Dept., Abdullah Gül University

Date: 08.06.2017

I hereby declare that all the information in this document has been obtained and presented in accordance with academic rules and ethical conduct. I also declare that, as required by these rules and conduct, I fully cited and referenced all the material and results that are not original to this work.

Name, Last name: Nyein Ei SAN

Signature:

ABSTRACT

INVESTIGATION OF ROCKFALL AROUND ANKARA CITADEL

San, Nyein Ei

M.S., Department of Geological Engineering

Supervisor: Prof. Dr. Tamer Topal

Co-Supervisor: Assist. Prof. Dr. Müge K. Akın

June 2017, 131 pages

Rockfall is one of the most important natural disasters affecting human life. Rockfall is the downward motion of a detached block or series of blocks with a small volume involving free falling, bouncing, rolling, and sliding. The reasons causing rockfall are mainly earthquakes, precipitation, freeze-thaw, physical-chemical weathering and joints.

Ankara Citadel is one of the important cultural heritages of the capital city of Turkey. It belongs to the oldest part of Ankara. The citadel is located on a steep hill and rockfall has occurred in the area where andesite is exposed. Since there are main road, floral shops, car parking and a school around the citadel, rockfall poses a great risk to the surrounding. The purpose of this study is to analyze the rockfall around Ankara Citadel with 2D and 3D models and suggest appropriate measures. In order to fulfill this scope, field studies and laboratory tests were carried out to collect the required data for analyses. Kinematic analysis was conducted to observe possible failure types. Limit equilibrium analysis was performed to calculate the safety factors of the slopes. 2D rockfall analyses were carried out with four different rock

weights. Then, the results were compared with 3D rockfall analysis. Based on the danger zones assessed from 2D and 3D rockfall analyses, the removal of the fallen and loosen andesite blocks and the installation of catch barriers with suggested properties were recommended.

Keywords: Andesite, Ankara Citadel, Danger Zone, Hazard Analysis, Rockfall Modelling.

ÖZ

ANKARA KALESİ ÇEVRESİNDE KAYA DÜŞMESİNİN İNCELENMESİ

San, Nyein Ei
Yüksek Lisans, Jeoloji Mühendisliği Bölümü
Tez Yöneticisi: Prof. Dr. Tamer Topal
Eş-Tez Yöneticisi: Yrd. Doç. Dr. Müge K. Akın

Haziran 2017, 131 sayfa

Kaya düşmesi insan hayatını etkileyen önemli doğal afetlerden birisidir. Kaya düşmesi, bağımsız bir bloğun ya da blokların serbest düşme, zıplama, yuvarlanma ya da kayma şeklinde aşağı doğru hareket etmesidir. Kaya düşmesine sebep olan başlıca nedenler depremler, yağış, donma-çözülme, fiziksel-kimyasal ayrışma ve süreksizliklerin varlığıdır.

Ankara Kalesi, Ankaranın önemli kültür miraslarından birisidir. Kale dik bir tepe üzerine kurulmuştur. Söz konusu kaya düşmeleri, andezit içeren birimlerde görülmektedir. Kale çevresinde ana yol, çiçek dükkanları, otopark ve bir okul olduğundan, kaya düşmesi çevre için büyük bir risk oluşturmaktadır. Bu çalışmanın amacı, Ankara Kalesinin etrafındaki kaya düşmelerini 2 ve 3 boyutlu modeller kullanarak analiz etmek ve uygun önlemleri önermektir. Bu amaçla, analiz için gerekli verileri toplamak amacıyla saha çalışmaları ve laboratuvar deneyleri yapılmıştır. Olası yenilme tiplerini gözlemlemek için kinematik analiz gerçekleştirilmiştir. Şevlerin güvenlik katsayılarını hesaplamak için limit denge analizleri yapılmıştır. İki boyutlu kaya düşme analizleri dört farklı kaya ağırlığı ile gerçekleştirilmiştir. Daha sonra, elde edilen sonuçlar 3 boyutlu kaya düşme analizi ile karşılaştırılmıştır. 2 ve 3 boyutlu kaya düşme analizileri ile değerlendirilen tehlike

bölgelerine dayanarak, düşmüş ve gevşemiş andezit blokların kaldırılması ve tavsiye edilen özelliklere sahip tutma bariyerlerinin kurulması önerilmiştir.

Anahtar Kelimeler: Andezit, Ankara Kalesi, Tehlikeli Bölge, Tehlike Analizi, Kaya Düşmesi Modellemesi.

To My Beloved Family

ACKNOWLEDGEMENTS

Firstly, I would like to thank my thesis supervisor, Prof. Dr. Tamer Topal for his support, encouragement, guidance, patience and for being always ready to answer my questions throughout my study. It was a privilege to have worked with you, Sir. I could not have completed this study without your kind support.

I wish to thank my co-supervisor Assist. Prof. Dr. Müge K. Akın for her valuable guidance and recommendations during my study.

I would like to thank my examining committee members; Prof. Dr. Nurkan Karahanoğlu, Prof. Dr. Erdal Çokça and Prof. Dr. Murat Ercanoğlu for their recommendations and constructive criticism.

I would like to express my gratitude to Yavuz Kaya and Timur Ersöz for kindly helping me with field study. I am greatly thankful for their support and encouragement, kindness and answering all my questions during my thesis study.

I also wish to thank Assoc. Prof. Dr. Mutluhan Akın for helping me with 3D rockfall analysis. I want to express my gratitude to Dr. Çağıl Kolat for helping me with TNT software.

I wish to thank Altindag municipality for their generous support of the data of the study area. I am also indebted and thankful to Rocscience for allowing me the access of the software programs to complete my work.

I am forever grateful to my late dad and my late brother for the love they had had shown me. You may not be with me anymore but I will always be heeding to your teachings for my life. I would like to thank my mom and my brother for being there for me whenever I needed, their love, understanding, encouragement, support and patience.

I also would like to express my gratitude to all my teachers and all of my colleagues from the Geological Engineering Department of Middle East Technical University, who were involved in preparing my thesis. I would also like to thank all my friends who supported me with encouragement, love and for wishing me my best. I will be forever grateful to everyone who has a role in the completion of my thesis.

Last but not the least, I wish to thank my husband for his support, encouragement, patience and the love he showed me. I could not have done this without him.

TABLE OF CONTENTS

LIST OF TABLES

TABLES

LIST OF FIGURES

FIGURES

CHAPTER 1

INTRODUCTION

Rockfalls can be a major hazard and a threat to life, properties and infrastructure (highways, railways, bridges, power lines, pipelines, buildings) in the mountain areas. Rockfall is a fragment of rock detached by sliding, toppling, or falling, that falls along a vertical or sub-vertical cliff and proceeds down slope by bouncing and flying along ballistic trajectories or by rolling on talus or debris slopes (Varnes, 1987). Rockfall can be caused by physical - chemical weathering, freeze-thaw, jointing, precipitation, seismic activity, tree roots and manmade activity (Chen et al., 1994; Wasowski and Gaudio, 2000; Marzorati et al., 2002; Dorren, 2003; Krautblatter and Moser, 2009; Wick et al., 2010; Topal et al., 2012).

Natural disasters such as earthquakes, landslides, flood and rockfall have taken place frequently in Turkey due to its geological, geomorphologic structures and climatic conditions. Rockfalls are one of four most important natural disasters that can occur in Turkey. From 1950 to 2008, the number of the provinces where rockfall occurred, is 79 with a total of 2956 rockfall events affecting 1703 settlements and 22157 victims. In Ankara, rockfall events generally occur in Altındağ, Beypazarı and Nallıhan districts where volcanic rocks are exposed. Ankara is one of 20 provinces that was most affected by rockfall, and Altındağ is the most affected district in Ankara (Gökçe et al., 2008).

Ankara Citadel is an important historical building and the symbol of Ankara City. The whole Citadel consists of an inner circle (İç Kale), an outer circle (Dış Kale) and

a northern part (Figure 1.1). The inner circle which is located at the top of the hill is mostly from Byzantine era, and the historical heritages are preserved in this part. This inner circle (wall) is called the castle and it is the oldest part in the whole compound. It is about 350m long along north-south direction and approximately 180 m wide on east-west direction. The outer circle was constructed around the west and south sides of the castle, and 100 to 150m apart. A cluster of structures was constructed downwards on the hill for the defense of the narrow valley (Tokmak, 2005). The northern part of the Citadel is very steep with a height of 986m.

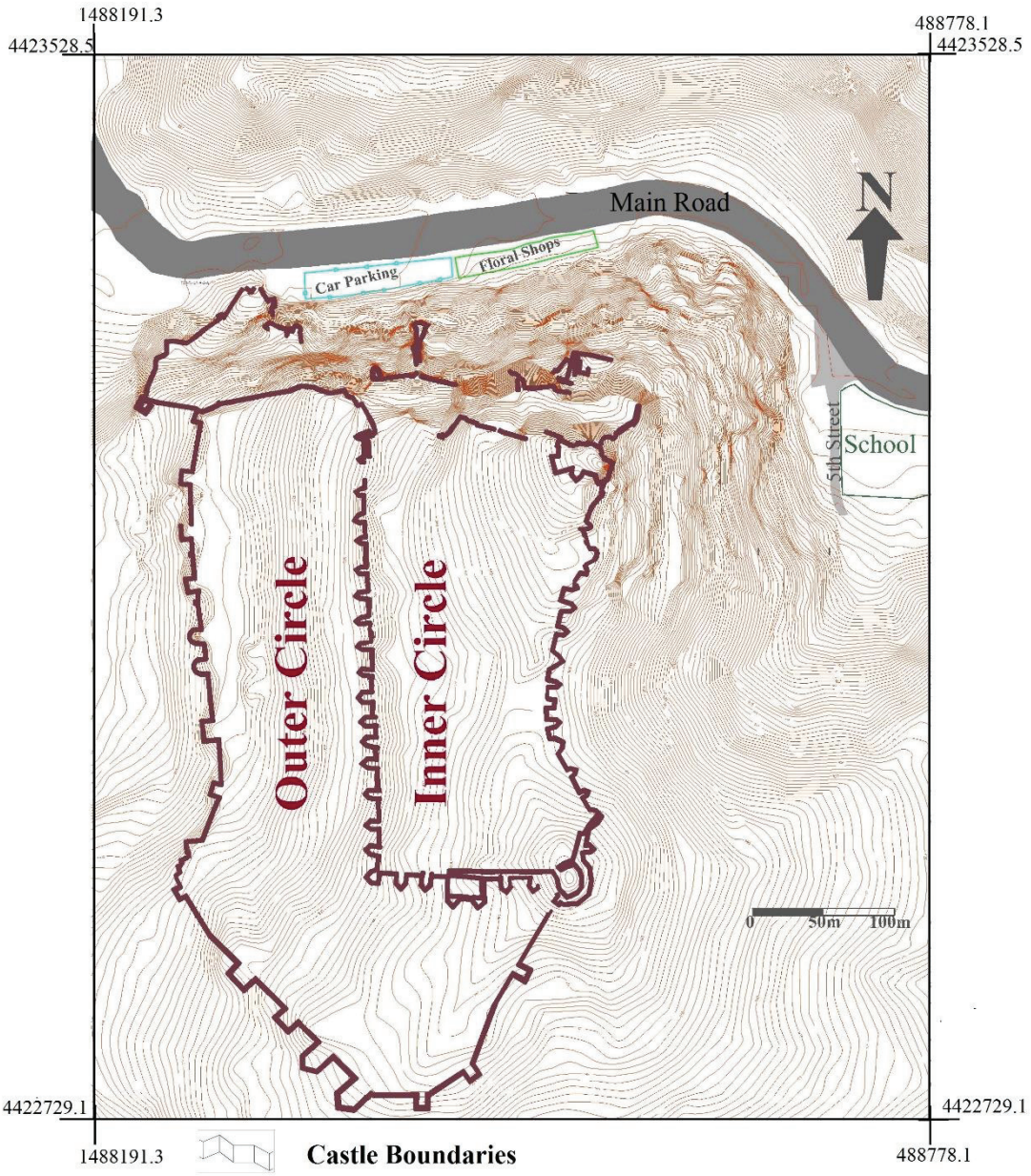

Figure 1.1 A sketch of Ankara Citadel on the topographic map provided by Altındağ municipality (2010).

There are settlements next to the bottom of the northern part of the hill. There are many fallen rocks observed very close to the main road (Bentderesi Street) around the hill (Figure 1.2). Therefore, it is important to investigate the rockfall hazard around the Ankara Citadel.

Figure 1.2 Fallen blocks seen in the study area and the floral shops at the bottom of the hill.

1.1 Purpose and Scope

This study aims to analyze the rockfall around Ankara Citadel. Since there are structures and road around the Citadel, potential rockfalls pose great threat to its neighborhood. Therefore, the purpose of this study is to develop the rockfall analysis

around the Citadel and suggest appropriate remedial measures based on the results of the analysis. The study took place on the northern and eastern part of the hill.

In the scope of the study, scanline survey, sample collections, laboratory studies were carried out to obtain data for the rockfall analysis. 2D and 3D analysis of the study area were done to predict a danger zone around the citadel. Based on the resultant danger zone, the most suitable remedial measures were recommended.

1.2 Location and Accessibility

Ankara Citadel is located in Altındağ District of Ankara Province in Turkey. The location map of the study area is presented (Figure 1.3). Altindağ province has become a region of intense settlement in Ankara (Ercanoğlu and Aksoy, 2004). A photograph of the Citadel taken by Altındağ municipality is shown in Figure 1.4. The topography of the study area and neighborhood is very steep. The hill of the Ankara Citadel is about 986m high on the northern part. Right next to the bottom of this part of the hill, there are parking lot, floral shops, a school and the main road. The Ankara Citadel is located close to the downtown of the city. The accessibility to the citadel is very easy by means of several ways such as buses and subways from every part of the city.

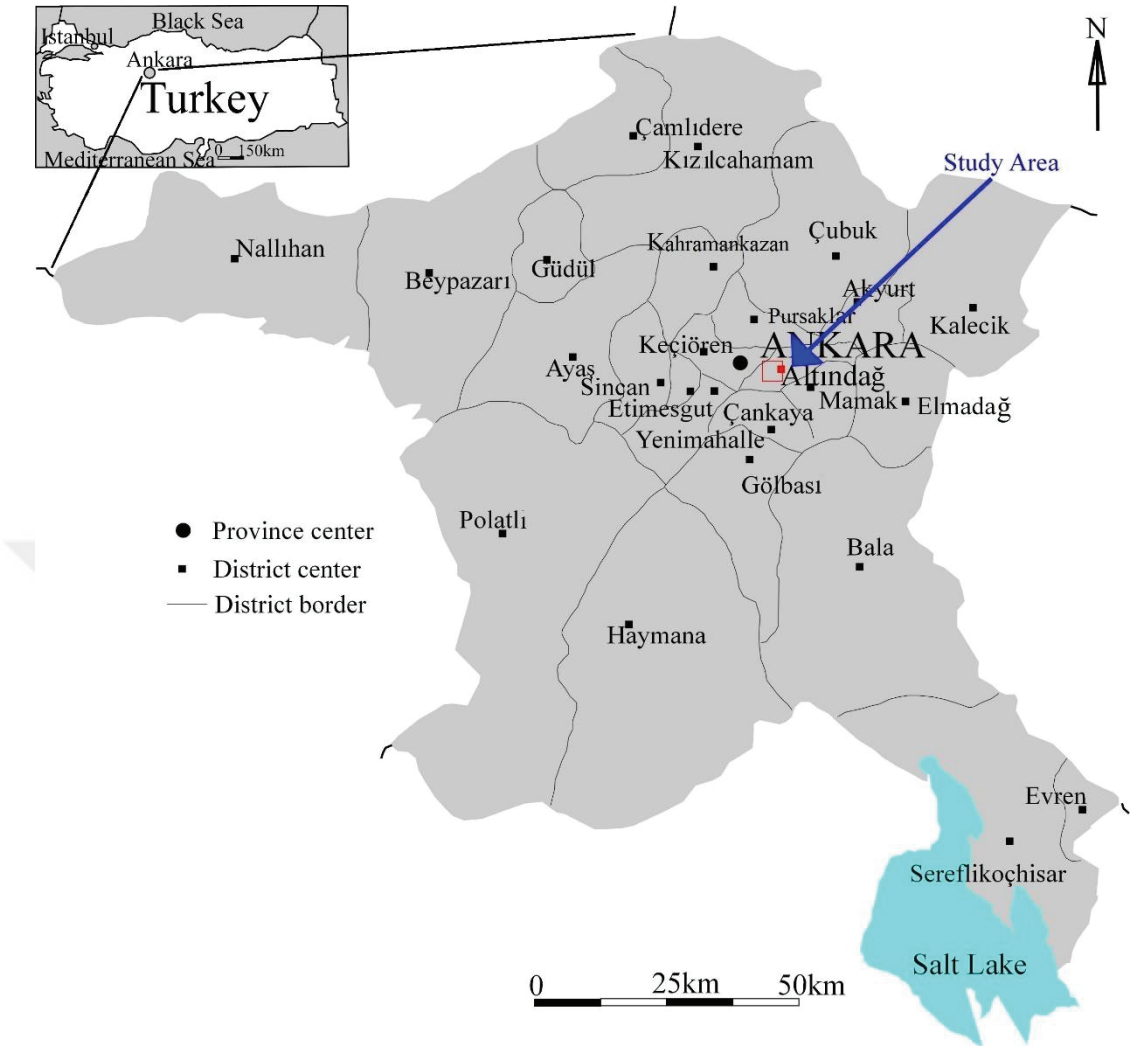

Figure 1.3 Location map of the study area (modified from Saygılı, 2016).

Figure 1.4 Ankara Citadel and its surrounding (Altındağ Municipality, 2010).

1.3 Topography

The slope, aspect and DEM maps of the study area are presented in Figures 1.5, 1.6 and 1.7, respectively. These maps were prepared by TNTmips (2012) software of Macromedia. The ITRF 1996 UTM coordinates of the maps are also given in the figures. DEM map was prepared by polynomial surface modeling method. The slope and aspect maps were derived from DEM. The slope map is divided into 4 groups as shown in Figure 1.5. The aspect map is also divided into 4 classes as North, South, East and West facing. The horizontal and vertical resolutions of the maps are 72dpi.

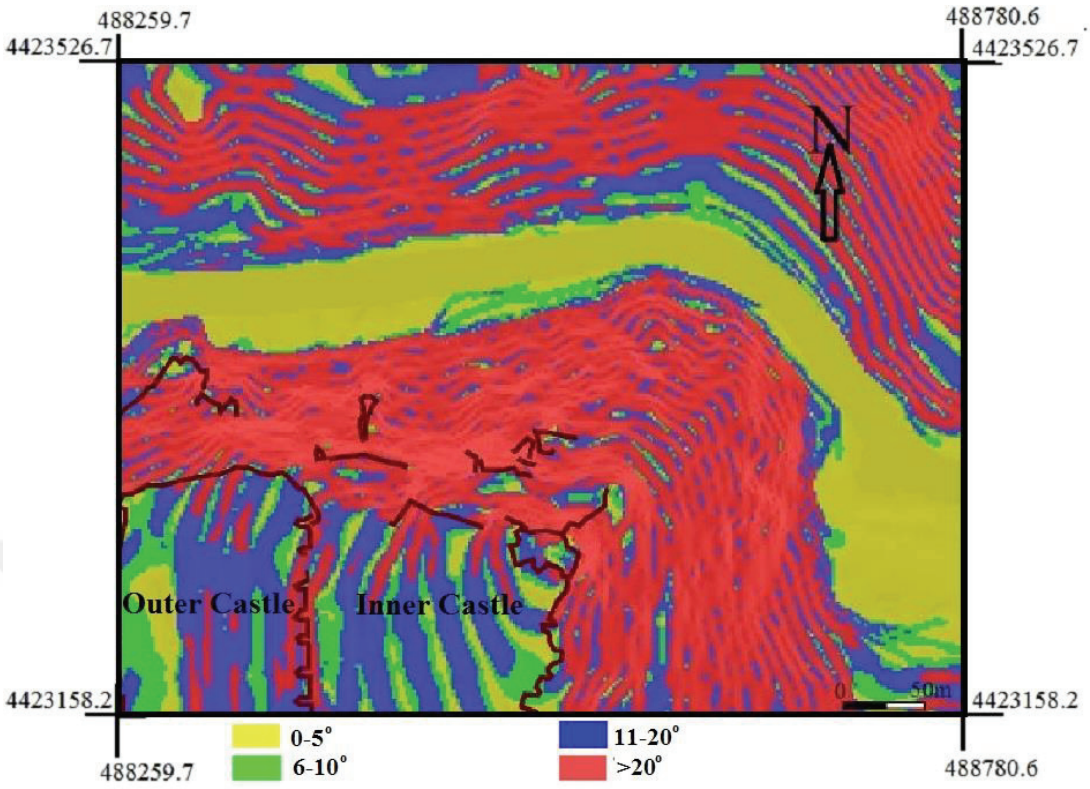

Figure 1.5 Slope map of the study area.

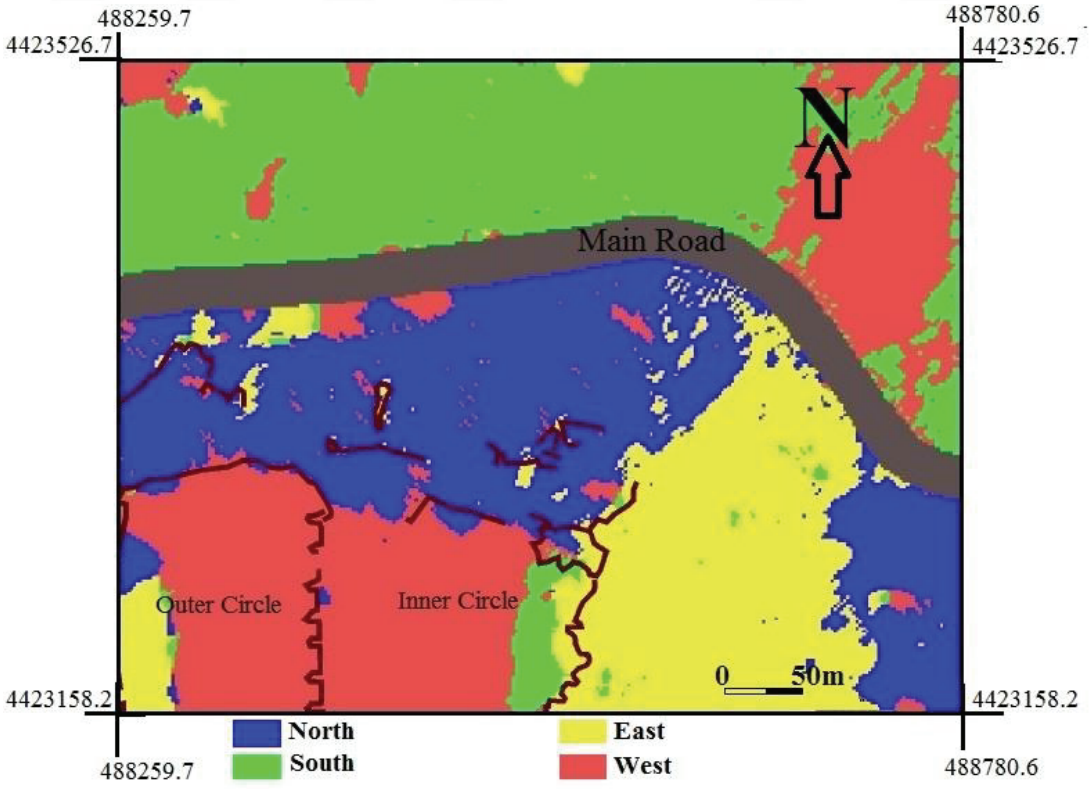

Figure 1.6 Aspect map of the study area.

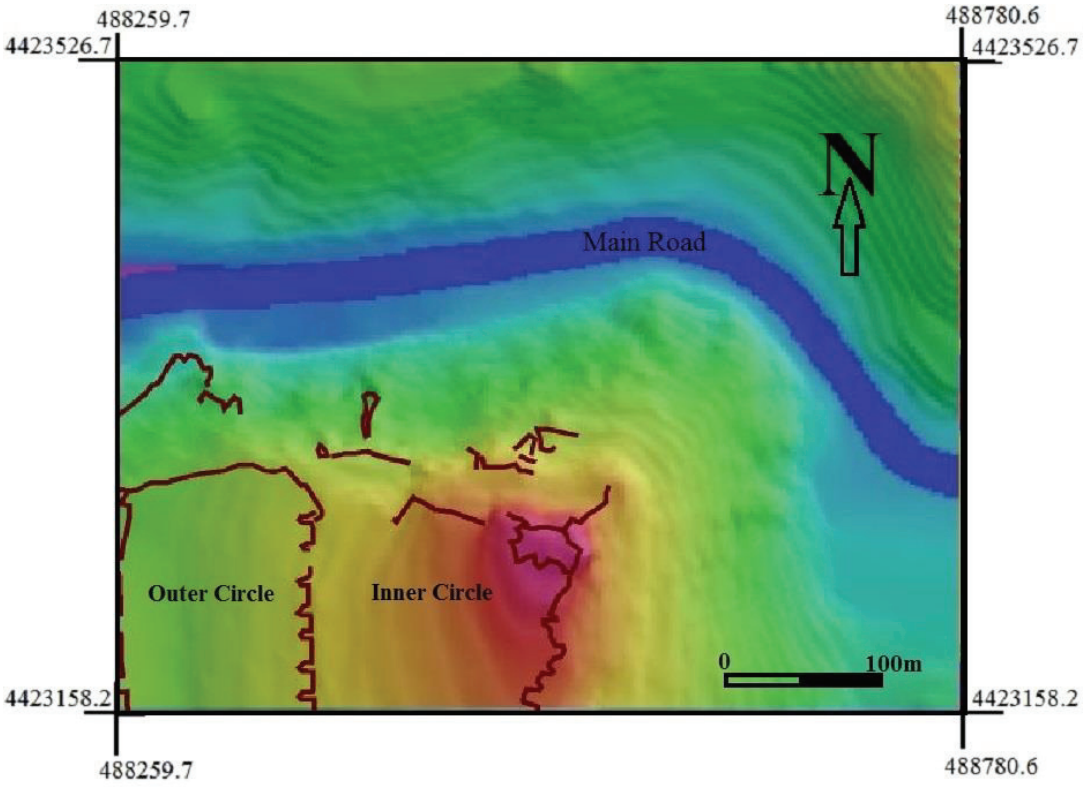

Figure 1.7 DEM of the study area.

1.4 Climate

Climatic changes can result in the freeze-thawing process of the rock which could lead to rockfall. Therefore, climatic conditions play an important role in rockfall events. Ankara has a moderately mild (continental) climate, even though all four seasons occur. Because of Ankara's elevation and inland location, winters are cold and snowy but summers are hot and dry with cool temperatures at nights. The statistical data of Ankara between 1954-2015 is given in Table 1.1. The coldest temperatures are in January and February as -3.0°C and -2.2°C. The highest temperatures are 30.2°C and 30.3°C in July and August, and the sharpest fluctuation of temperatures are also spotted in these months with 14.3°C difference. Rainfall occurs mostly during the spring and autumn. The highest average precipitation occurs in May and the lowest in August.

Table 1.1 Statistical meteorological data of Ankara between 1954 – 2015 (TSMS,2016).

ANKARA	Jan.	Feb.	Mar.	Apr.	May	Jun.	Jul.	Aug.	Sep.	Oct.	Nov.	Dec.
Average Temperature (°C)	0.4	1.9	6	11.3	16.1	20.1	23.6	23.4	18.8	13	7	2.6
Average Highest Temperature (°C)	4.4	6.6	11.6	17.3	22.2	26.6	30.2	30.3	26	19.8	12.9	6.6
Average Lowest Temperature (°C)	-3	-2.2	0.9	5.6	9.7	13	15.9	16	11.8	7.2	2.4	-0.7
Average Sunny Time (hour)	2.5	3.5	5.2	6.4	8.4	10.2	11.3	11.6	9.2	6.5	4.4	2.4
Average Precipitation Days	12.3	11	11.1	11.7	12.6	8.9	3.7	2.8	3.9	6.9	8.4	11.5
Monthly average Precipitation Amount (kg/m^2)	42.1	36.6	40.3	46.5	52	36.7	14.2	10.9	18.7	29.1	32	43.1

1.5 Methodology

This study includes several steps. First of all, detailed literature survey was carried out to acquire the geological setting of the study area and research previous studies. Topographic map of the study area with 1/4000 scale was obtained from the Altındağ municipality (Figure 1.1).

Secondly, field studies were conducted. During field studies, detailed scanline surveys were performed at 21 different locations. Potential rockfall sources were determined in the field. Samples were collected for laboratory studies. The sizes of the fallen blocks were measured to assist the analysis. Schmidt rebound measures were taken with the L-type Schmidt hammer.

Thirdly, laboratory studies were conducted on the collected samples. Porosity, unit weight, water absorption, sonic velocity and uniaxial compressive strength values of the rocks were obtained from different laboratory tests. Back analysis was conducted to find rolling friction coefficient of the rock.

Kinematic analyses were performed to estimate what types of rock failures are possible. Then, limit equilibrium analyses were done to detect the stability of the rock slope. Next step is the analysis of the rockfall with 2D and 3D methods. 22 profiles were determined and rockfall analyses were carried out with RocFall 5.013 software (Rocscience, 2015c) for each profile. Different block sizes measured in the field were also considered for the analysis. 3D analyses were conducted by ROTOMAP32 (Geo&soft, 2005). The results from both analyses were compared to obtain a danger zone.

For the final step of the study, remedial measures were suggested to mitigate the effects of rockfall in the study area based on the results of the analysis.

1.6 Geology

The geological units seen around the study area are Elmadağ formation, Ortaköy formation, Keçikaya formation, Mamak formation, Tekke volcanics, Gölbaşı formation and alluvium (Figure 1.8).

Lower, Middle and Upper Triassic aged Elmadağ formation extends along south west - north east direction. This formation consists of metaconglomerate, metasandstone, mudstone, sandy limestone, limestone, sandstone, volcanogenic sandstone, agglomerate and metavolcanics with or without greenschist facies. Metamorphism of this formation reduces upward progressively. This formation is

generally yellow, gray and brown colored. The stratification of this unit is thin and medium thickness, and is frequently folded. This formation overlays Emir formation, and overlaid by Keçikaya formation (Akyürek et al., 1997).

Mid-Upper Triassic aged Ortaköy formation consists of spilite, diabase, tuff, volcanogenic sandstone and agglomerate. Spilite and diabase partly preserve the primary structure, but partly metamorphosed. Pillow structures can rarely be seen in dark green, black colored basalt. There are void spaces inside spilite, and they are filled by calcite. The petrographic examinations of the rock types forming the Ortaköy formation are as follow. In spilite, albite microlites are distributed in a paste of calcite, chlorite, opaque grains. The voids of the rocks are filled with calcite, chlorite and albite. This formation laterally intrudes Elmadağ formation and bottom part of Keçikaya formation. Keçikaya formation covers the upper part of Oraköy formation (Akyürek et al., 1997).

Mid-Upper and Upper Triassic aged Keçikaya formation is composed of gray, white colored limestone and sandy limestone. It has characteristic of partly crystallized and partly dolomitic. The medium and thick stratified unit is abundantly fractured and cracked. Nevertheless, the stratification cannot be observed clearly everywhere, due to the easy abrasion characteristic of the surface. Gray colored limestone inside this formation has fossils in it. Keçikaya formation overlays Ortaköy and Elmadağ formations. It is overlaid by Hasanoğlu formation with an unconformity (Akyürek et al., 1997).

Upper Miocene aged Mamak formation is composed of the lava mix of aglomerate, tuff, andesite and basalt. Agglomerates in this formation consist of white, gray, red colored andesite, dacite and basalt pebbles in various sizes attached by tuff. Layering can be seen clearly in some sections. The tuffs seen in the agglomerates are of different colors, and generally thinly stratified. Andesites are observed as sills in the agglomerates. Mamak formation overlays Kumartaş formation. Mamak formation is laterally intruded by Tekke Volcanics and Hancili formation. It is overlaid by Bozdağ basalt (Akyürek et al., 1997).

Upper Miocene aged Tekke volcanics is composed of andesite, trachyandesite, basalt and less amount of tuff, aglomerate and dacite. Andesites are red, pink, gray and black. Flow tracks can be observed in andesites. Gray and white colored tuff are generally seen inside andesite and agglomerate. They are finely grained with andesite fragments in it. This formation intrudes Mamak formation. It can also be seen in Kumartaş ve Hançili formation as sills (Akyürek et al., 1997).

Pliocene aged Gölbaşı formation is composed of grey, red coloured and unpacked or loosely packed conglomerate, sandstone and mudstone of different origins. Generally, there is no stratification, but horizontal strata can be observed in some sections. Cement is calcite and clay. Quartzite, basalt, various limestones, diabase, metamorphic rocks, radiolarite serpentinite, gabbros compose the grains and gravels of sandstones and conglomerate. This formation is mostly observed as decomposed. Gölbaşı formation overlays Bozdağ basalt and other older formations with an unconformity. The upper margin of this formation cannot be traced. Alluvium unit consists of unpacked or loosely packed sand, milestones and gravel from river beds of the region (Akyürek et al., 1997).

However, the only geological unit covered the study area is the andesite belonging to the Upper Miocene aged Mamak formation. The andesites in the study area are generally steeply jointed, and were considered as the products of Miocene volcanism in Central Anatolia (Erol, 1961; Erentöz, 1975). The rock has generally pinkish gray color and was slightly to moderately weathered. The andesite in the study area is generally highly jointed having cooling joints and flow layers forming the steep topographic features.

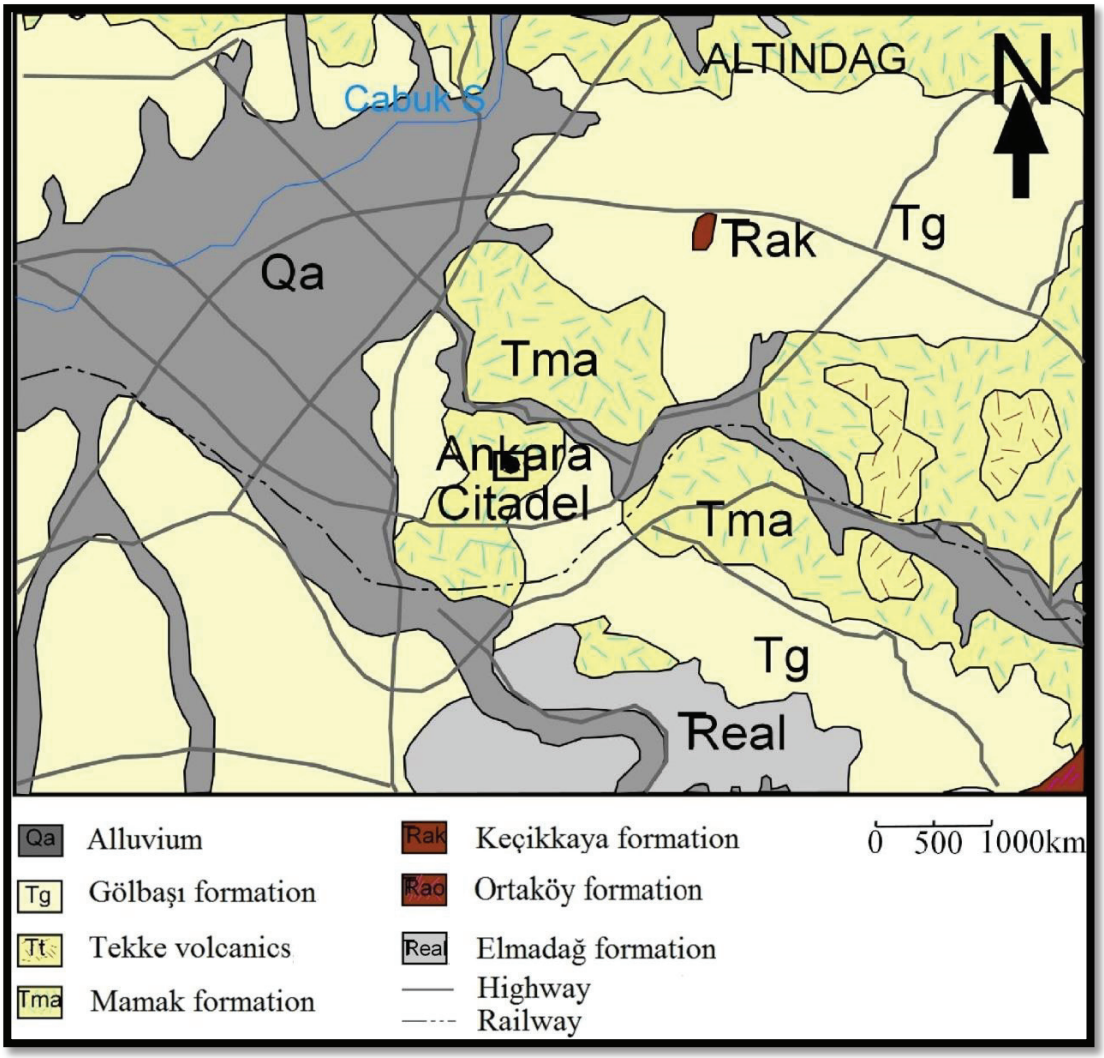

Figure 1.8 Regional geologic map of the study area (modified from Akyürek et al., 1997).

The petrographic analysis of the thin sections the andesites shows plagioclase, hornblende and biotite as the main minerals. Some volcanogenic fragments were also spotted, and opaque amorphous formations and clay minerals were detected as secondary minerals. As a result of weathering, secondary clay formations were seen surrounding plagioclase minerals, weathered zone around hornblendes and chlorite formation in biotites were also detected (Tokmak, 2005).

In The earthquake zoning map of Ankara (Figure 1.9) shows the earthquake zones of the region (AFAD, 1996). 1st degree earthquake zone means the acceleration values

expected in the area is more than 0.4g. 2nd degree earthquake zone is acceleration values between 0.3 and 0.4g, while 3rd degree earthquake zone is between 0.2 and 0.3g. 4th degree earthquake zone is between 0.2 and 0.1g and 5th degree earthquake zone is expected to have acceleration less than 0.1g. The study area which is located in Altındağ is in the 3rd degree earthquake zone of Turkey.

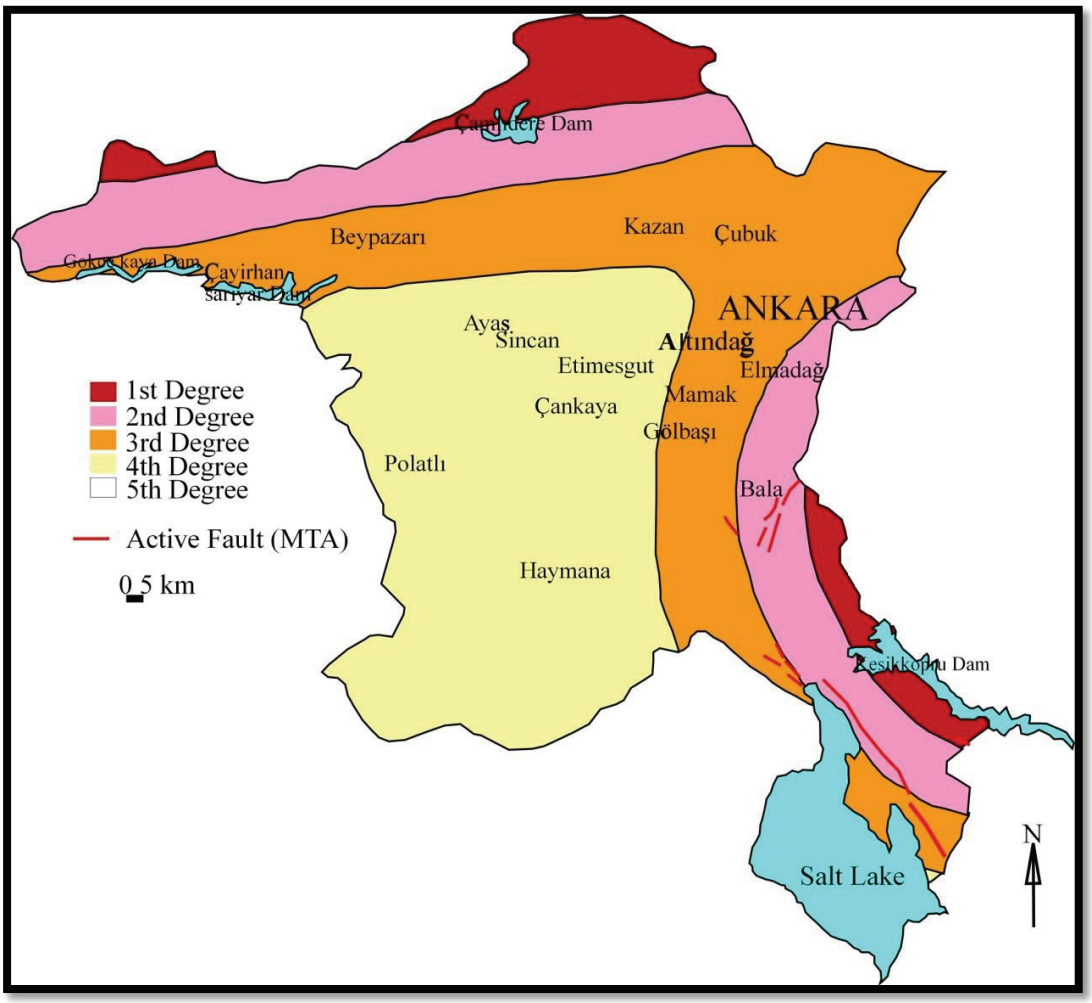

Figure 1.9 Earthquake zoning map of Ankara (modified from AFAD, 1996).

1.7 Previous Study

The study area and its surroundings have been the subject of many studies.

Erol (1961) studied the tectonic development of Ankara region. He considered the andesites of the study area as the products of Miocene volcanism in Central Anatolia.

As for the hydrological studies around the study area, hydrogeological survey along Southern part of Ankara by Müller (1957) and Hatip and Mürted plain's hydrogeological study carried out by DSI (1957, 1956), and studies relating to Ankara's water needs by Yalçın (1988) can be shown as examples.

Ulusay (1975) observed slope instability in Ankara andesites by field studies. Öncül (1978) carried out study about the rock strength and Karacan (1984) did the studies relating to geomechanical properties of discontinuities on Ankara andesites.

Kasapoğlu (1980) studied on the geo-engineering properties of the ground in the City of Ankara for his thesis. He observed three groups of the Ankara andesites according to their colors; as bluish grey, pinkish and blackish purple, and explained this as the results of three different phases of volcanic flows. The color of andesite ranges from pinkish red to whitish yellow. The whitish yellow color symbolizes that the andesite was weathered. According to Kasapoğlu (1980), generally the phenocrystals of the porphyritic andesites has plagioclase and/or quartz minerals with sizes range between 1 and 5 mm. One of the most obvious characteristics of these andesites is cooling joints developed in the vertical directions.

Gokceoglu et al. (2000) developed a discontinuity controlled probabilistic risk maps of the Altındağ (settlement) region. By applying kinematic rules and digital elevation model of the study area, the probabilistic risk maps were developed for planar, toppling and wedge failures. By comparing the distribution of the actual failures in the area with the probabilistic risk maps developed for the study area, all of the identified failures were discovered in the higher risk zones on the probabilistic risk maps.

Ercanoğlu and Aksoy (2004) studied the Ankara castle and its vicinity to investigate the probable modes of instabilities using kinematic analysis technique and to construct potential instability map of the study area with the aid of Geographic Information Systems (GIS). Existence of three major discontinuity sets were found. Planar, wedge and toppling type of failures were analyzed using a computer program called DIKA (Digital Kinematic Analysis). From the instability map developed,

28%, 15% and 10% of the study area were observed as potentially susceptible to toppling, wedge and planar failures, respectively. Because of the high and steep topographical features, it was observed that the potential instabilities can be transformed into rockfalls after initial failures.

Aksoy and Ercanoglu (2006) studied an urban settlement area to determine the rockfall source by using a rule-based fuzzy evaluation. It was analyzed based on the discontinuity data of the andesites in the central part of Ankara city including the Ankara Citadel. A rule-based fuzzy evaluation contained the altitude difference, the number of discontinuities, the number of wedges and the number of potential slides as the parameters of the fuzzy sets. In order to access rock source areas (RSAs), data from field studies and a rule-based fuzzy evaluation were combined. As the results of the RSA maps, 1.7% and 5.8% of the study area were discovered to have “high RSA” and “medium RSA”, respectively. Potential hazard map was also prepared. Finally, “high rockfall potential” was found to cover 3.6% of the study area and “medium rockfall potential” 7.9% based on the high and medium RSAs.

CHAPTER 2

BACKGROUND INFORMATION ON ROCKFALL

Rockfall tends to occur on rocky terrains. Danger of rockfall can lead to indirect loses such as building damage and services delay or direct loses like human casualties. Because of the fact that rockfall events are sudden, their frequency and magnitude are unforeseeable, and they pose a great danger to infrastructures and human lives (Dorren, 2003; Pantelidis, 2009; Pantelidis, 2010). Many damaging rockfall events have taken place all over the world. When the rockfall events occurred on the highway in Vancouver on July 29th, 2008, the rock blocks covered the road between Furry Creek Bridge and Horseshoe Bay (Figure 2 .1) (Volkwein et al., 2011).

Figure 2.1 A rockfall event blocked the highway Sea to Sky joining Vancouver to the ski resort Whistler (Volkwein et al., 2011).

Rockfalls are abrupt movements of rocks and boulders that become detached from steep slopes or cliffs, and proceeds downward by free falling, bouncing or rolling (Varnes, 1978).

2.1 Rockfall Mechanics

The assessment of the rockfall initiation mechanism is one of major concerns in proceeding with further steps of rockfall investigation (Aksoy and Ercanoglu, 2006). Rockfall mechanics can be separated in two parts such as triggering mechanism and modes of motions of falling rocks.

2.1.1 Rockfall Triggering Mechanism

The causes of rockfall can actually be divided into rockfall promoters and reasons of the initiation of the movement (Dorren, 2003). The rockfall promoters produce the discontinuities in the rocks which may lead to detachment of the rocks from the bedrocks. The degree of rockfall promotion depends on the environmental factors causing physical and chemical weathering, and on the bedrock type (Schumm and Chorley, 1964; Day, 1997). Regions with heavy precipitation, frequent freeze-thaw cycles and seismic events are greatly prone to dangers of rockfall (Turner and Schuster, 1996). Rockfalls are strongly influenced by gravity, mechanical weathering, and the presence of interstitial water (Varnes, 1978). When mountain sheep and goats move around on the slope, they may initiate the rockfall though this is a less usual cause. The study of MaCauley (1985) stated that the animal movement resulted in 0.3% of rockfalls on California highways. In wet climates, vegetation and tree growth can be the cause of rockfall by cracking the rock and allowing the water to enter into the cracks (Wyllie, 2015). Rockfall can also be caused by poor blasting practices during original construction or reconstruction (Brawner, 1994).

In general, rockfalls are reported caused by numerous factors and whether a rock can fall or not depends on a combination of topographical, geological and climatological factors and the time (Dorren, 2003).

2.1.2 Modes of Motion of Falling Rocks

Once the rock has been broken off the bed rock and begins to move, it proceeds downwards in different modes of motions which depend on the mean slope gradients (Dorren, 2003). According to Varnes (1978), the modes of the motions are freefall, bounce and roll.

Freefalling of rocks are seen in the steep slopes. The characteristic of the freefall is that motions occur in the air, and therefore, there is no contact with the slope (Azzoni et al., 1995). Figure 2.2 shows the mode of motion of the rocks changing from freefalling to bouncing and rolling as the mean slope gradient decreases according to

Ritchie (1963). However, the values of the mean slope gradients may differ based on the different field situations (Dorren, 2003).

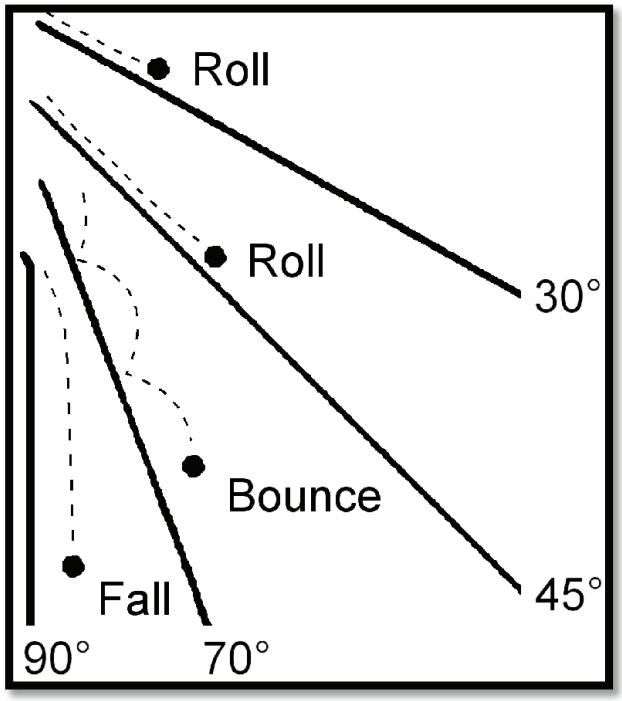

Figure 2.2 General modes of motion of rocks on slopes associated with the mean slope gradients (Ritchie, 1963).

Freefalls occurs on the very steep slope. According to Azzoni et al. (1995), in freefalling of rocks there are two different movements which are translation of the centre of rock and the rotation of the block around its center. These two movements are essential, because in reality, falling rocks are rarely ever round. Once the block comes in contact with a slope, it may roll, slide or a combination of both (Ateriou and Tsiambaos, 2015).

If the mean slope gradient decreases in the down-slope section, a rock collides on the slope surface after freefalling, which is defined as bouncing (Dorren, 2003). Where a rock falls on the slope that is covered by blocks of similar dimensions, a series of bounces may occur (Bozzolo and Pamini, 1986).

Where the mean slope gradient is less than approximately 45°, a rock slowly changes its motion from bouncing to rolling because of rotational momentum accumulated at

the rock (Dorren, 2003). If the falling rock's dimensions are much greater than those of the roughness of the slope, the rock rolls with simultaneous slippage at the point of contact (Bozzolo and Pamini, 1986).

Sliding occurs only at the initial stage of motion or when a rock ceases moving (Bozzolo and Pamini, 1986). After different modes of motion, a moving rock stops (Dorren, 2003).

Rock mass may break up when impacting on the ground during its descent (Copons et al., 2009). This breaking up produces individual rock blocks, or fragmental blocks, which move independently when the size of the detached rock mass is roughly less than 10^5 m^3 (Evans and Hungr, 1993).

2.2 Rockfall Models

Many different models are developed to calculate the runout zones of the rockfall events. According to Dorren (2003), all existing rockfall models can be classified into three main groups: (1) empirical models, (2) process-based models and (3) GIS-based models.

2.2.1 Empirical Models

Empirical models of rockfall events are usually derived from the way how topographical factors and the length of the runout zone relate with each other (Dorren, 2003). They are the models which apply statistical methods to analyze the data obtained from a study area (Copons et al., 2009). In the studies of empirical models, simplified assumptions are made in the rockfall scenarios such as rockfall size and slope characteristics. Therefore, empirical models have error margins, and the work has to be done on a huge area at a medium scale (Copons et al., 2009).

Two main basic empirical models are widely adopted for the study of rockfalls based on geometrical approaches. They are reach angle and shadow angle. Toppe (1987) and Evans and Hungr (1993) suggest the *Fahrböschung* principle (Heim, 1932) to predict runout zones of rockfall events. The angle between the highest point of the

rockfall source and the stopping point of the longest runout boulder is defined as the *Fahrböshung* (Figure 2.3) (Evans and Hungr, 1993). Following Lied (1977), another principle suggested by Evans and Hungr (1993) is the minimum reach angle. The minimum angle is the angle between the highest point of the talus slope and the stopping point of the longest runout boulder for any given rockfall (Figure 2.3) (Dorren, 2003). There are several values of minimum shadow angle suggested in the literature, and Lied (1977) suggested that minimum shadow angle should be between 28°-30° (Copons et al., 2009). After compilation of 16 profiles of rockfall paths on talus slope from south western British Columbia, Evans and Hungr (1993) subjected the minimum shadow angle of 27.5°.

In addition to the length of the runout, Asteriou and Tsiambaos (2016) proposed an empirical model which estimates the post trajectory directions of a block by examining the effects of shape, slope angle, and the deviation of the post impact trajectory as a function of the pre-impact trajectory direction. Basically, the empirical models are the easiest type of rockfall models.

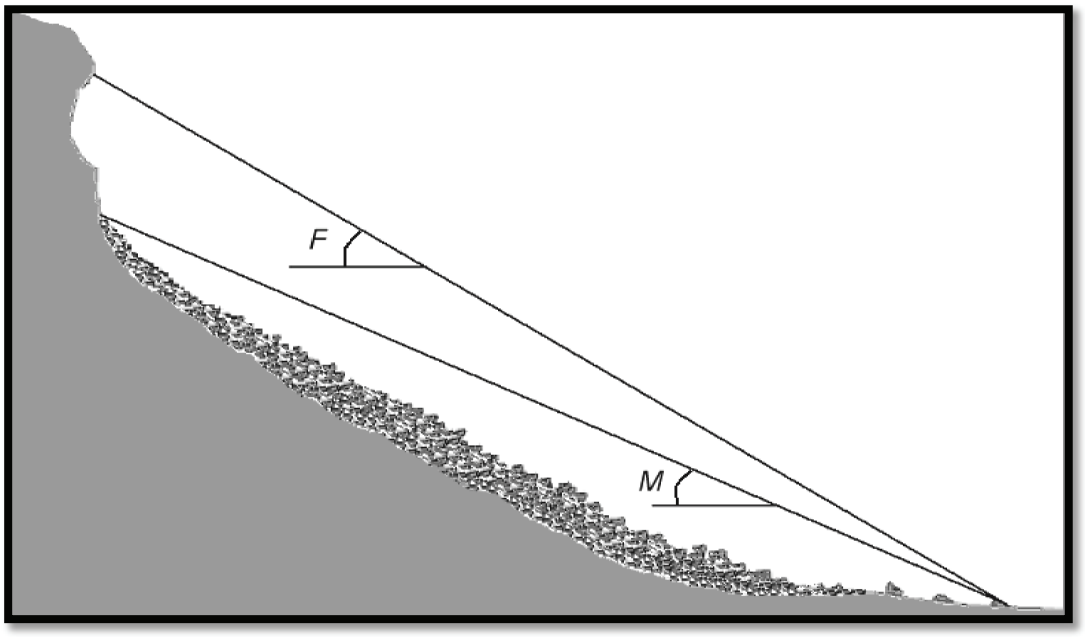

Figure 2.3 The *Fahrböschung* (*F*) and the minimum shadow angle (*M*) of a talus slope (Dorren, 2003).

2.2.2 Process-based Models

Process-based models are the simulations of the modes of motion of falling rocks over slope surfaces (Dorren, 2003). Kirkby and Statham (1975) and Statham (1976) developed a process-based rockfall model for movement of rocks over talus slopes with the presumption of rocks only to slide over a talus. Keylock and Domaas (1999) developed simple dynamic rockfall model which was proposed based on the model outlined by Kirby and Statham (1975). This model presumed that insignificant energy loss and a zero-horizontal velocity component during freefall. With that presumption, the model assessed the downslope motion over talus and runout zone. There are plenty of process-based models that describes rockfall process (Wu, 1985; Bozzolo and Pamini, 1986; Pfeiffer and Bowen, 1989; Kobayashi et al., 1990; Evans and Hungr, 1993; Budetta and Santo, 1994; Azzoni et al., 1995).

According to Dorren (2003), these models are in agreement with three factors. The first factor is that the rockfall process is in two-dimensional section where the lateral dispersion is not considered. Secondly, a straight line was assumed with a slope angle, which is the mean slope gradient on each represented segment of the rockfall track and combination of these lines represented the rockfall track (Figure 2.4). Finally, in the simulations, the motions were in the sequence of flying phase and contact phase. The flying stage were modeled with a parabolic equation based on the initial velocity in x and y directions and the acceleration due to gravity. The intersection of the parabolic function and the straight slope segments was considered as the collision point.

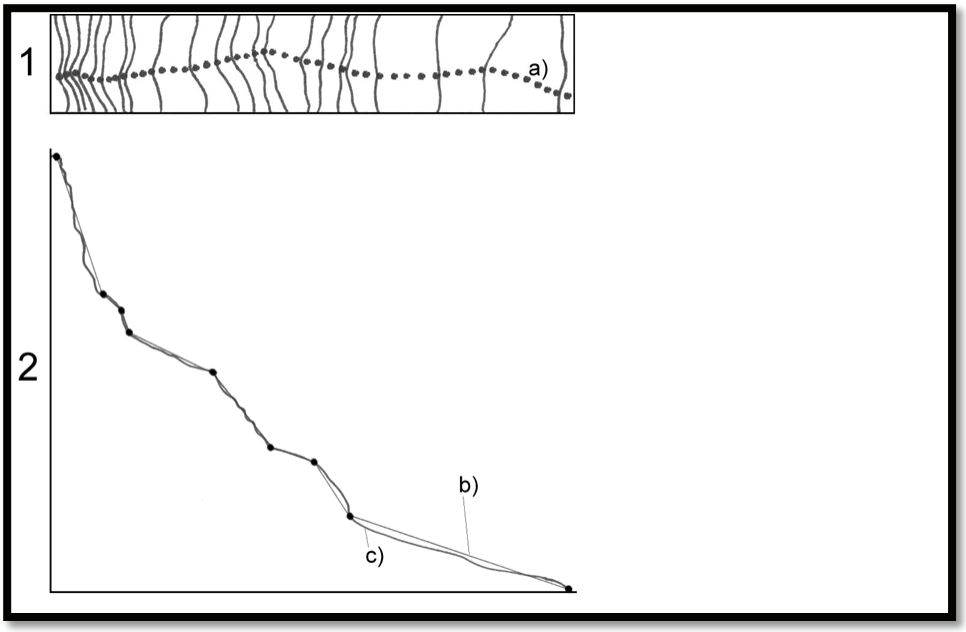

Figure 2.4 The upper figure (1) shows the actual rockfall path (a) projected on a contour line map. The lower figure (2) shows the slope segments (b), used in two-dimensional rockfall models representing the actual slope of the rockfall path (c) (Dorren, 2003).

Different simulation techniques of today can be categorized into two as multi-mass and non-multi-mass system techniques. As the falling rocks are only considered as particles without mass or size, the first category has the problem that the shapes of the falling rocks are not taken into account. On the other hand, the energy loss at the collision time cannot be assessed exactly in the second category affecting the determination of rockfall behaviors on the slope (Ma et al., 2011).

The process-based models can also be divided into the spatial dimensional groups. The majority of the process-based models are in the group of 2D models, which operate on the line of slope profiles (Ritchie, 1963; Bozzolo and Pamini, 1986; Pfeiffer and Bowen, 1989; Spang, 1995). 3D process-based are run on three-dimensional space (x, y, z) which requires spatially continuous parameter maps. As scanning method of rocky terrain such as LiDAR (Light Detection and Ranging), are successfully developed to create digital terrain models (DEM), 3D analyses become

feasible by importing DTM's into rockfall modeling programs (Lan et al., 2007; Lan et al., 2010; Wyllie, 2015).

2.2.3 GIS-based Models

Geographical Information Systems (GIS) are computer-based systems applied to reserve, exploit and present geographic information (Barreca et al., 2013). GIS has already been recognized as a beneficial tool for better managing, interpreting and maintaining resources in addition to verified decision support system (McNeil et al., 2002). The rockfall models operating within a GIS environment or the raster-based models with input data provided by GIS analysis, are called GIS-based models (Dorren, 2003). There are three procedures associated with GIS based rockfall modeling. Hegg and Kienholz, (1995) defined those procedures as identifying the rockfall source areas in the region of interest, determination of the fall track and the calculation of the length of the runout zone.

Dorren and Seijmonsbergen (2003) developed three GIS-based models to predict rockfall runout zones at Montafon region, Austria, namely ROCKY1, ROCKY2 and ROCKY3. The first model is based on the algorithms illustrated by Scheidegger (1975) and van Dijke and van Westen (1990). ROCKY2 is an extended version of ROKCY1 and is based on the Sturzgeschwindigkeit model developed by Meissl (1998). This model simulated freefalling and sliding modes of motion (Dorren, 2003). ROCKY3 is a combination of a GIS-based model and a process-based model, in which simulation of the motion of falling rocks are thorough. The major distinction between ROCKY3 and the other two models is that ROCKY3 is capable of simulating multiple bounces of a falling rock within a pixel.

Meissl (1998) also developed two GIS-based rockfall models using an empirical model for calculating the runout zone (Dorren, 2003). The first model was *Schattenwinkel* based on the minimum shadow angle principle (Evans and Hungr, 1993). The second model of Meissl (1998) was called *Geometrische Gefäll* which was based on the angle of the shortest line between the top of the rockfall source scar and the stopping point (Dorren, 2003).

Lan et al. (2007) developed RockFall Analyst (RA) in ArcGIS using ArcObjects and C# (multi-paradigm programming language) which has the ability to manage huge amounts of geospatial information relative to rockfall behaviors. RA supplies powerful and unique modeling, and analysis means for 3D rockfall process models and danger estimation.

A pilot GIS-based system was applied for the evaluation and analysis of rockfall hazard associated with active faults affecting the eastern and southern flanks of Mt. Etna (Barreca et al., 2013). This database was planned to reserve all geometric and kinematic parameters of all elements, and to be continuous upgraded when new valuable data are accessible so that a more thorough hazard assessment of the Etna region can be obtained. Combining GIS-based models with 3D physical rockfall process-models becomes a valuable tool to evaluate the rockfall hazard in large regions (McNeil et al., 2002; Agliardi and Crosta, 2003; Dorren, 2003; Dorren et al., 2004; Guzzetti et al., 2004).

RocFall 5.013 (Rocscience, 2015c) and ROTOMAP 32 (Geo&soft, 2005) that are used in this study are process-based rockfall models. RocFall is a powerful, user-friendly 2D computer program that performs a probabilistic simulation of rockfalls, and can be applied to design remedial measures by checking their effectiveness (Stevens, 1998). The ROTOMAP32 (Geo&soft, 2005) module is for 3D rockfall analysis, and allows the complete design of rockfall protective system presenting real 3D modeling and many other options for model calibration and barrier design.

2.3 Key Parameters in Analysis of Rockfall

Slope geometry, slope material properties, rock geometry and rock material properties have effects on the way the falling rocks act (Ritchie, 1963). Analysis of rockfall involves study of both trajectories and impacts (Wyllie, 2015). The main parameters concerned with rockfall analysis are trajectories, impact energy, coefficients of restitution and friction coefficient.

Trajectories: The path of rockfall trajectories is parabolic according to Newtonian mechanics, and the fall is interrupted by the three points on the parabolic. Trajectories depend on the velocities of the falling bodies. Its length and height (bounce height) are defined by the distance between impact points and the height of the rockfall path above the ground surface. They are helpful in determination of locations and heights of protection system (Wyllie, 2015).

Impact energy: Since the physical interpretation of instant of impact with the slope is complicated, certain assumption has to be done to simplify the situation (Bozzolo and Pamini, 1986). As a rockfall event is made up of sequences of impacts, a trajectory follows each impact. A rock will proceed downward, as long as the velocity and energy loss during impact is less than the velocity and energy gained during the following trajectory (Wyllie, 2015). When a rock impacts on the slope, kinetic energy is lost due to inelastic components of collisions. Kinetic energies before and after impact can be calculated from velocities and masses of the blocks (Li et al., 2016).

Coefficients of Restitution: The ratio of rebounding velocity to incoming velocity is defined as the coefficient of restitution (Li et al., 2016). The change in normal velocity during impact is defined as the normal coefficient of restitution (Wyllie, 2015). It measures the degree of elasticity in collision normal to the slope (Pfeiffer and Bowen, 1989). The reduction in tangential velocity during impact is called the tangential coefficient of restitution, and it is related to the friction force produced between the contact surface (Wyllie, 2015). In the rockfall analysis, one of the most important and most difficult parameter to assess for the analysis is the coefficient of restitution (Topal et al, 2007; 2012; Kaya and Topal, 2015).

Friction coefficient: Sliding or rolling friction is a factor resisting motion parallel to the slope, also causing the loss of kinetic energy (Pfeiffer and Bowen, 1989). The friction coefficient is a parameter that involves both the material forming the slope surface and the roughness of the surface (Wyllie, 2015). Rolling friction coefficient can be expressed as the tangent of the angle at which a boulder initially at rest starts

rolling. Coefficient of friction can be calculated as the tangent of the angle at which a boulder initially at rest starts sliding (Peng, 2000).

2.4 Rockfall Remediation and Mitigation Methods

Because of the unpredictability of rockfall events, to prevent and reduce the risk, it is imperative that the analyses of rockfall hazards are carried out and the optimal measures are suggested for damage control. There are several options for remediation and mitigation strategies. Remediation methods are the processes that treat the slope to prevent the fall, and mitigation on the other hand is the process that make the risk of the potential fall less severe (Maerz, 2014). The choice of techniques depends on several factors, including the size or volume of rockfall, access to the rockfall source, maintenance limitations, the budget, and the desired result (FHWA,1993). Rockfall protection can be supplied by many different structures that are effectively certified by the makers with substantial trials of the systems and their utilization in fields (Wyllie 2015).

2.4.1 Remediation Methods

Remediation methods can be considered as method of stabilizing the slope (Maerz, 2014). These methods are rock scaling, flattening the slope, removal of pore water pressure, and support systems (Brawner 1994).

Rock scaling: It is the removal of loose rock from slope by means of hand tools and mechanical equipment. It is commonly used in conjunction with most other design elements (FHWA, 1993).

Flattening the slope: It can be applied to change the slope geometry that is in favor of rockfall.

Removal of pore water pressure: It is reduction of the water level within a slope through installation of horizontal drains or adits (FHWA, 1993). They are usually used with other designs such as retaining wall (Figure 2.5).

Figure 2.5 Horizontal drainage system installed on the retaining wall to reduce pore water pressure (Ischebeck Titan, 2016).

Support system: They can be applied to the slope to reinforce the rock. For example, rock bolts and retaining walls can be constructed to hold the rock blocks and rock masses in place and to prevent them from falling (Maerz, 2014). Figure 2.6 shows the rock bolts applied on a wall to stabilize the slope.

Figure 2.6 Rock bolts applied on the slope to stabilize unstable blocks (Skylinesteel, 2016).

2.4.2 Mitigation Methods

The selection of rockfall protection structures that are appropriate for the site conditions depends on a combination of factors that include design impact energy,

topography, slope, geometry and the type of facility that is to be protected (Wyllie, 2015). The structures that are used to mitigate the rockfall are berm, ditch, fence, wire mesh and rock shed. The impact energy and fall trajectories are needed to determine the strength, the height and the location of the structure on the slope for the design of rockfall protection (Wyllie, 2015; Li et al., 2016). These design parameters are usually assessed from computer simulation programs.

Berms: They are used to retard the energy of the falling rock, and they may also increase factor of safety against sliding. Their design is supposed to retain fallen rock from the higher slopes and prevent the further movement of the rock down the slope. To prevent the likelihood of falling rock to bounce off, the berms must be covered with energy absorbing material like sand and gravel (Maerz, 2014). Figure 2.7 shows the typical application of berms on the road cut on North Dakota, USA.

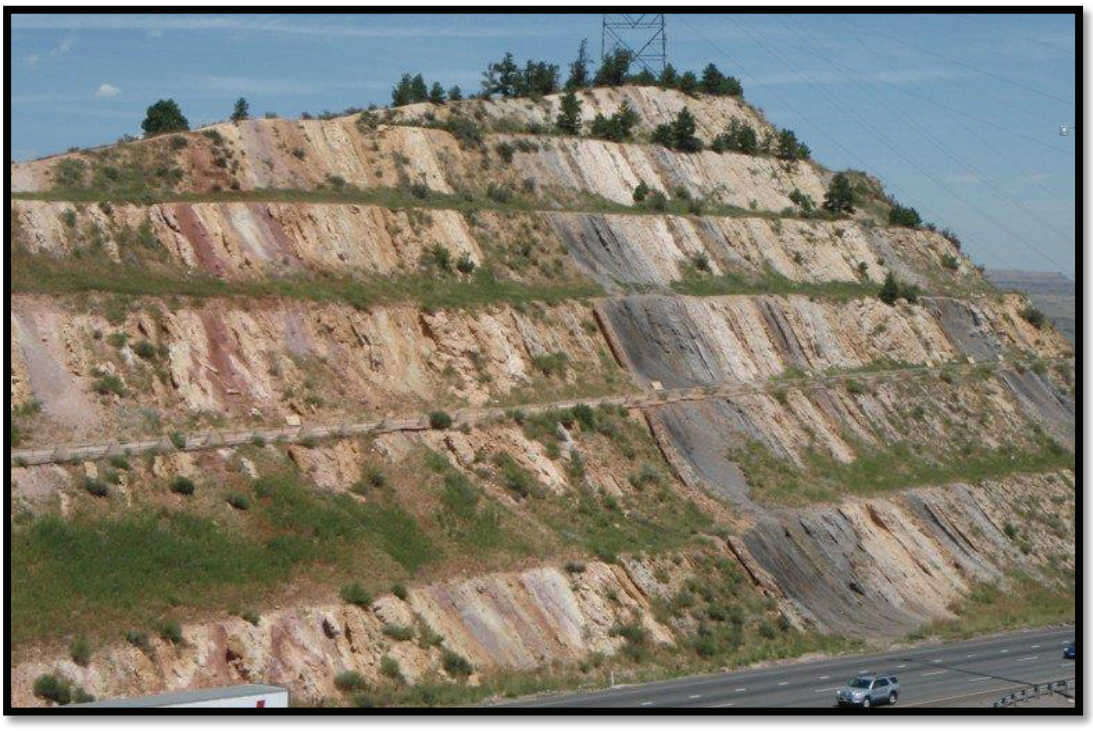

Figure 2.7 Typical berms structure on the road cut from North Dakota, USA (Panoramio, 2016).

Ditches and barriers: They are the structures, that are usually installed at the base of the slope. They are often reliable, low-cost and low maintenance protection

structures. Required dimension of a ditch is defined by its base width, inclination and depth, and is related to the height of the face and its slope angle (Wyllie, 2015). Figure 2.8 shows Ritchie's chart for designing ditches, and Figure 2.9 shows a sketch of typical ditch section.

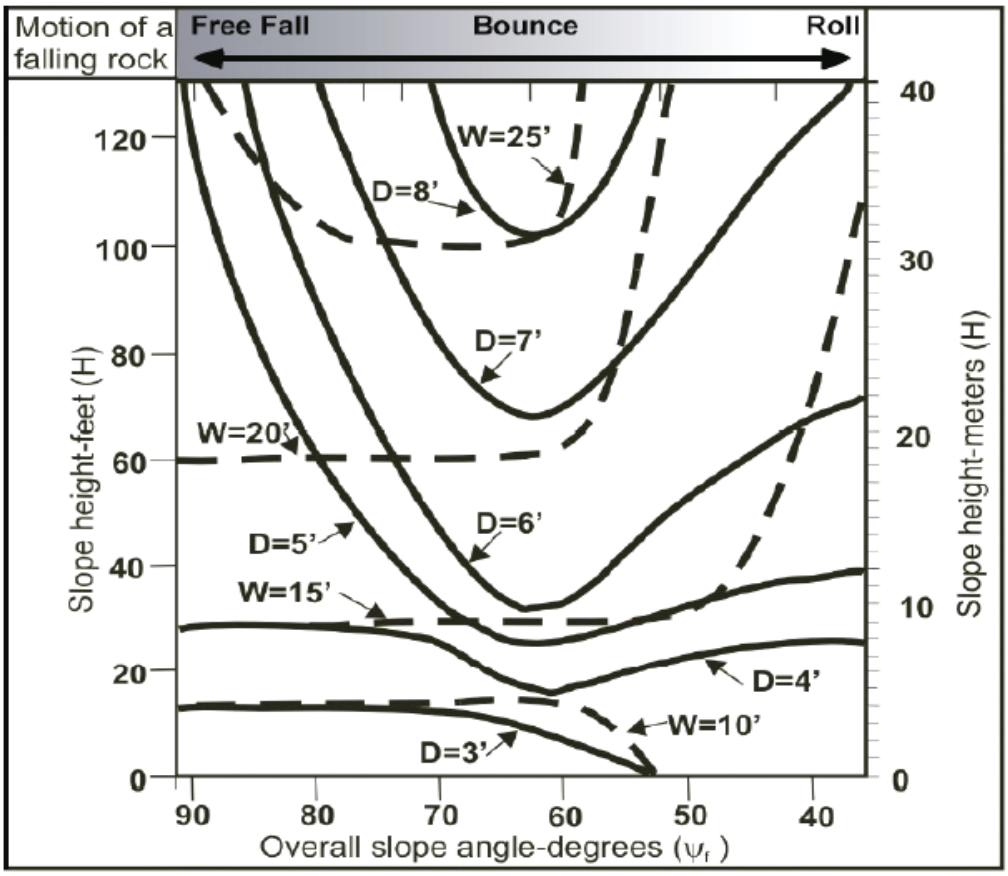

Figure 2.8 Ritchie's design chart for determining required width (W) and depth (D) of rock catch ditches in relation to height (H) of hill slope (Ritchie, 1963).

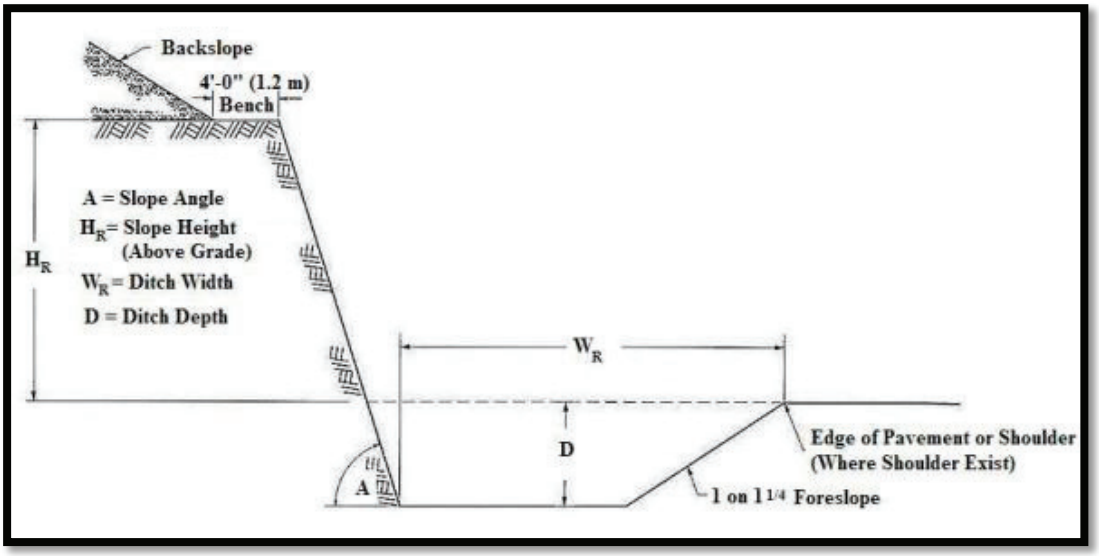

Figure 2.9 Typical Ritchie ditch section (Munfakh et al., 1998).

Fences: They can be built either on the slope or at the base of the slope. Impact energies and trajectories data are necessary for good designs (Wyllie, 2015). The design of the fences is to slow down the rolling rocks and its angular velocity (Ritchie, 1963). An application of fences to prevent fallen rocks to the road is shown in Figure 2.10.

Figure 2.10 Fences to catch the fallen rocks (Bright Hub Engineering, 2016).

Wire Mesh: In the cases where there is no suitable space for structures like ditches, wire mesh may be draped over the slope surface (Wyllie, 2015). They can be designed to prevent the detached blocks from reaching the road and enable them to drop only vertically and slowly (Maerz, 2014). The rock slope covered with a typical design of wire mesh on Kayseri-Develi highway is shown in Figure 2.11.

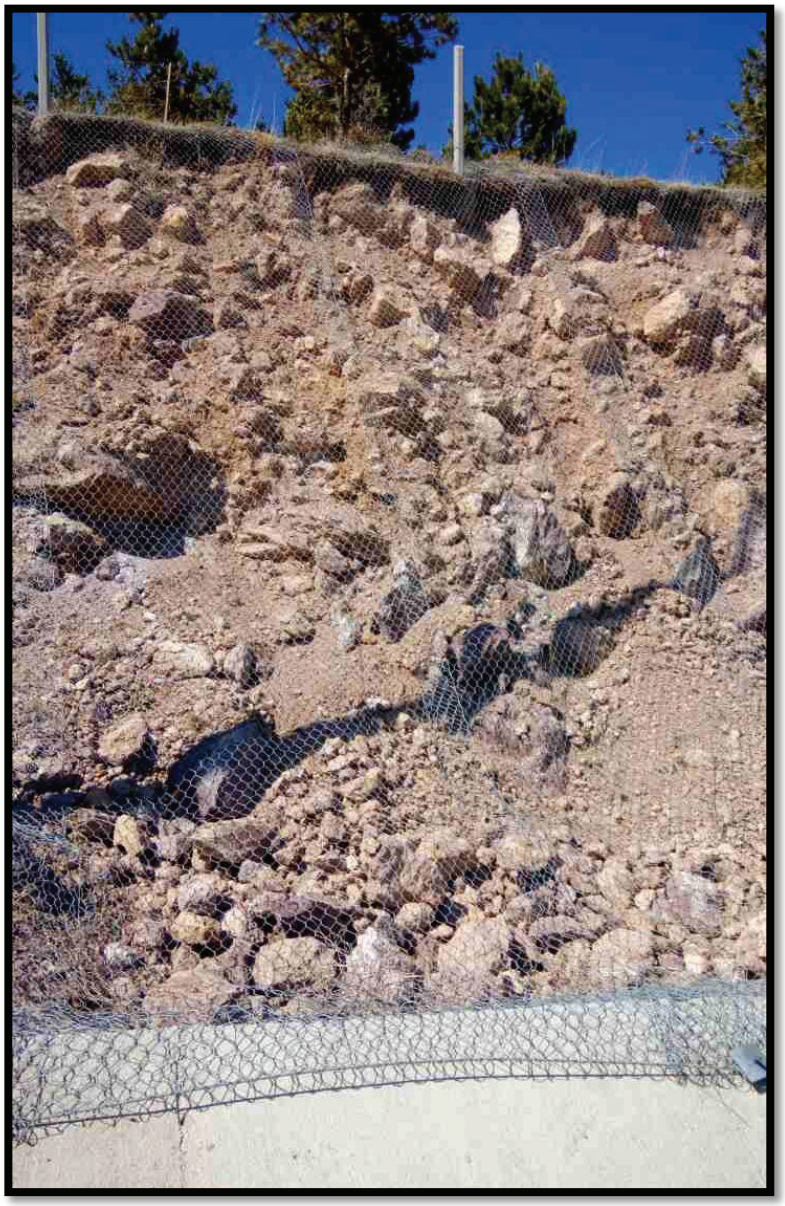

Figure 2.11 Wire mesh protection over the slope on Kayseri-Develi highway.

Reinforced concrete sheds: They are usually constructed at the locations where rockfalls are frequent and very sound protection system is necessary for essential facilities such as high traffic volume highway and high speed train (Wyllie, 2015). They can be designed to withstand a high specific energy impact, but they are quite expensive structures (Maerz, 2014). A picture of Rain Rocks rock shed in California is shown in Figure 2.12.

Figure 2.12 The Rain Rocks rock shed and Pitkins Curve Bridge opened officially in January of 2014 (Discover Central California, 2016).

CHAPTER 3

FIELD AND LABORATORY STUDIES

To be able to perform rockfall analysis around Ankara Citadel, firstly, data including topographic map, reports and photographs were collected from Altındağ municipality. The 1/4000 scaled electronic map of Ankara Citadel neighborhood, that was supplied by Altındağ Municipality was digitized and used as base map. Then, field studies including scanline surveys (ISRM, 1981; Priest, 1993), determination of potential rockfall sources and sample collections were conducted.

3.1 Field Studies

The study area was investigated totally, and field data were collected at 21 stops based on the accessibility of the outcrops. Every stops' coordinates were recorded with GPS. Later, the stops were marked on Google Earth. Google Earth view of the study area with marked 21 stops and 2 fallen block spots is shown in Figure 3.1. Scanline surveys were performed along these 21 stops.

The andesite exposed in the study area is generally pinkish grey in color and mostly slightly weathered. The highly jointed outcrops have cooling joints and flow layers in different directions. At each stop, orientations of the discontinuities were taken. The persistence, spacing, aperture, infilling, weathering state, roughness, wall strength and ground water condition of the discontinuities were noted. The northern part of the study area with locations of stops, fallen blocks and sample location is shown in Figure 3.2.

Figure 3.1 Google Earth view of the northern part of the Ankara Citadel with measurement locations.

Figure 3.2 The northern part of the Ankara Citadel.

Based on the field studies done around the Ankara Citadel, it was observed that previous rockfall events of various block sizes occurred. The spacing values of flow layers and cooling joints define the sizes of the blocks. The discontinuity data of the scanline survey made at 21 stops around the castle were contoured (Figure 3.3) with the aid of DIPS 6.0 software (Rocscience, 2013).

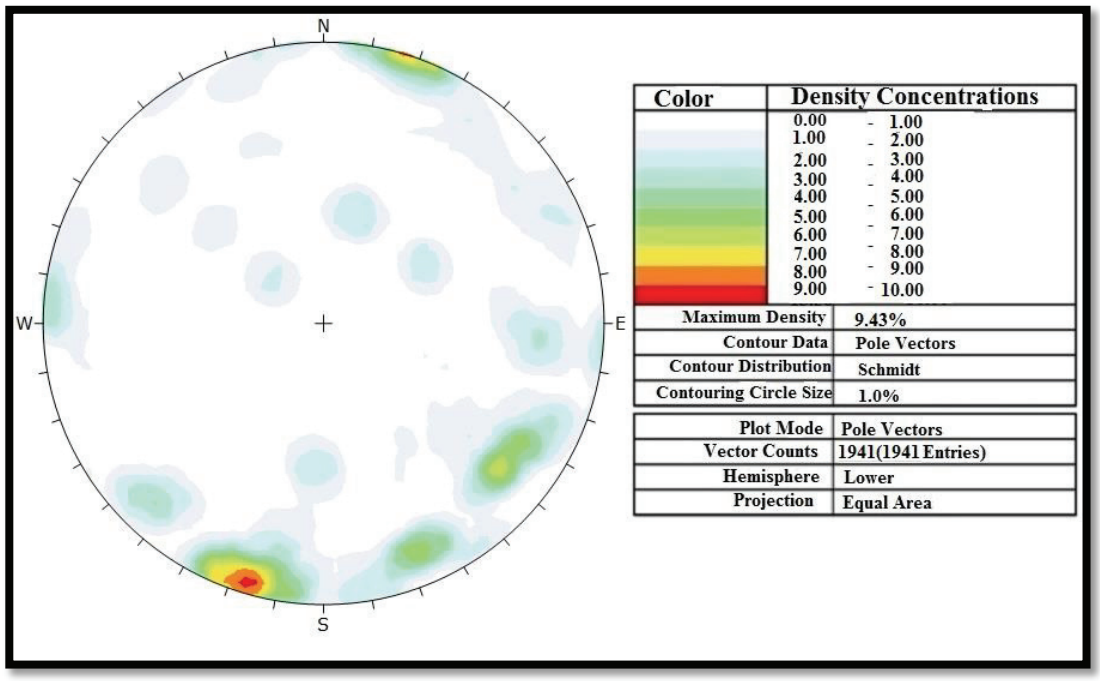

Figure 3.3 Contour diagram of the discontinuities measured during the scanline survey.

According to the discontinuity measurements made in the field, there are flow layers with low dip angles. These flow layers are visible but scattered in the areas near the center of the contour diagram in Figure 3.3. There are also a large number of steeply dipping cooling joints that develop in different directions perpendicular to the flow layers. This is evidence that the andesite is highly fractured. Therefore, the discontinuities set are non-systematic.

The persistence of cooling joints is usually less than 5m, but locally around 15m. The spacing ranges from 2 to 200cm. However, the spacing value is concentrated mostly around 20 to 60cm (Figure 3.4). The apertures are often tight, but there are

also clay-filled openings reaching 2cm in areas close to the surface. However, the apertures of the flow layers do not have infilling material because of their alignment of nearly horizontal. Other properties of the flow layers are similar to cooling joints. The Schmidt hardness values ranges from 25 to 41. The andesite is slightly to moderately weathered. The discontinuity surface of the andesite is undulating rough. JCS was determined as 3.55MPa from the Schmidt rebound hammer results by using the table of estimate of joint wall compressive strength from Schmidt hardness proposed by Deere and Miller (1966). The ground water is not observed in the study area.

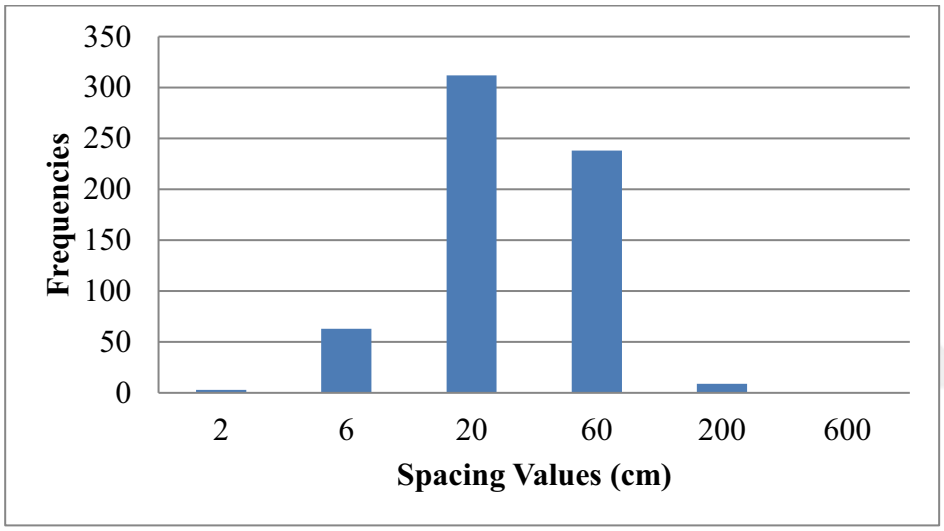

Figure 3.4 Frequency distribution of discontinuities spacing in the study area.

At the first stop, the andesite is pinkish grey. The rock shows slightly weathered state. The surface of the discontinuity is undulating rough. The dip amounts and dip directions of the flow layers in this stop are concentrated at 22º/254º and 36º/295º. The slope of this stop has dip and dip direction of 80º/310º. The contour diagram of the discontinuities is shown in Figure 3.5. The Schmidt rebound hardness of the rock at this stop ranges from 36 to 41. The spacing values of the cooling joints vary between 20cm and 70cm. However, the persistence of the joints ranges from 0.5m to 2m. The apertures between them are tight to 2 mm, and the infilling material is silty clay only at the surface. The flow layers have properties similar to those of the

cooling joints except that they do not infilling material. An outcrop of the andesite is shown in Figure 3.6.

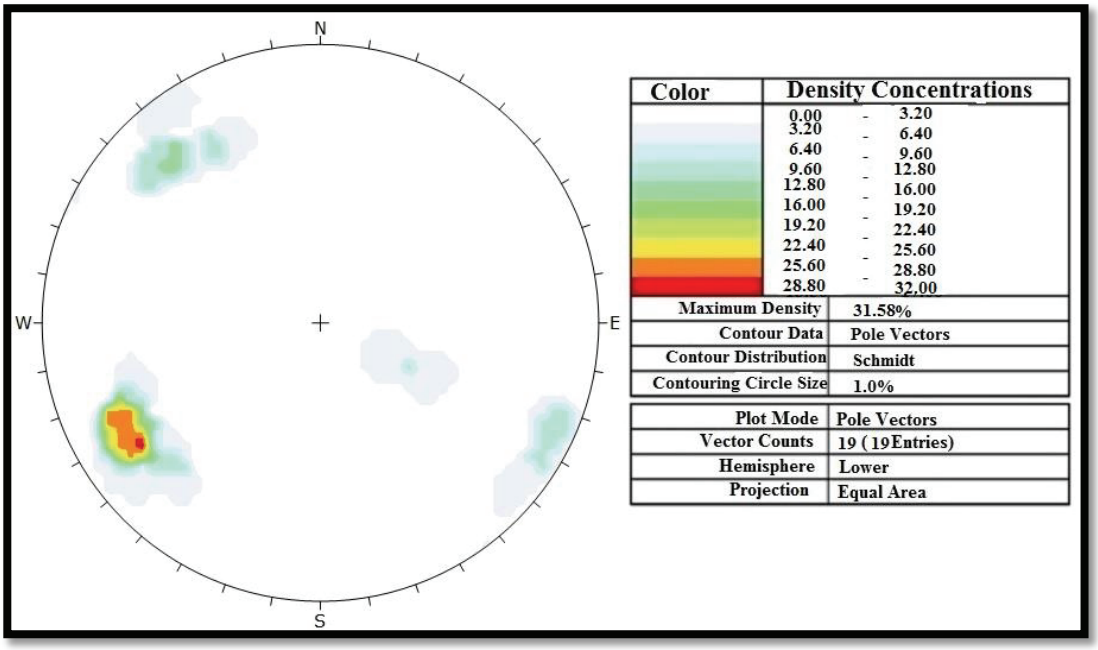

Figure 3.5 Contour diagram of the discontinuities at the 1st location.

Figure 3.6 Photograph of the andesite at the 1st location.

At the second stop, the rock is pinkish grey and slightly weathered. The surface of the discontinuity is undulating rough. The main dip amounts and dip directions of the flow layers are 04º/022º, 05º/022º and 04º/023º, and those of the slope is 82º/315º. The contour diagram of the discontinuities is shown in Figure 3.7. The Schmidt rebound hardness ranges from 28 to 38. The joints have spacing values between 30cm and 70cm. The persistence of the joints varies between 50cm and 70cm. The joints have tight to 2mm apertures filled with silty clay only at the surface. The properties of the flow layers are similar to those of the cooling joints but they do not infilling material.

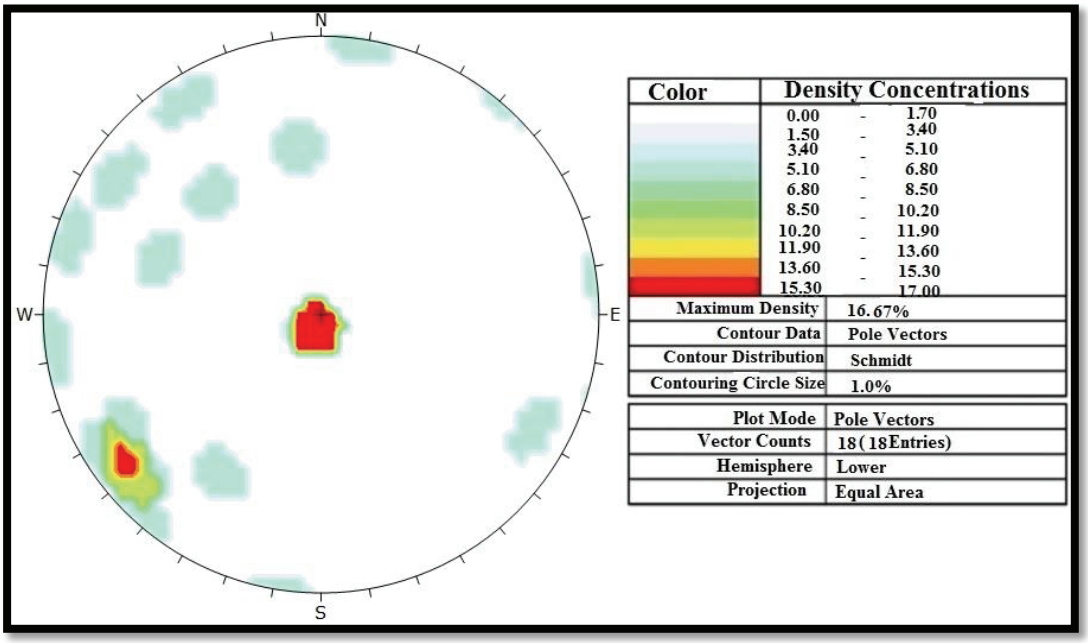

Figure 3.7 Contour diagram of the discontinuities at the 2nd location.

The andesite at the third stop is pinkish grey. The rock shows slightly weathered state. The surface of the discontinuity is undulating rough. The dip amount and dip directions of the slope is 56º/325º. The contour diagram of the discontinuities is shown in Figure 3.8. The Schmidt rebound hardness ranges from 25 to 30 in this stop. The spacing values of the joints vary between 30cm and 40cm. The persistence of joints ranges from 50cm to 150cm. The apertures are tight to 3cm, and filled with silty clay only at the surface. The flow layers have properties similar to those of the cooling joints except that they do not infilling material.

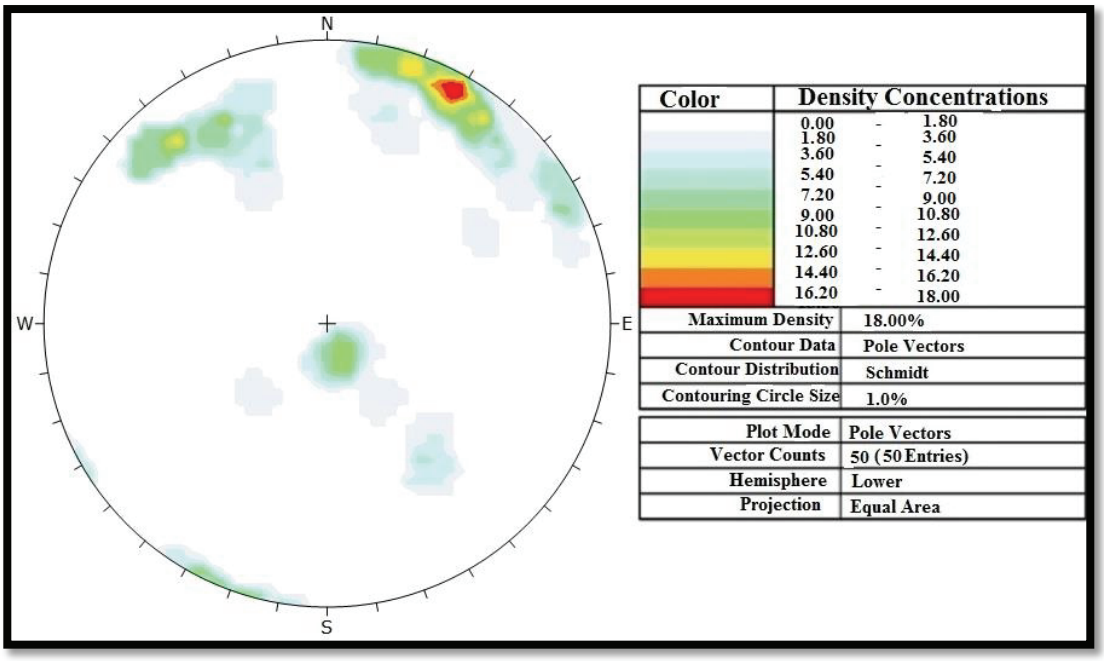

Figure 3.8 Contour diagram of the discontinuities at the 3rd location.

At the fourth stop, the rock is pinkish grey and slightly weathered. The surface of the discontinuity is undulating rough. The dip amounts and dip directions of the flow layers are concentrated at $13^o/331^o$ and $21^o/270^o$. Two slope surfaces were recorded in this stop, and their dip amounts and dip directions are $62^o/277^o$ and $76^o/336^o$. The contour diagram of the discontinuities is shown in Figure 3.9. The joints have spacing values between 50cm to 110cm. The persistence of the joints ranges from 100cm to 150cm. The apertures are tight to 3cm, and filled with silty clay only at the surface. The properties of the flow layers are similar to those of the cooling joints but they do not have infilling material. An outcrop of the highly fractured andesite is illustrated in Figure 3.10.

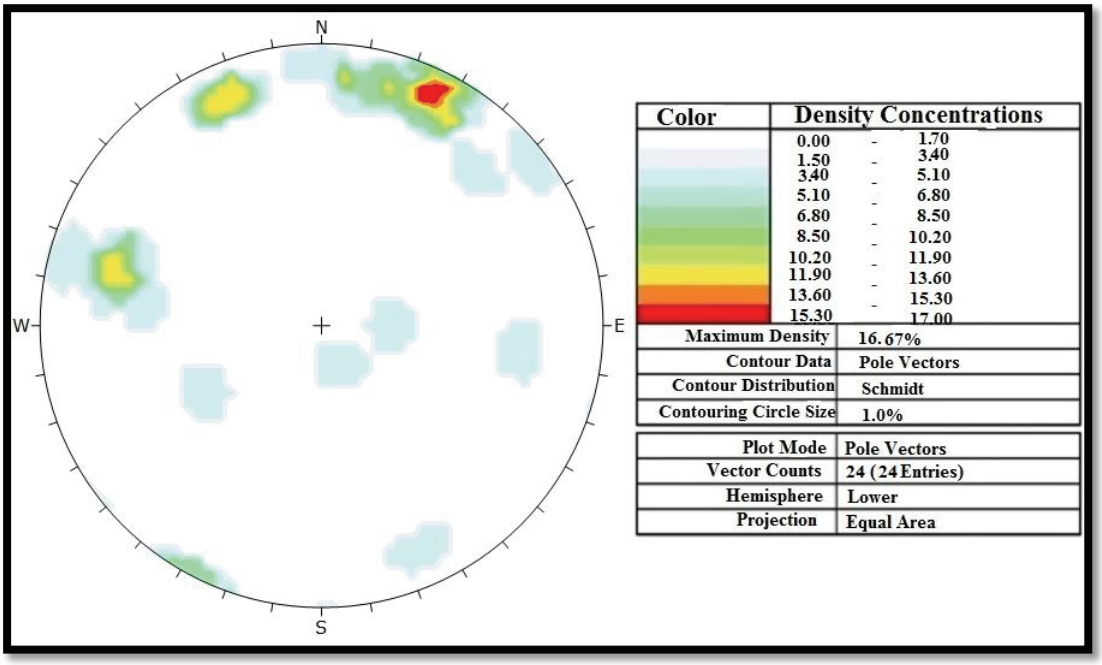

Figure 3.9 Contour diagram of the discontinuities at the 4th location.

Figure 3.10 The highly fractured andesite seen at the 4th location.

The andesite at the fifth stop is pinkish grey. The rock shows slightly weathered state. The surface of the discontinuity is undulating rough. The dip amounts and dip

directions of the flow layer and the slope are 18º/324º and 84º/340º, respectively. The contour diagram of the discontinuities is shown in Figure 3.11. The joints spacing varies between 20cm and 60cm. The persistence of the joints ranges from 60cm to 80cm. The apertures between them are tight to 2 mm, and filled with silty clay only at the surface. The flow layers have properties similar to those of the cooling joints except that they do not infilling material.

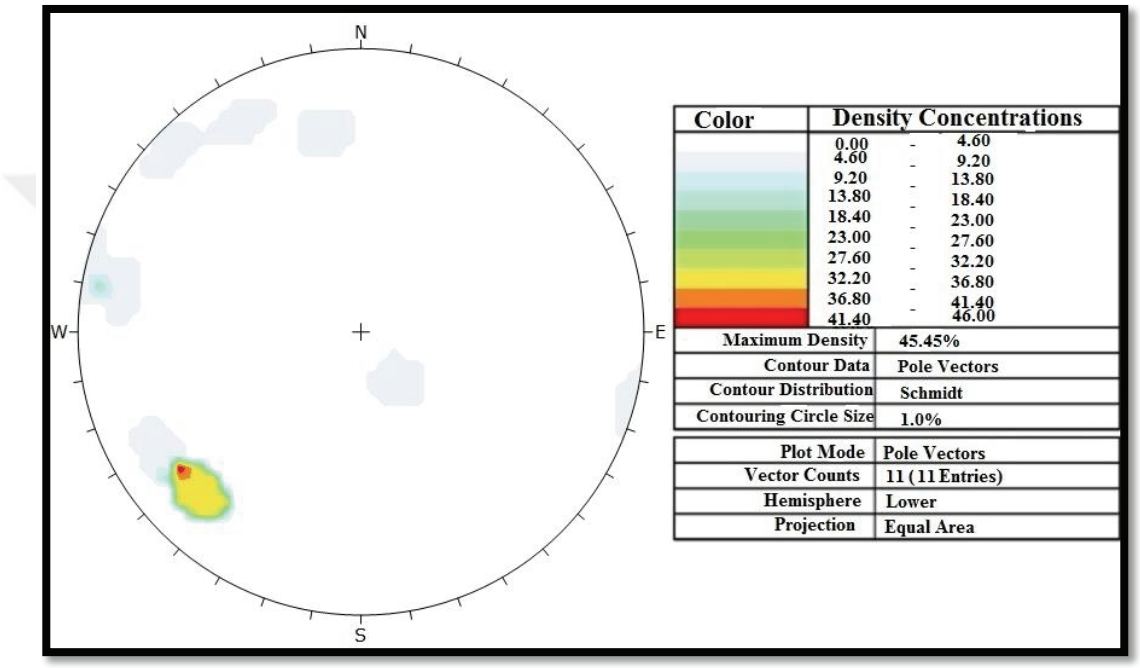

Figure 3.11 Contour diagram of the discontinuities at the 5th location.

At the 6th stop, the rock is pinkish grey and slightly weathered. The surface of the discontinuity is undulating rough. The dip amount and dip direction of the slope is 74º/326º. The contour diagram of the discontinuities is shown in Figure 3.12. The joints have spacing values between 30cm and 60cm. The persistence of the joints ranges from 30cm to 700m. The apertures are tight to 3cm, and filled with silty clay only at the surface. The properties of flow layers are similar to those of the cooling joints but they do not infilling material.

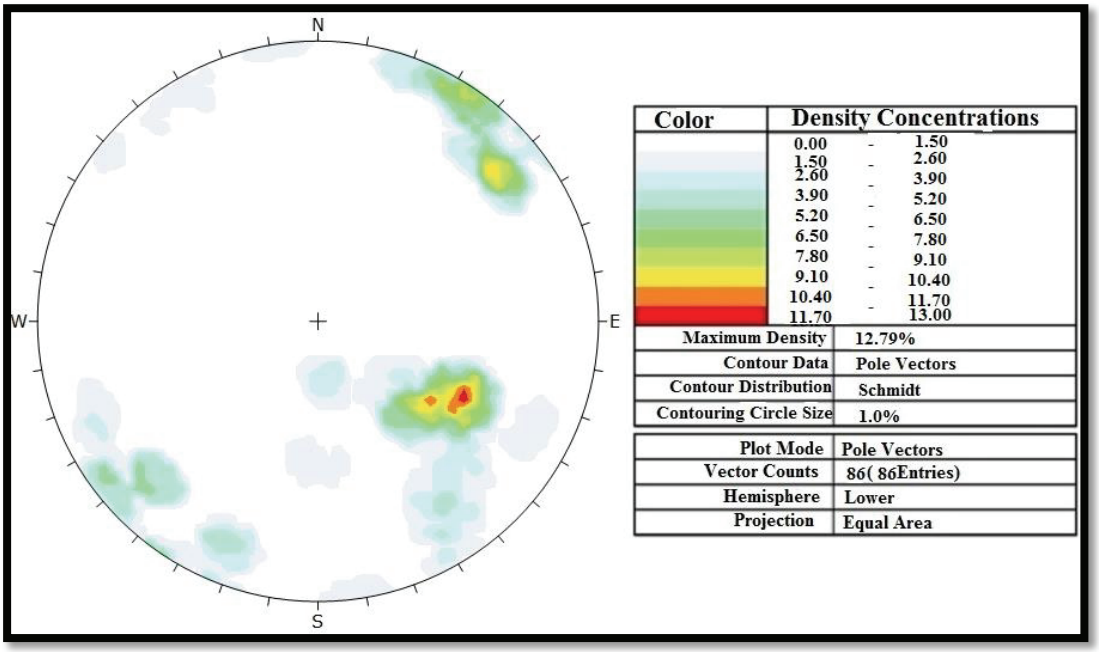

Figure 3.12 Contour diagram of the discontinuities at the 6th location.

The andesite at the seventh stop is pinkish grey. The rock shows moderately weathered state. The surface of the discontinuity is undulating rough. The dip amounts and dip directions of the flow layers are concentrated at 21º/033º and 24º/060º. Those of the slope is 80º/350º. The contour diagram of the discontinuities is shown in Figure 3.13. The Schmidt rebound hardness ranges from 35 to 40 in this stop. The spacing values of the joints vary between 5cm and 110cm. The persistence of the joints ranges from 0.3cm to 6m. The apertures between them are tight to 2cm, and filled with silty clay only at the surface. The flow layers have properties similar to those of the cooling joints except that they do not infilling material.

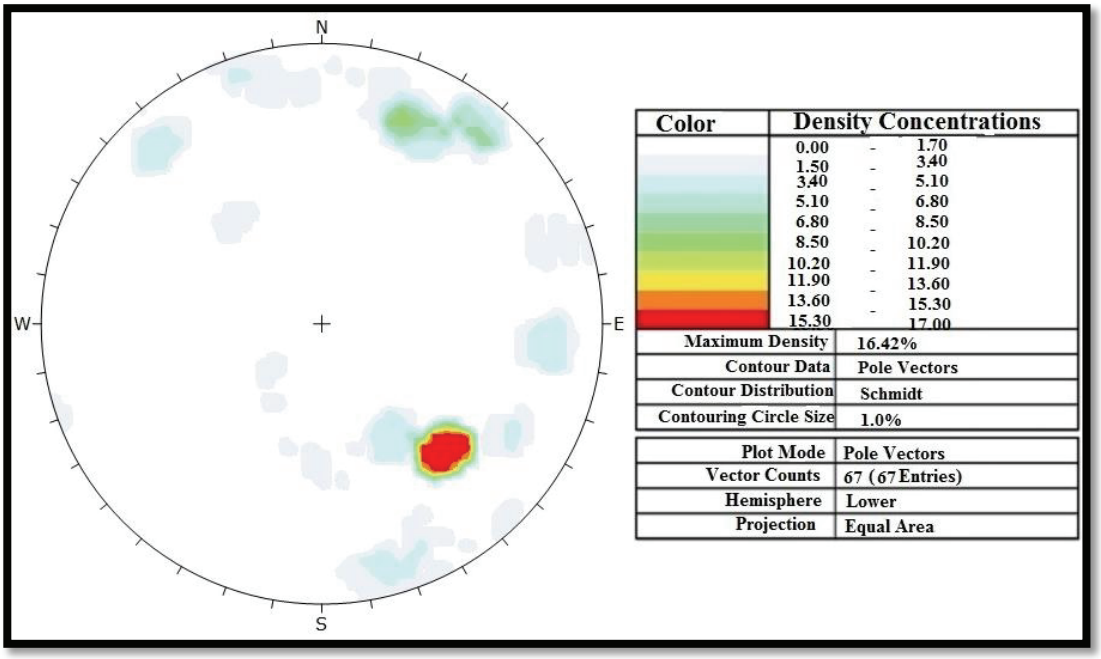

Figure 3.13 Contour diagram of the discontinuities at the 7th location.

At the eighth stop, the rock is pinkish grey and slightly weathered. The surface of the discontinuity is undulating rough. The dip amount and dip direction of the slope is 83°/054°. The contour diagram of the discontinuities is shown in Figure 3.14. The joints have spacing values between 15cm and 120cm. The persistence of the joints varies between 0.15m and 5m. The apertures are tight to 1cm, and filled with silty clay only at the surface. The properties of the flow layers are similar to those of the cooling joints but they do not infilling material.

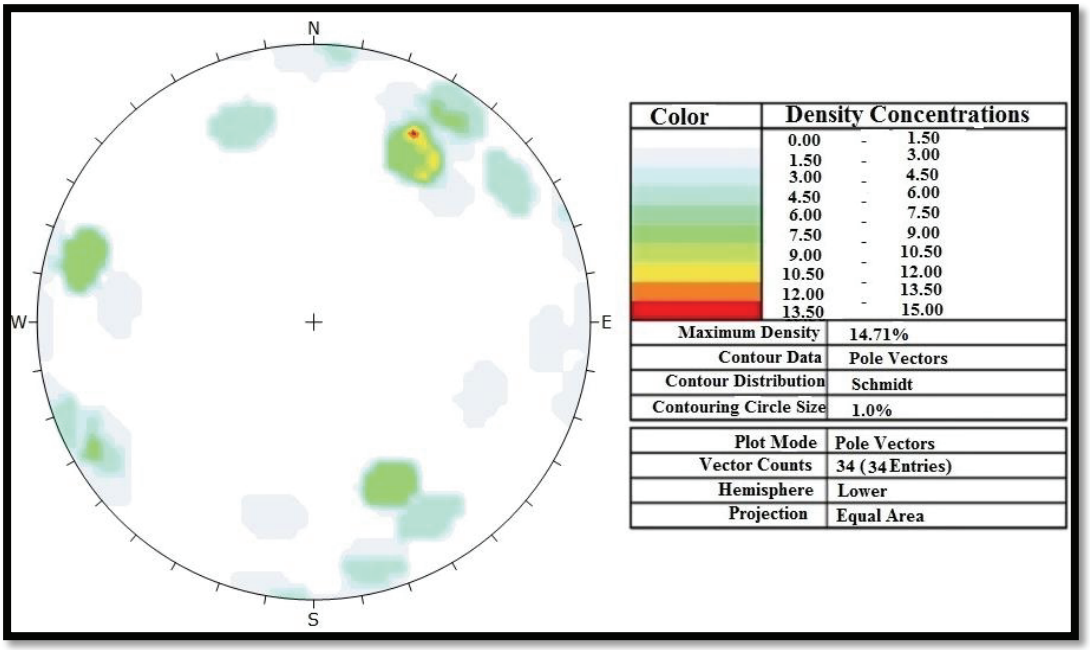

Figure 3.14 Contour diagram of the discontinuities at the 8th location.

The andesite at the 9th stop is pinkish grey. The rock shows slightly weathered state. The surface of the discontinuity is undulating rough. The dip amount and dip direction of the slope is 89°/110°. The contour diagram of the discontinuities is shown in Figure 3.15. The joints spacing varies between 0.1m and 1m. The persistence of the joints ranges from 0.4m to 9m. The apertures between them are tight to 2cm, and filled with silty clay only at the surface. The flow layers have properties similar to those of the cooling joints except that they do not infilling material. Figure 3.16 shows the cooling joints in the study area with high persistence value.

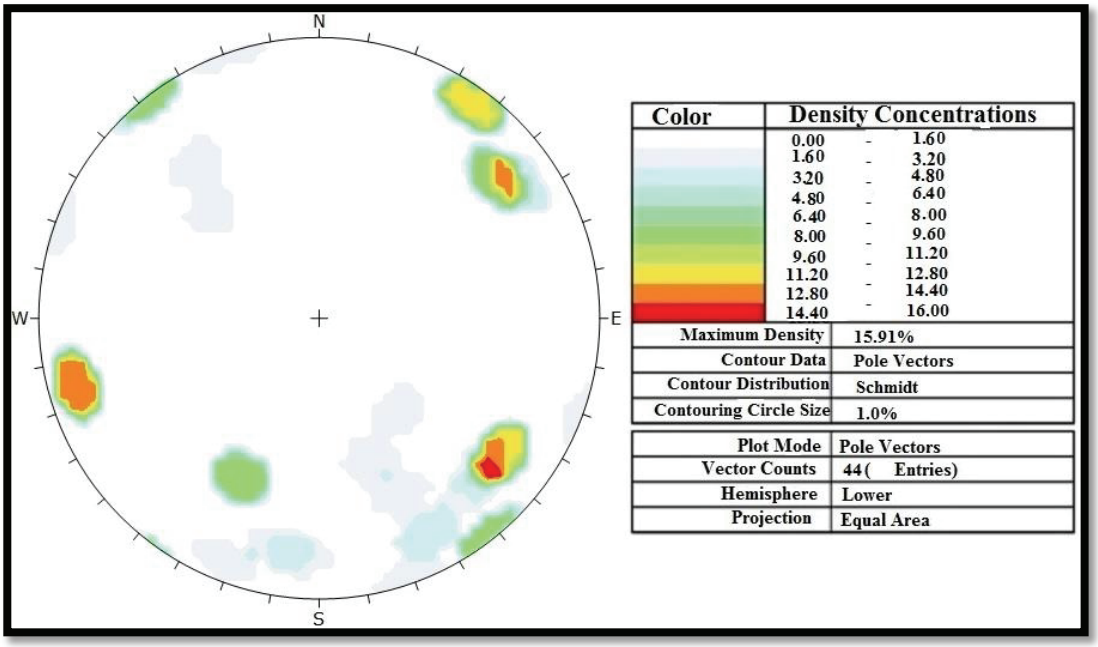

Figure 3.15 Contour diagram of the discontinuities at the 9th location.

Figure 3.16 Cooling joints of the andesite with high persistence.

At the tenth stop, the rock is pinkish grey and slightly to moderately weathered. The surface of the discontinuity is undulating rough. The dip amount and dip direction of the slope is 25°/199°. The contour diagram of the discontinuities is shown in Figure 3.17. The joints have spacing values between 2cm to 60cm. The persistence of the joints ranges from 0.05m to 2m. The joints have tight to 1cm apertures filled with silty clay only at the surface. The properties of the flow layers are similar to those of the cooling joints but they do not infilling material.

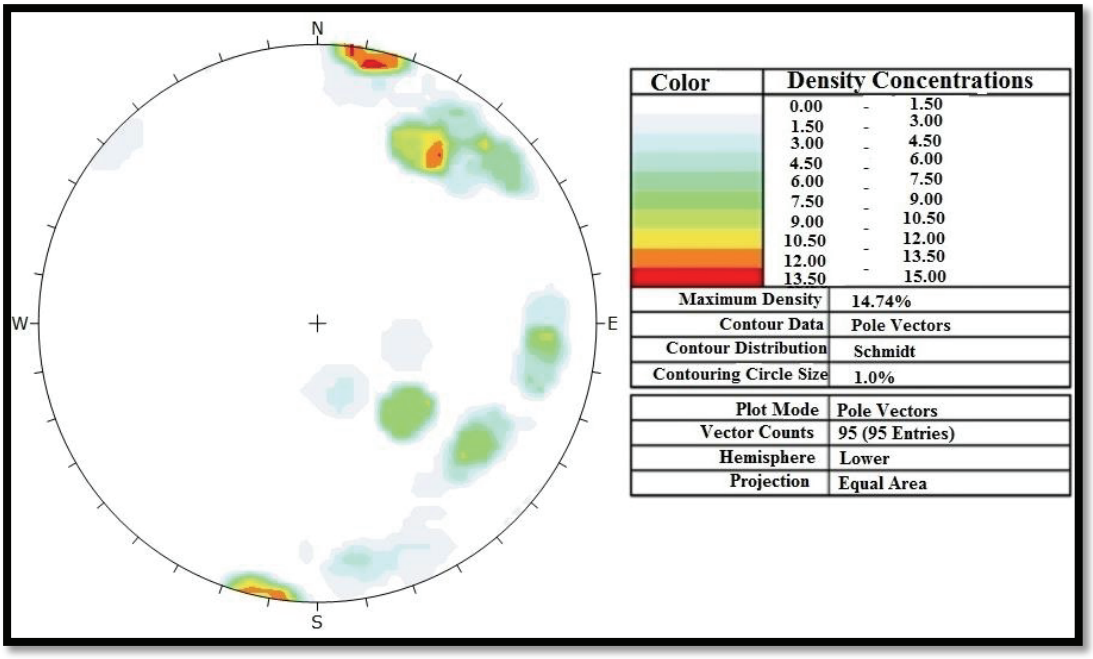

Figure 3.17 Contour diagram of the discontinuities at the 10th location.

The andesite at the eleventh stop is pinkish grey. The rock shows slightly weathered state. The surface of the discontinuity is undulating rough. The dip amount and dip direction of the slope is 85°/030°. The contour diagram of the discontinuities is shown in Figure 3.18. The spacing values of the joints vary between 4cm and 70cm. The persistence ranges from 10cm to 2m. The apertures between them are tight to 1cm, and filled with silty clay only at the surface. The flow layers have properties similar to those of the cooling joints except that they do not infilling material.

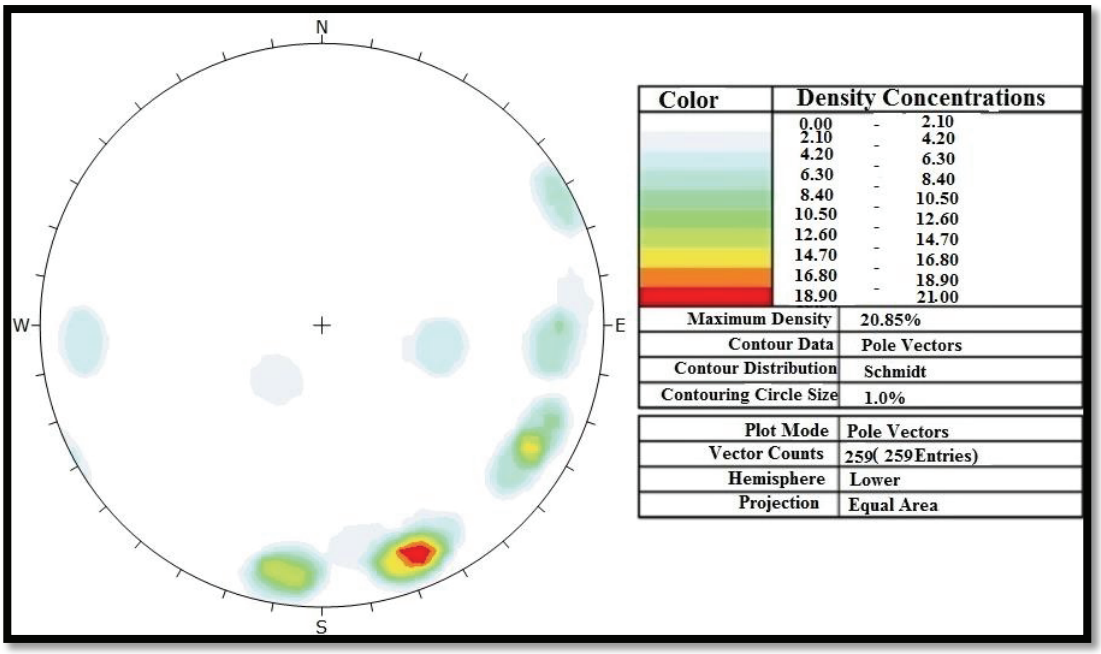

Figure 3.18 Contour diagram of the discontinuities at the 11th location.

At the 12th stop, the rock is pinkish grey and slightly weathered. The surface of the discontinuity is undulating rough. The main dip amounts and dip directions of the flow layers are 25º/200º, 26º/200º, 26º/200º and 25º/199º, and those of the slope is 49º/325º. The contour diagram of the discontinuities is shown in Figure 3.19. The joints have spacing values between 3cm to 86cm. The persistence of the joints ranges from 0.1cm to 1m. The apertures are tight to 2cm, and filled with silty clay only at the surface. The properties of the flow layers are similar to those of the cooling joints but they do not infilling material.

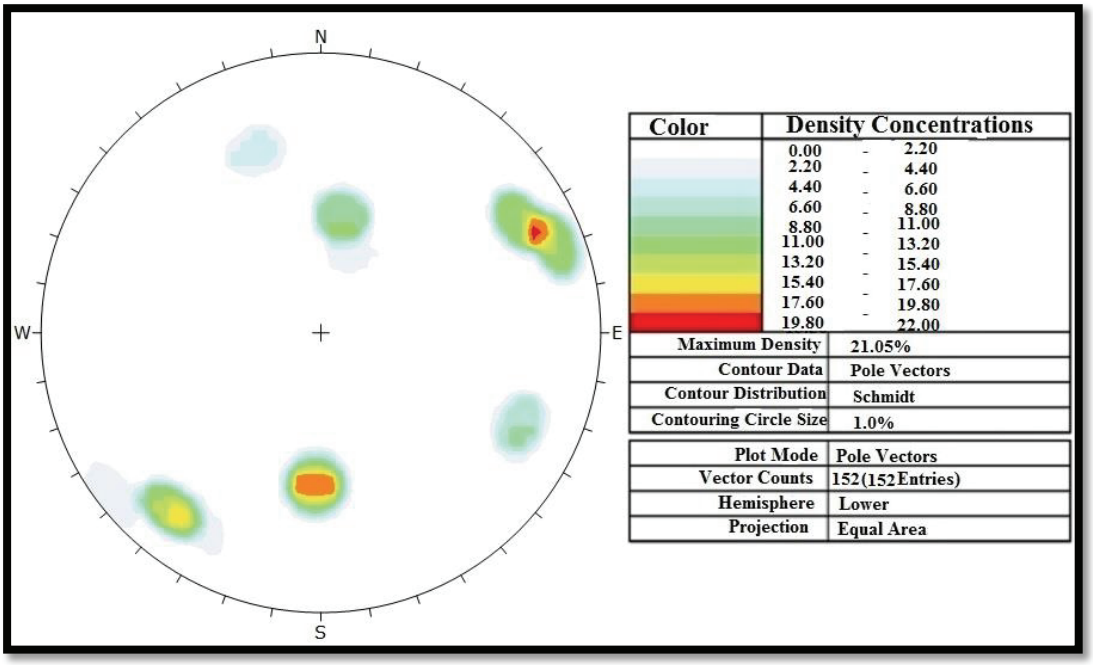

Figure 3.19 Contour diagram of the discontinuities at the 12th location.

The andesite at the 13th stop is pinkish grey. The rock shows slightly weathered state. The surface of the discontinuity is undulating rough. The dip amount and dip direction of the slope is 19º/190º. The contour diagram of the discontinuities is shown in Figure 3.20. The joints spacing varies between 3cm and 49cm. The persistence of the joints ranges from 4cm to 70cm. The apertures between them are tight to 2cm, and filled with silty clay only at the surface. The flow layers have properties similar to those of the cooling joints except that they do not infilling material.

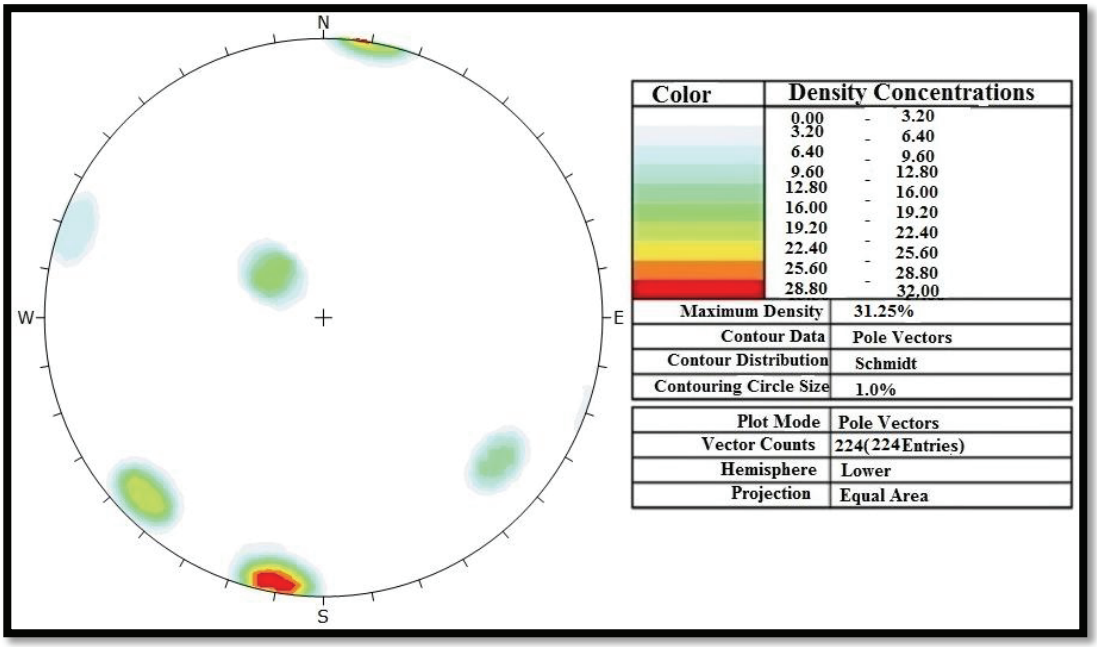

Figure 3.20 Contour diagram of the discontinuities at the 13th location.

At the 14th stop, the rock is pinkish grey and slightly weathered. The surface of the discontinuity is undulating rough. The dip amount and dip direction of the slope is 86º/340º. The contour diagram of the discontinuities is shown in Figure 3.21. The cooling joints have spacing values between 5cm and 70cm. The persistence of the joints ranges from 0.2m to 1m. The apertures are tight to 2cm, and filled with silty clay only at the surface. The properties of the flow layers are similar to those of the cooling joints but they do not infilling material. In Figure 3.22, the highly fractured andesite with detached blocks can be seen.

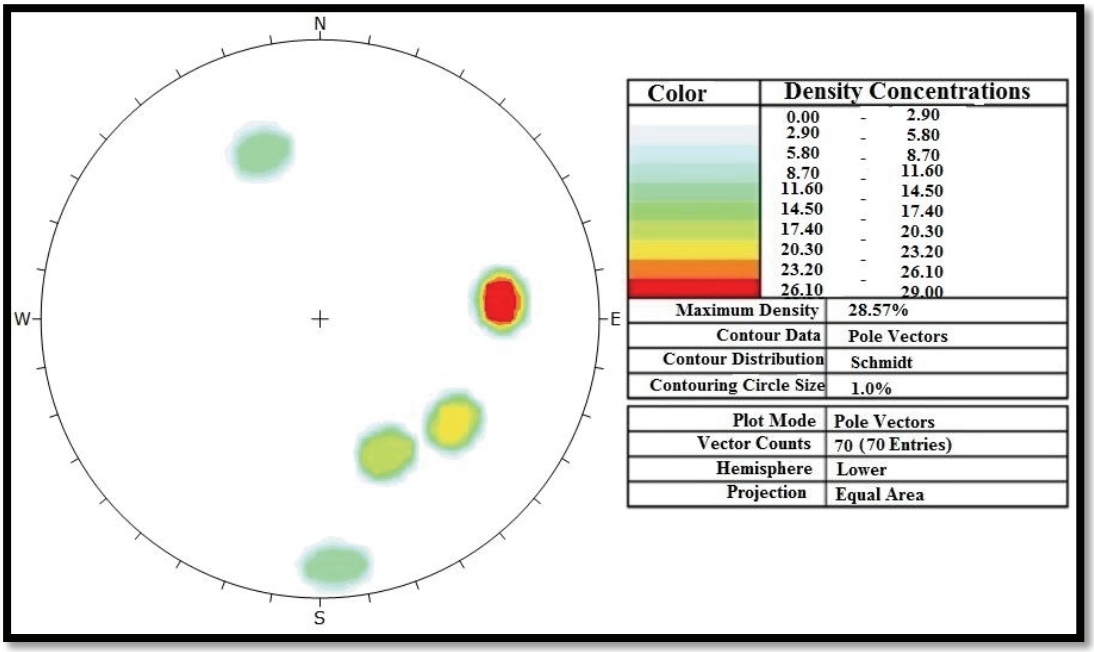

Figure 3.21 Contour diagram of the discontinuities at the 14th location.

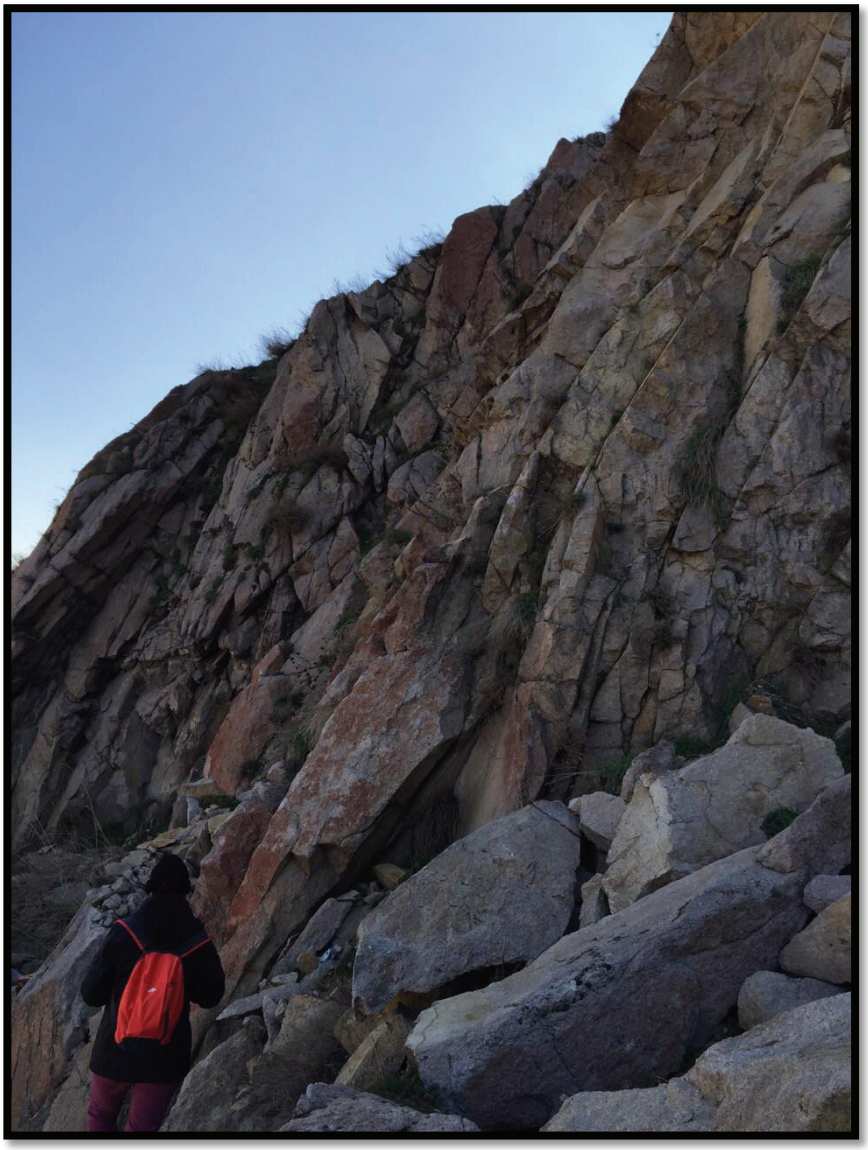

Figure 3.22 Outcrop of the highly fractured andesite with some blocks already detached and fallen down.

The andesite at the fifteenth stop is pinkish grey. The rock shows slightly weathered state. The surface of the discontinuity is undulating rough. The dip amounts and dip directions of the flow layer and the slope are 19º/190º and 84º/330º, respectively. The contour diagram of the discontinuities is shown in Figure 3.23. The joints spacing varies between 5cm and 49cm. The persistence of the joints ranges from 0.1m to 1m. The apertures between them are tight to 2cm, and filled with silty clay

only at the surface. The flow layers have properties similar to those of the cooling joints except that they do not infilling material.

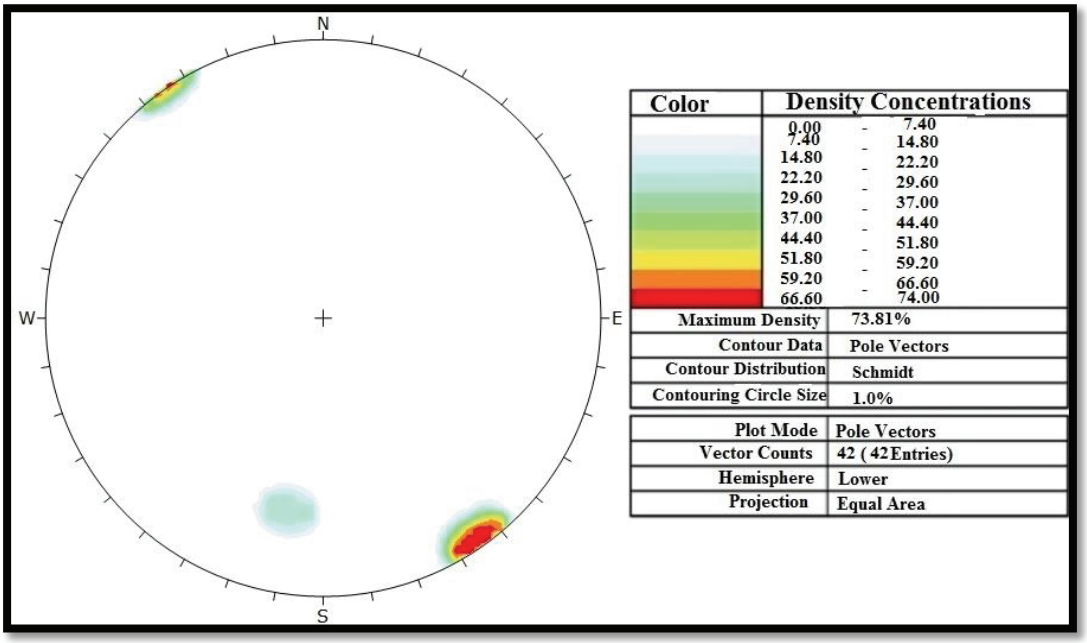

Figure 3.23 Contour diagram of the discontinuities at the 15th location.

At the 16th stop, the rock is pinkish grey and moderately weathered. The surface of the discontinuity is undulating rough. The dip amount and dip direction of slope is 88°/345°. The contour diagram of the discontinuities is shown in Figure 3.24. The joints have spacing values between 4cm and 60cm. The persistence of these joints ranges from 0.1m to 1m. The apertures are tight to 4cm, and filled with silty clay only at the surface. The properties of the flow layers are similar to those of the cooling joints but they do not infilling material.

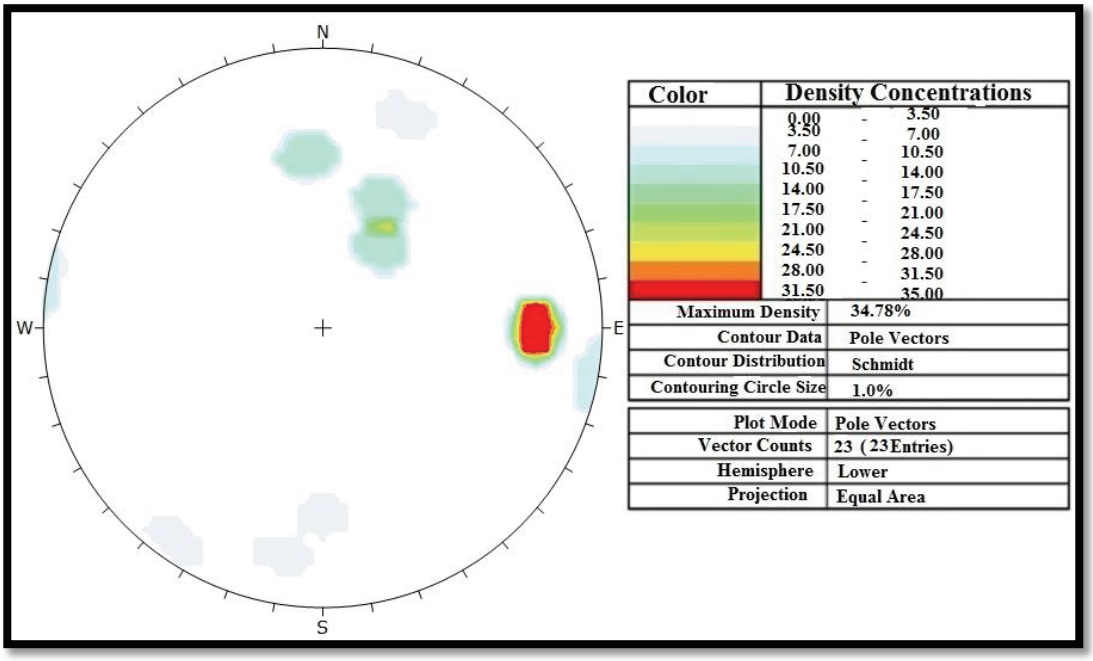

Figure 3.24 Contour diagram of the discontinuities at the 16th location.

The andesite at the seventeen stop is pinkish grey. The rock shows slightly weathered state. The surface of the discontinuity is undulating rough. The dip amount and dip direction of the slope is 70^{o}/030^{o}. The contour diagram of the discontinuities is shown in Figure 3.25. The spacing values of the cooling joints vary between 2cm and 65cm. The persistence varies between 0.07m and 1m. The apertures between them are tight to 1mm, and filled with silty clay only at the surface. The flow layers have properties similar to those of the cooling joints except that they do not infilling material.

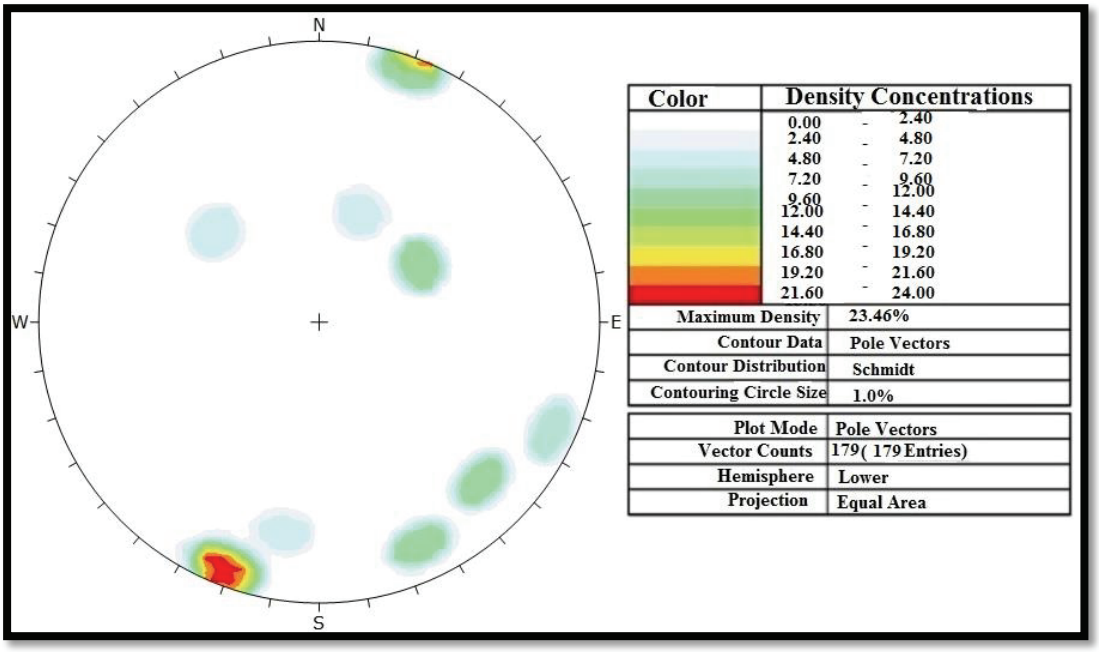

Figure 3.25 Contour diagram of the discontinuities at the 17th location.

At the 18th stop, the rock is pinkish grey and moderately weathered. The surface of the discontinuity is undulating rough. The dip amount and dip direction of the slope is 71°/029°. The contour diagram of the discontinuities is shown in Figure 3.26. The joints have spacing values between 2cm and 66cm. The persistence of the joints ranges from 0.07m to 1m. The apertures are tight to 1mm, and filled with silty clay only at the surface. The properties of the flow layers are similar to those of the cooling joints but they do not infilling material.

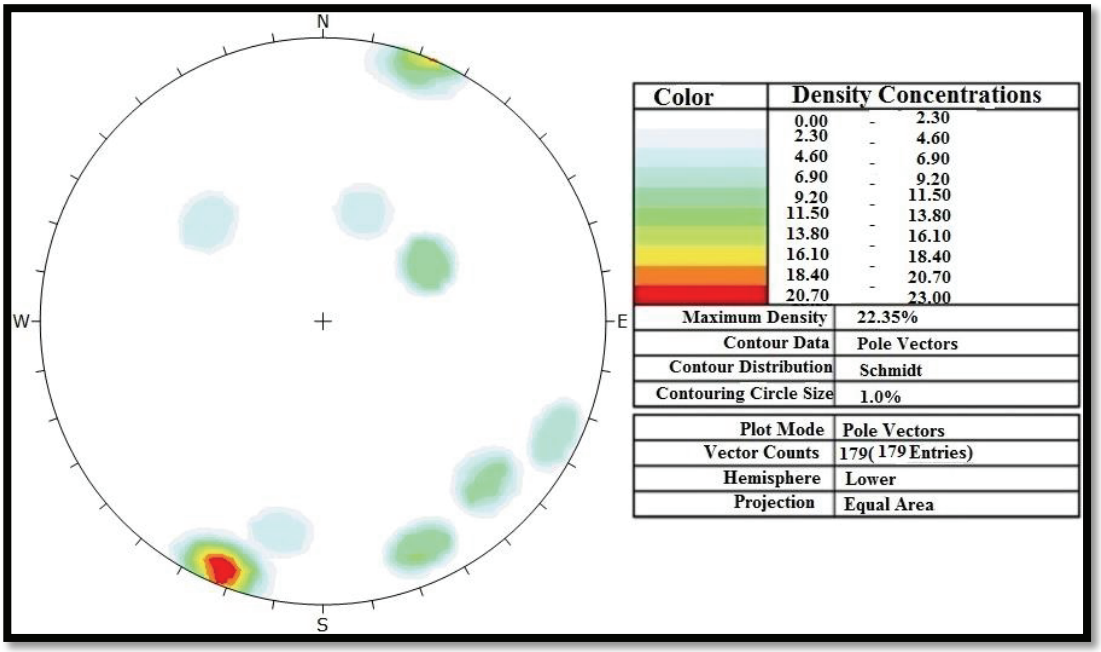

Figure 3.26 Contour diagram of the discontinuities at the 18th location.

The andesite at the nineteenth stop is pinkish grey. The rock shows slightly weathered state. The surface of the discontinuity is undulating rough. The dip amount and dip direction of the slope is 55^{o}/070^{o}. The contour diagram of the discontinuities is shown in Figure 3.27. The joints spacing values varies between 3cm and 60cm. The persistence of the joints varies between 0.13m and 3m. They have tight to 2mm apertures filled with silty clay only at the surface. The flow layers have properties similar to those of the cooling joints except that they do not infilling material.

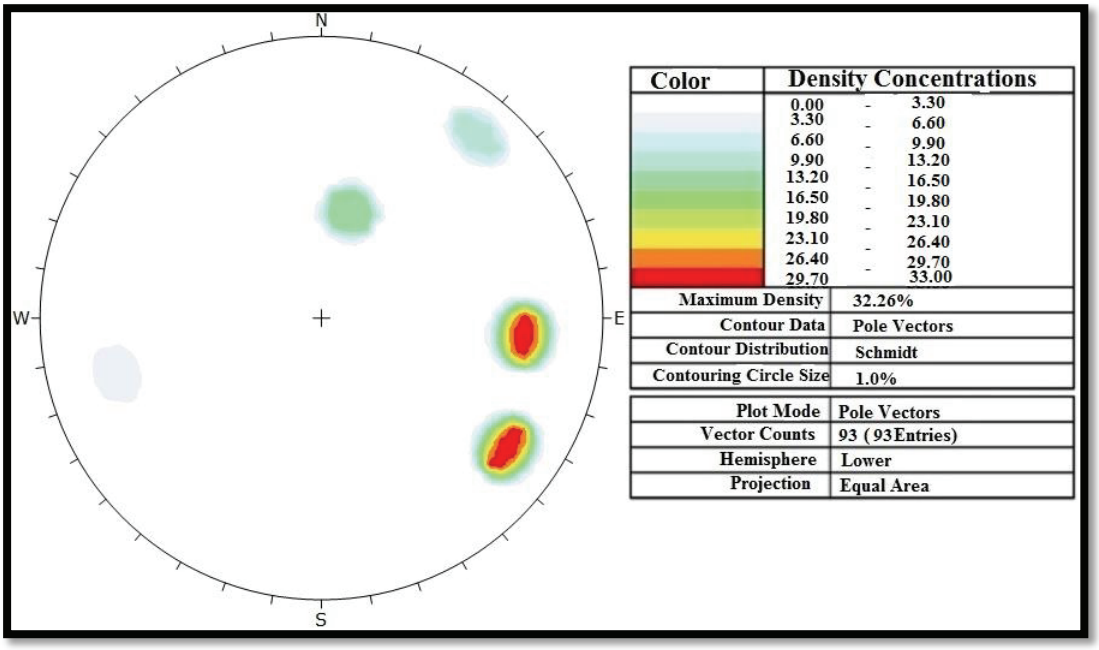

Figure 3.27 Contour diagram of the discontinuities at the 19th location.

At the 20th stop, the rock is pinkish-yellowish brown and slightly weathered. The surface of the discontinuity is undulating rough. The dip amount and dip direction of the slope is 74°/015°. The contour diagram of the discontinuities is shown in Figure 3.28. The cooling joints have spacing values between 11cm and 87cm. The persistence of these joints varies between 0.07m and 1m. The apertures are tight to 2cm, and filled with silty clay only at the surface. The properties of the flow layers are similar to those of the cooling joints but they do not infilling material.

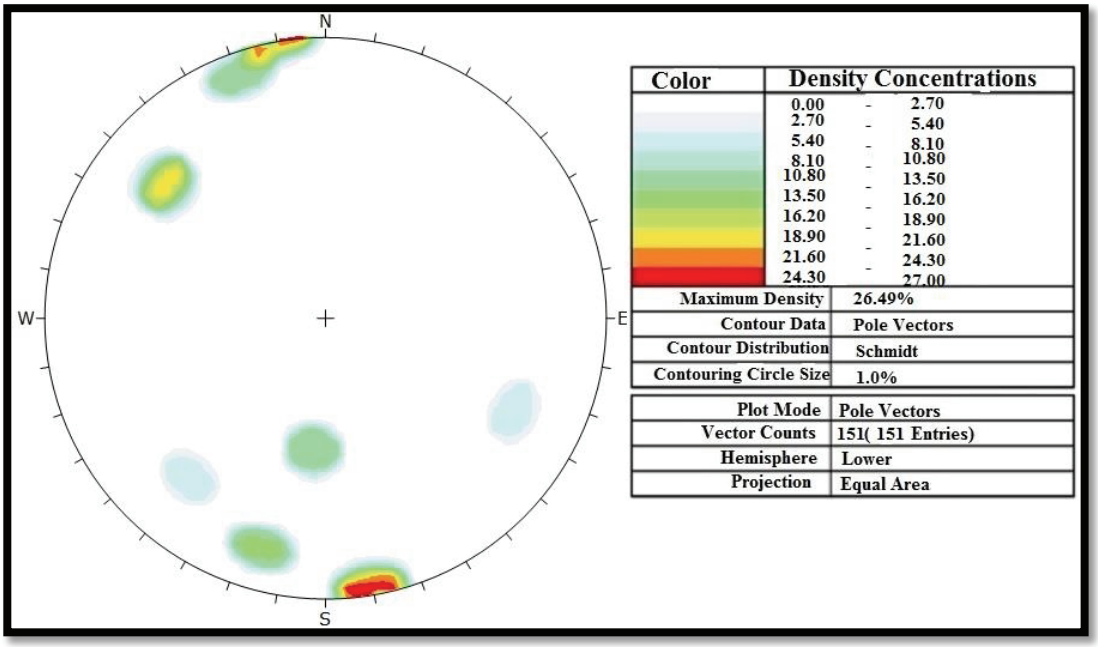

Figure 3.28 Contour diagram of the discontinuities at the 20th location.

The andesite at the last stop is pinkish. The rock shows slightly weathered state. The surface of the discontinuity is undulating rough. The dip amounts and dip directions of the flow layer and the slope are 37º/290º and 80º/015º, respectively. The contour diagram of the discontinuities is shown in Figure 3.29. The spacing values of the cooling joints vary between 2cm and 66cm. The persistence of the joints ranges from 0.3m to15m. The apertures between them are tight to 2cm, and filled with silty clay. The flow layers have properties similar to those of the cooling joints except that they do not infilling material. This stop is right outside of the wall of the main castle. Figure 3.30 shows the long cooling joints of the andesite surrounding the northern part of the main castle walls. The summary table of the discontinuity data taken at 21 stops is given in Appendix A.

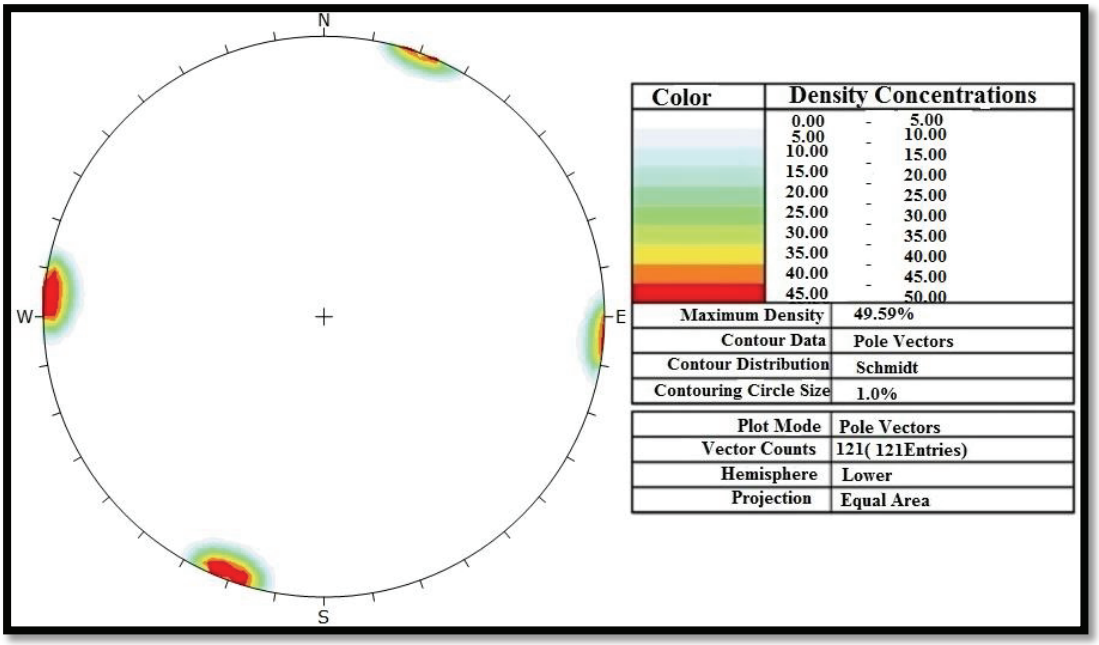

Figure 3.29 Contour diagram of the discontinuities at the 21th location.

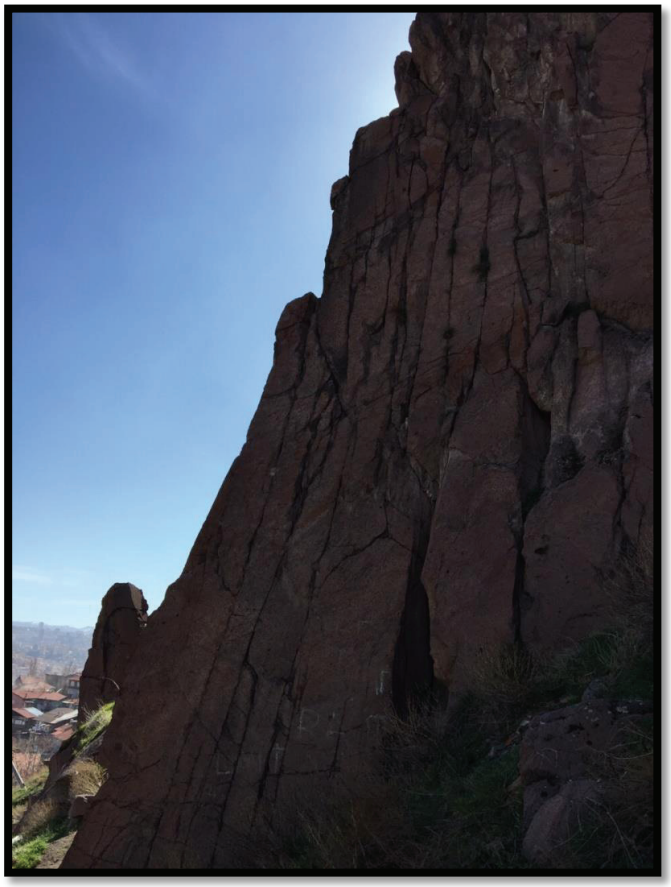

Figure 3.30 Outcrop of the andesite just around the main castle (northern part of the inner circle) on top of the hill.

Additionally, the potential rockfall sources were identified visually in the field to carry out the 2D and 3D analyses on the northern and eastern hill of the Castle. The map of the study area with identified potential rockfall sources in blue lines is presented in Figure 3.31 below. The size of the biggest fallen block seen in the study area is 160cm x 80 cm x 60 cm weighting nearly 1789.4kg.

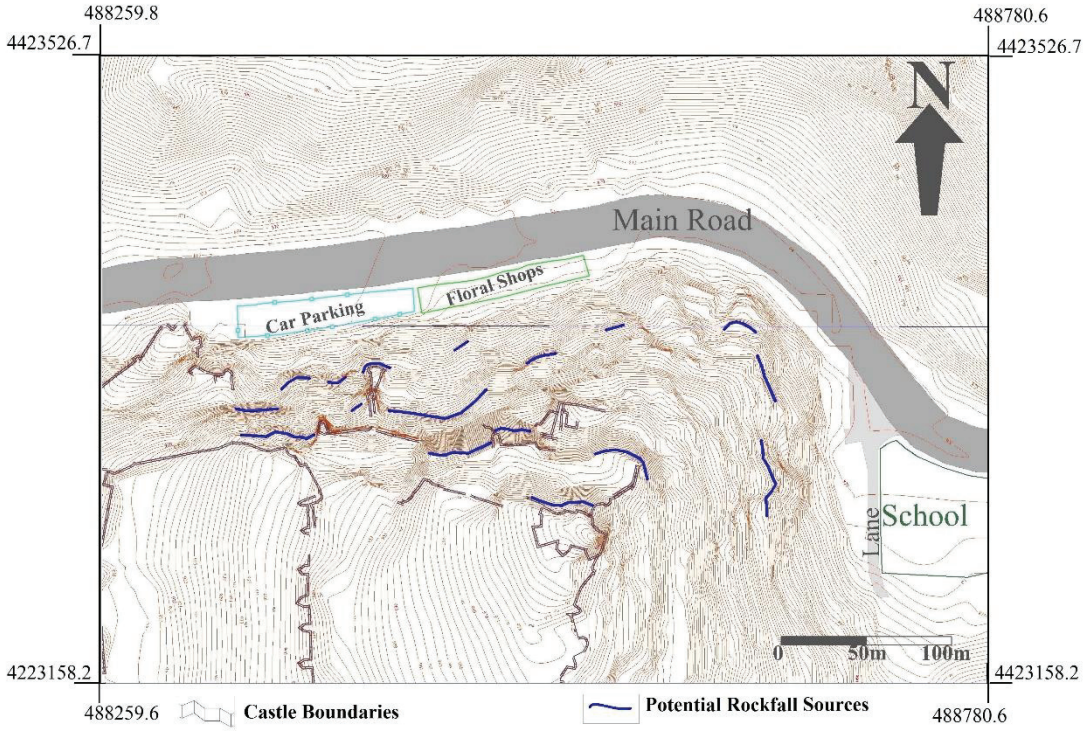

Figure 3.31 The study area showing the potential rockfall sources.

3.2 Laboratory Studies

During the field study, block samples (Figure 3.32) were taken from fallen blocks to identify the engineering properties of the andesite. On these samples, effective porosity, unit weight, water absorption, sonic velocity and uniaxial compressive strength tests were carried out, and direct shear test was performed along saw-cut surfaces of the andesite discontinuities. Except from the direct shear test, all the tests

were carried out in the Engineering Geology Laboratory in the Geological Engineering Department. The laboratory tests were done according to ISRM (1981).

Figure 3.32 Andesite samples used for the laboratory tests.

3.2.1 Effective Porosity and Unit Weights

The effective porosity and unit weight are the important index parameters of the rocks. The pores present in the structure of the material not only reduce the strength of the material but also increase its weathering. The presence of pores also affects the unit weight. The apparatus used in calculating effective porosity test is shown in Figure 3.33. The average effective porosity and unit weights (dry and saturated) values measured from the laboratory results are given in Table 3.1. According to the laboratory results, the porosity values of the andesite samples vary between 6 and 11%, and have an effective porosity of 8.2% on average. The porosity and density of the andesites are in the "medium" category according to Anon (1979).

Figure 3.33 The vacuum apparatus used to determine the effective porosity and unit weight of the andesite.

Table 3.1 The effective porosity and unit weight values of the andesite.

Samples No	Effective Porosity (%)	Unit Weight (kN/m^3)	Unit Weight (kN/m^3) (Saturated)	Engineering Classification (ANON, 1979)
K1	7.87	22.3	23.08	Medium
K2	8.76	22.05	22.91	Medium
K3	6.91	22.2	22.87	Medium
K4	7.02	22.04	22.73	Medium
K5	9.67	22.28	23.23	Medium
K6	8.26	22.05	22.86	Medium
K7	9.8	22.31	23.27	Medium
K8	6.79	22.09	22.76	Medium
K9	7.71	21.72	22.48	Medium
K10	10.28	21.39	22.39	Medium
K11	7.3	22.13	22.84	Medium
K12	7.43	22.08	22.81	Medium
K13	10.86	23.79	24.85	Medium
K14	9.85	22.24	23.2	Medium
K15	8.39	22.18	23.01	Medium
K16	6.88	22.17	22.84	Medium
K17	6.89	22.1	22.78	Medium
K18	6.96	22.55	23.23	Medium
Average	**8.2**	**22.2**	**23.01**	**Medium**
Standard Deviation	**1.31**	**0.45**	**0.51**	

3.2.2 Water Absorption under Atmospheric Pressure

In this experiment, the amount of water that the rocks absorb under atmospheric pressure is measured and expressed as percentage. Water absorption, which is one of the important parameters affecting the strength of rocks, has an important role in the behavior of the water-borne salts in the rock pores and during freeze-thaw events arising from temperature difference of daytime and night. The samples prepared for water absorption test is shown in Figure 3.34. The water absorption percentages by weight and volume are presented in Table 3.2.

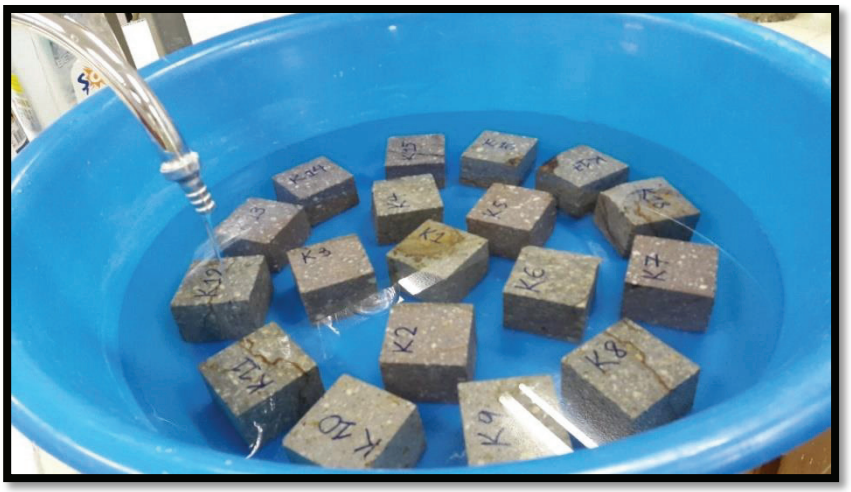

Figure 3.34 Water absorption test samples under atmospheric pressure.

Table 3.2 Water absorption values of the andesite by weight and volume.

Samples No	Water Absorption by Weight(%)	Water Absorption by Volume (%)
K1	3.21	7.29
K2	3.68	8.28
K3	2.82	6.37
K4	3.02	6.77
K5	4.12	9.34
K6	3.61	8.12
K7	4.15	9.43
K8	3.02	6.79
K9	3.51	7.78
K10	4.69	10.23
K11	3.17	7.13
K12	3.34	7.49
K13	4.21	9.55
K14	4.2	9.52
K15	3.45	7.8
K16	3.04	6.87
K17	2.96	6.66
K18	2.81	6.44
Average	**3.5**	**7.88**
Standard Deviation	**0.55**	**1.20**

3.2.3 Uniaxial Compressive Strength (UCS)

Uniaxial compressive strength (UCS) is one of the important parameters used when classifying strengths and characterizing solid rocks (ISRM, 1981). For this experiment, 6 x 6 x 6 cm cube samples were used (Figure 3.35). The results of uniaxial compressive strength obtained from dry and saturated samples are given in

Table 3.3. The andesites of the study area are "moderately strong" according to ISRM (1981).

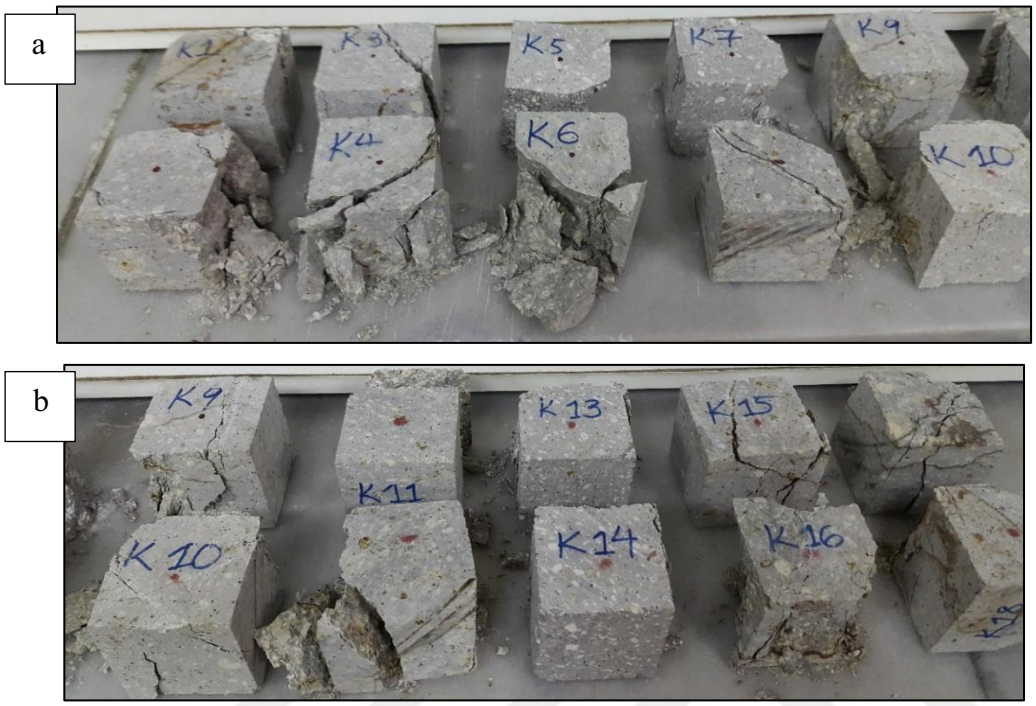

Figure 3.35 (a) Dry and (b) Saturated samples after UCS test.

Table 3.3 The results of dry and saturated UCS values of the andesite.

Samples No	UCS (Dry-MPa)	Strength Classification (ISRM, 1981)	Samples No	UCS (Saturated–MPa)	Strength Classification (ISRM, 1981)
K1	39.98	Moderate	K10	26.01	Moderate
K2	44.81	Moderate	K11	21.58	Moderate
K3	47.5	Moderate	K12	43.59	Moderate
K4	43.66	Moderate	K13	23.31	Moderate
K5	47.56	Moderate	K14	18.15	Moderate
K6	57.19	Moderate	K15	25.79	Moderate
K7	42.95	Moderate	K16	54.08	Moderate
K8	48.1	Moderate	K17	39.23	Moderate
K9	41.96	Moderate	K18	30.84	Moderate
Average	**45.97**			**31.4**	
Standard Deviation	**4.75**			**11.17**	

3.2.4 Sonic Velocity Test

The sonic velocity test can be used to assess the degree of fracturing of the rock. Moreover, it is also possible to obtain information about the degree of weathering by means of the sonic velocity experiment. The sonic test measures the velocity of the elastic waves (P-waves) sent into the rock. By this way, information on joint systems and porosity can be indirectly assessed. Cube-shaped andesite samples were tested both in saturated and dry conditions. The sonic velocity of the rock is calculated by the following equation.

$$V=LT$$

where; V = velocity, L = length that the wave passed through, and T = time that the wave took to pass through.

Sonic velocity tests were performed with the PUNDIT-PLUS model test device. The transit time of the transmitted wave was measured by placing the transducers on opposite sides of the cubic sample. Then, the sonic velocity was calculated by the above equation. The results are given in Table 3.4. The sonic velocity values obtained are 2154.99m/s for dry samples and 3367.60m/s for saturated samples.

The values obtained from both conditions (dry and saturated) indicate that there is no structural softening / deformation in the rocks when the samples are saturated. The velocity of the andesite is in low to very low and medium to low category (Anon, 1979). Very low velocity values, especially in dry conditions, are considered to be related to the presence of micro-fractures in the andesite samples.

Table 3.4 The values of sonic velocities measured on andesite samples for dry and saturated conditions.

Sample No	Dry Sonic Velocity (m/s)	Engineering Classification (ANON, 1979)	Sample No	Saturated Sonic Velocity (m/s)	Engineering Classification (ANON,1979)
K1	2565.96	Low	K10	3768.75	Medium
K2	1080.94	Very Low	K11	3666.67	Medium
K3	1563.64	Very Low	K12	3378.53	Low
K4	2321.71	Very Low	K13	2675.56	Low
K5	1838.41	Very Low	K14	3384.18	Low
K6	2010.07	Very Low	K15	3145.08	Low
K7	2693.69	Low	K16	3556.89	Medium
K8	2508.33	Low	K17	3365.17	Low
K9	2812.21	Low			
Average	**2154.99**			**3367.6**	
Standard Deviation	**544.49**			**319.18**	

3.2.5 Direct Shear Test Along Saw-Cut Samples

This test is used to measure the shear strength parameters of rock discontinuities quickly. In this experiment, at least three different samples with saw-cut surface are subjected to different normal loads and the shear strength of the specimens under normal stress is determined with deformation control. The selected normal loads are planned to represent the site conditions on which the samples are taken from. As a result of the experiment, basic shear strength parameters of rock material, which are c (cohesion) and ϕ (internal friction angle) values, are found. 6 square-shaped samples with widths of 6cm and heights of 1cm were prepared for this experiment. Direct shear test was performed in Laboratory of Akademi Geologic

Geotechnical Construction. The results of the experiment are given in Table 3.5. According to the direct shear test of the saw-cut andesite, the peak cohesion and internal friction angle are 32.81kPa and 28.2°, and residual cohesion and internal friction angle is 4.21kPa and 23°.

Table 3.5 Results of the direct shear test along saw-cut andesite.

	Peak Values			**Residual Values**		
	Sample 1	**Sample 2**	**Sample 3**	**Sample 1**	**Sample 2**	**Sample 3**
Width (cm)	6	6	6	*6*	*6*	*6*
Height (cm)	1	1	1	*1*	*1*	*1*
Vertical Load (kg)	2	4	8	*2*	*4*	*8*
Vertical Stress(kgf/cm^2)	0.556	1.111	2.222	*0.556*	*1.111*	*2.222*
Direct Shear (kgf/cm^2)	0.539	1.055	1.476	*0.273*	*0.516*	*0.982*
Vertical Stress (kN/m^2)	55.56	111.11	222.22	*55.56*	*111.11*	*222.22*
Direct Shear (kN/m^2)	53.87	105.49	147.57	*27.49*	*51.62*	*98.19*
Cohesion (c)	32.81 kPa			*4.21 kPa*		
Internal Friction Angle (ϕ_b)	28.2°			*23°*		

CHAPTER 4

SLOPE STABILITY ANALYSIS

Kinematic analysis, limit equilibrium analysis, and 2D and 3D rockfall analyses were carried out as parts of slope stability analysis in this thesis.

4.1 Kinematic Analyses

When there are many sets of discontinuities intersecting in oblique angles, kinematic studies may be helpful in anticipating the most likely pattern of slope failure. Kinematic analyses were carried out to determine whether or not planar, wedge and toppling failures are possible. Kinematic analyses were performed with Dips 6.0 software (Rocscience, 2015c). Dips is designed for the interactive analysis of orientation based geological data. It allows analyzing and visualizing structural data following the same techniques used in manual stereonets. Analyses were carried out at all 21 stops individually in the study area with discontinuity data measured during the scanline surveys in the field.

The internal friction angle was taken as 30^{o} by considering that the blocks have not moved yet. It was determined by Barton failure criterion (1976) using basic friction angle, joint roughness coefficient (JRC) and joint wall compressive strength (JCS). The basic friction angle was determined from the peak internal friction angle of from the direct shear test. JRC was measured in the field with hand profilometer. JCS was determined from the Schmidt rebound hammer results by using the table of estimate of joint wall compressive strength from Schmidt hardness proposed by Deere and Miller (1966).

For each stop, its slope angle was used to determine if the potential failures can occur or not. The kinematic analyses for the 10th stop are shown in Figures 4.1, 4.2 and 4.3 for planar, wedge and toppling failure, respectively. From the results of the analyses, all planar, wedge and toppling failures are possible at the 10th stop.

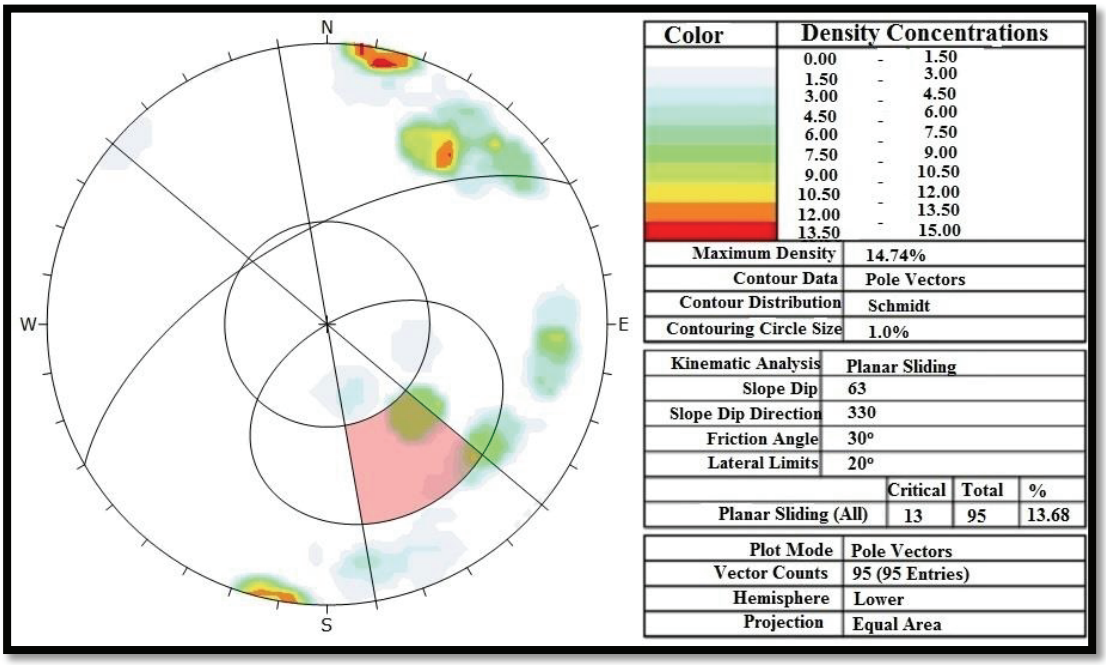

Figure 4.1 Kinematic analysis for planar failure of the 10th stop.

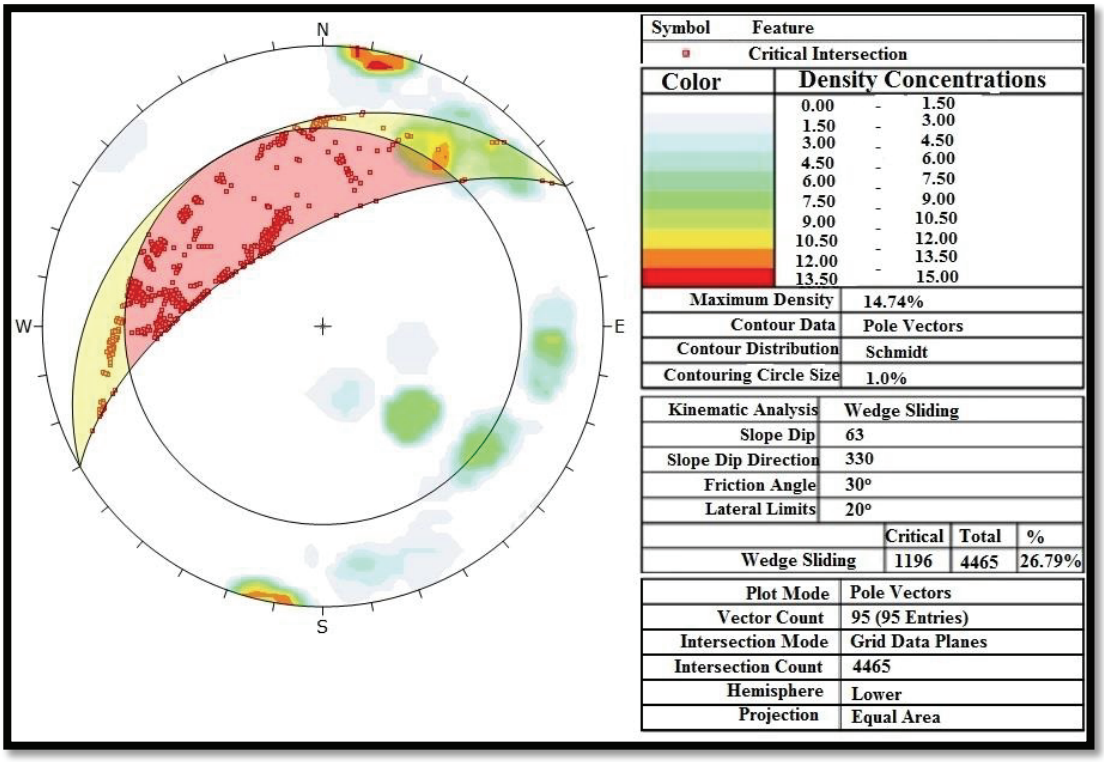

Figure 4.2 Kinematic analysis for wedge failure of the 10th stop.

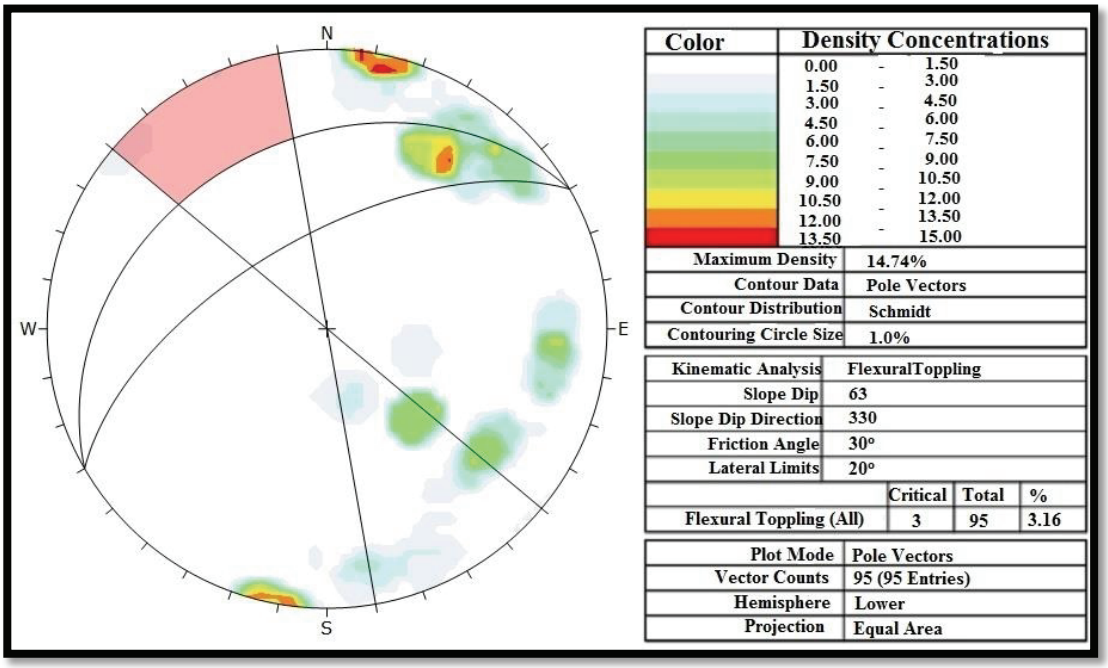

Figure 4.3 Kinematic failure for toppling failure of the 10th stop.

The results of the kinematic analyses for all the stops are shown in Table 4.1. According to the analyses of the data taken from the field, the wedge failure is expected to happen at all the stops of the study area. The planar failure is likely to happen to all the stops except 5th, 12th, 13th, 14th, 19th and 21th stops. The toppling failure is probable to occur in most stops, excluding 12th,13th,19th and 20th stops.

Table 4.1 Kinematic failure results for all the stops in the study area.

	Kinematic Failure Types		
STOPS	Planar	Wedge	Toppling
1	+	+	+
2	+	+	+
3	+	+	+
4	+	+	+
5	-	+	+
6	+	+	+
7	+	+	+
8	+	+	+
9	+	+	+
10	+	+	+
11	+	+	+
12	-	+	-
13	-	+	-
14	-	+	+
15	+	+	+
16	+	+	+
17	+	+	+
18	+	+	+
19	-	+	-
20	+	+	-
21	-	+	+

4.2 Limit Equilibrium Analyses

By taking possible failure modes determined in the kinematic analyses into consideration, limit equilibrium analyses were conducted to investigate the stability of the slopes. This method of analysis enables the calculation of the safety factor

which is unitless indicator of the stability. RocPlane 3.0 (Rocscience, 2015c), Swedge 6.0 (Rocscience, 2015c) and RocTopple 1.0 (Rocscience, 2015c) were used to calculate the safety factors of planar, wedge and toppling failure, respectively. RocPlane is a tool for performing planar rock slope stability analysis and design. Swedge is an analysis tool for evaluating the geometry and stability of surface wedges in rock slopes. RocTopple is an interactive software tool for performing toppling analysis and support design of rock slopes. The popular block toppling method of Goodman and Bray, 1976 is the base of this analysis. The analyses were carried out under two conditions as static and dynamic.

The parameters used for limit equilibrium analyses are given in Table 4.2. The unit weight was determined by the laboratory test. Barton-Bandis shear strength model was chosen in the input data. ϕ was taken from the peak internal friction angle of the direct shear test. JRC and JCS were determined from the field studies. The heights of the slopes were observed generally about 10m in the field and the upper face angle was taken as 2^o to represent the almost horizontal upper surface of the very steep slopes.

Table 4.2 Parameters used in the limit equilibrium analyses.

Unit weight	22.88kN/m^3
ϕ	28.2^o
JRC	13 (3.28*)
JCS	3.55MPa
Height	10m
Upper face angle	2^o

*Size corrected value of JRC.

Typical outputs of limit equilibrium analysis for planar, wedge and toppling failures are shown in Figures 4.4, 4.5 and 4.6, respectively.

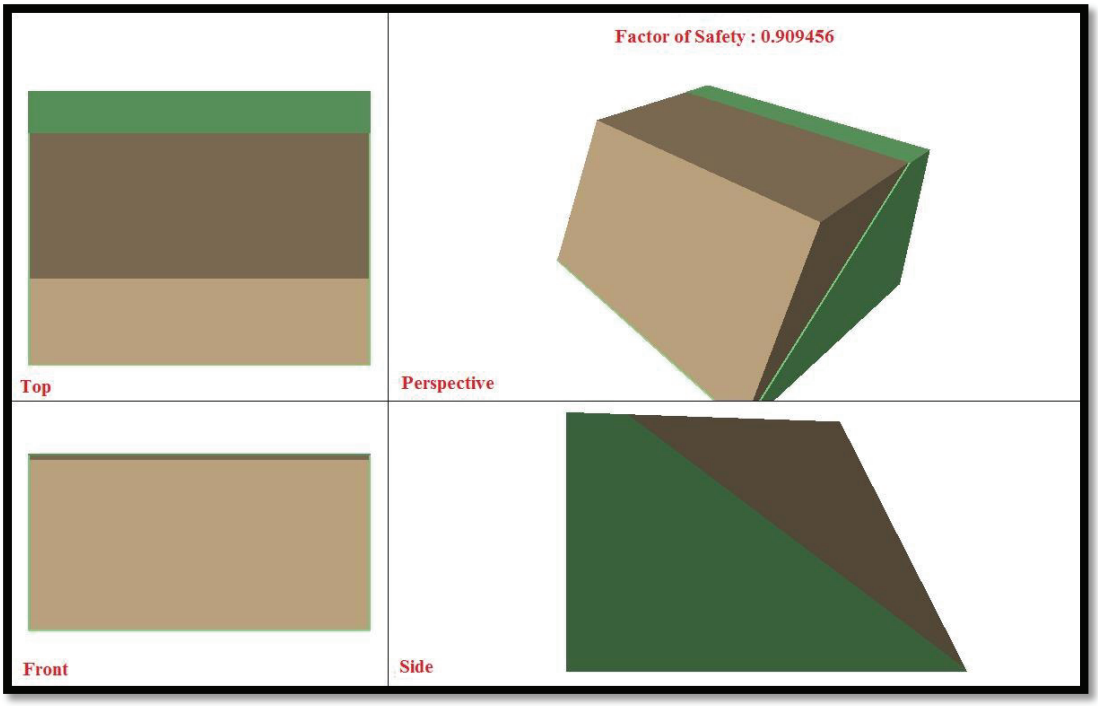

Figure 4.4 The result of the limit equilibrium analysis of planar failure for the 10th stop.

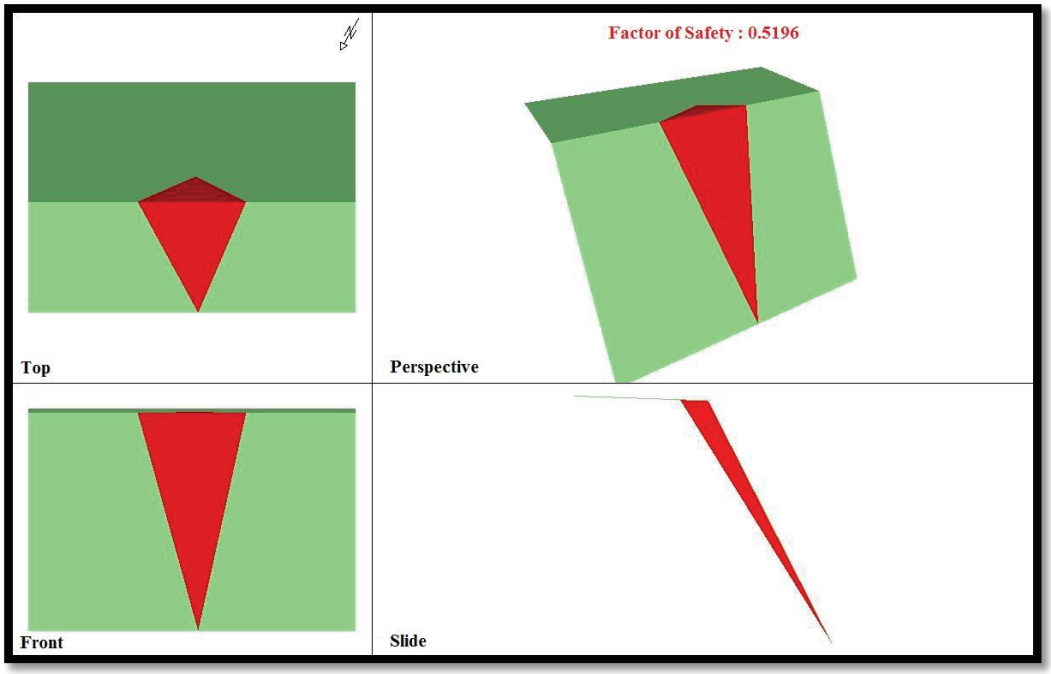

Figure 4.5 The result of the limit equilibrium analysis of wedge failure of the 10th stop.

For the toppling analyses, the spacing value of each stop was used from its range individually, and the angle of the base slope was determined by considering the persistence of the joints in each slope separately.

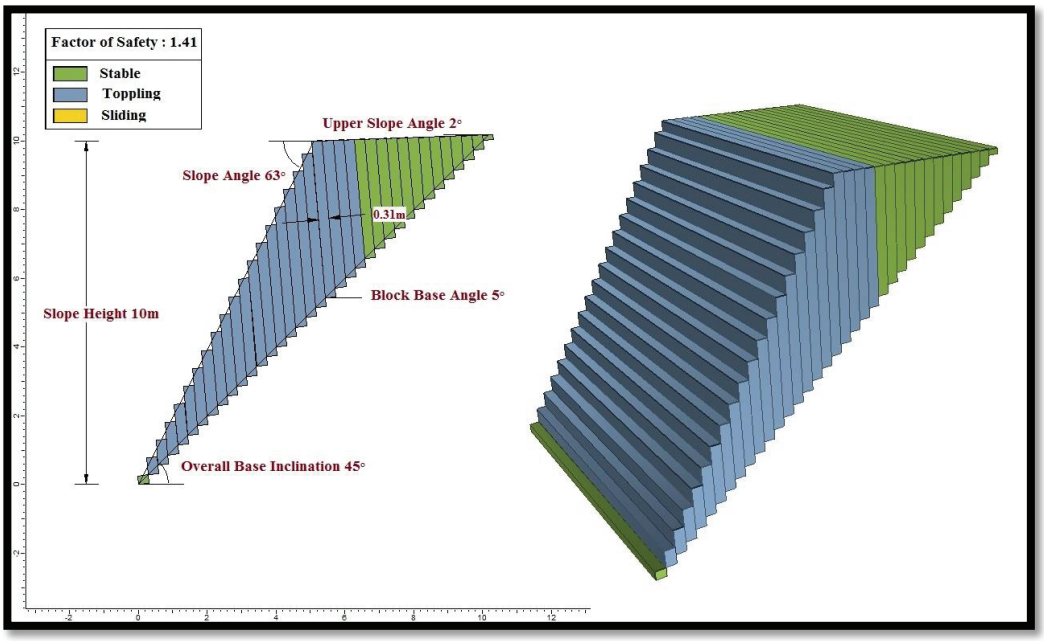

Figure 4.6 The result of limit equilibrium analysis of toppling failure of the 10th stop.

Safety factors of the slopes calculated from limit equilibrium analysis of planar, wedge and toppling failures for static conditions are given in Table 4.3. Almost all of the safety factors except wedge failure of 3rd and 7th stop, and toppling failure of 10th stop, are very low.

Table 4.3 Safety factor values resulted from limit equilibrium analyses for static conditions.

	Safety factors for static conditions		
STOPS	Planar	Wedge	Toppling
1	0.893	0.293	0.467
2	0.209	0.228	0.668
3	0.659	1.132	0.760
4	0.438	0.658	0.844
	0.248	0.866	0.617
5	-	0.886	0.364
6	0.312	0.956	0.526
7	0.201	1.169	0.634
8	0.147	0.407	0.436
9	0.088	0.402	0.490
10	0.909	0.520	1.410
11	0.181	0.451	0.391
12	-	0.996	-
13	-	0.445	-
14	-	0.354	0.536
15	0.133	0.475	0.493
16	0.469	0.154	0.538
17	0.360	0.880	0.483
18	0.370	0.471	0.459
19	-	0.842	-
20	0.300	0.864	-
21	-	0.407	0.362

For dynamic conditions, by considering the seismic intensity of Ankara region (Teoman et al., 2004), horizontal seismic ground acceleration was taken as 0.05g. This seismic acceleration value was calculated by taking the North Anatolian Fault as reference because it is the biggest seismic source around the area. Other faults

may also affect the study area. However, the biggest impact would be the ones generated from the North Anatolian Fault. Safety factor values decrease slightly for dynamic conditions because the seismic accelerations affect the stability of the rock negatively. Safety factors of the slopes calculated from limit equilibrium analyses of planar, wedge and toppling failures for the dynamic conditions, are tabulated in Table 4.4.

Table 4.4 Safety factor values resulted from limit equilibrium analyses for dynamic conditions.

	Safety factors for dynamic conditions		
STOPS	Planar	Wedge	Toppling
1	0.808	0.252	0.458
2	0.170	0.186	0.662
3	0.598	1.025	0.736
4	0.391	0.594	0.732
	0.206	0.778	0.588
5	-	0.803	0.342
6	0.270	0.861	0.494
7	0.161	1.061	0.359
8	0.106	0.360	0.435
9	0.047	0.355	0.486
10	0.822	0.465	0.491
11	0.142	0.396	0.390
12	-	0.902	-
13	-	0.388	-
14	-	0.306	0.536
15	0.092	0.424	0.190
16	0.422	0.109	0.345
17	0.316	0.779	0.440
18	0.326	0.410	0.439
19	-	0.772	-
20	0.258	0.783	-
21	-	0.360	0.347

Based on the results of limit equilibrium analyses, many failures are expected to occur in both static and dynamic conditions. Moreover, by taking current topography into account, after the discontinuity-controlled failure, it is thought that the blocks will go into "rockfall" mode.

4.3 Rockfall Analyses

Within the scope of the study, rockfall analyses were performed using the potential rockfall sources determined in the field. 2D and 3D rockfall analyses were carried out separately with different softwares. Then, their results are compared in Chapter 5.

4.3.1 2D Rockfall analyses

2D analyses were carried out with RocFall 5.013 (Rocscience, 2015c). RocFall is a robust, easy-to-use program that can be used to simulate almost all rockfall events. RocFall utilizes a particle analysis to assess the movement of the rock (Stevens, 1998). RocFall 5.013 (Rocscience, 2015c) has an additional engine, rigid body formulation, compared to the older versions. It integrates the shape of the rocks into impact calculations. In this study, rigid body approach was preferred.

A total of 20 profiles where steep slopes exist were selected to cover the study area entirely. The analyses were carried out along those 20 profiles (Figure 4.7). As it can be seen in Figure 4.7, some of the profiles have more than one potential rockfall source. The analyses were performed for each profile from every single potential rockfall source affecting the profile.

The parameters used in 2D analyses are tabulated in Table 4.5. The normal and tangential coefficients of restitution of the rock are taken as 0.46 and 0.71, respectively for the 2D analyses. These values were taken from Topal et al. (2007) due to the similarities of the andesites exposed in Afyon Castle and those in this study area. Back analysis to determine Rn and Rt were not carried out in the field because the falling rocks may hit the road, cars or floral shops, since they were just

right next to the bottom of the hill. The dynamic friction coefficient of 0.58 was calculated as tangent of the international friction angle, tan (ϕ) (Rocscience, 2015).

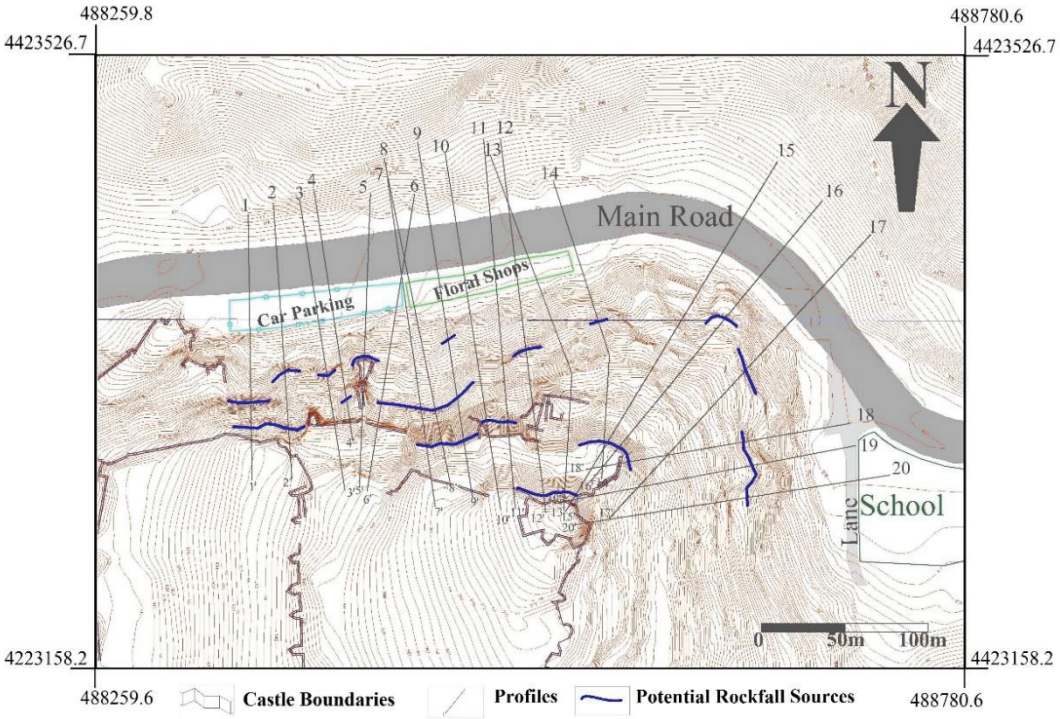

Figure 4.7 20 profiles used for 2D rockfall analyses. Rockfall source areas are shown by blue color.

Table 4.5 Parameters used for 2D rockfall analyses.

Parameters	**Value**
Normal coefficient of restitution	0.46±0.05
Tangential coefficient of restitution	0.71±0.05
Dynamic friction coefficient	0.58±0.04
Rolling resistance	1.31±0.02
Initial velocity (m/s)	1
Number of throws	1000 rocks
Minimum velocity cut-off (m/s)	0.1
Shape of the rocks thrown	Hexagonal

To be able to obtain the value of rolling resistance, back analysis was carried out in RocFall 5.013 (Rocscience, 2015c) by using the largest fallen block in the study area. The block location is known from the field study, and the rockfall source area was also determined in the field. Therefore, the rocks were thrown on 3-3' profile with different rolling resistance values from the range of the values provided by Rocscience (2015). The result of 1.31, where the rocks fell closest to the fallen block spot was taken. The analyses' results are shown in Figure 4.8.

A series of different weights of rocks such as 250kg, 500kg, 750kg and 1800kg were thrown, and their results were examined. The weights of the blocks were calculated from dimensions of the fallen block seen in the study area. As the results of 2D analysis, rock's end point locations, bounce heights and total kinetic energy values were obtained from every profile and every potential rockfall source. Typical graphs of end point, bounce height and total kinetic energy values yielded by the software are shown in Figure 4.9. The rockfall mode of the 2D analysis is bouncing.

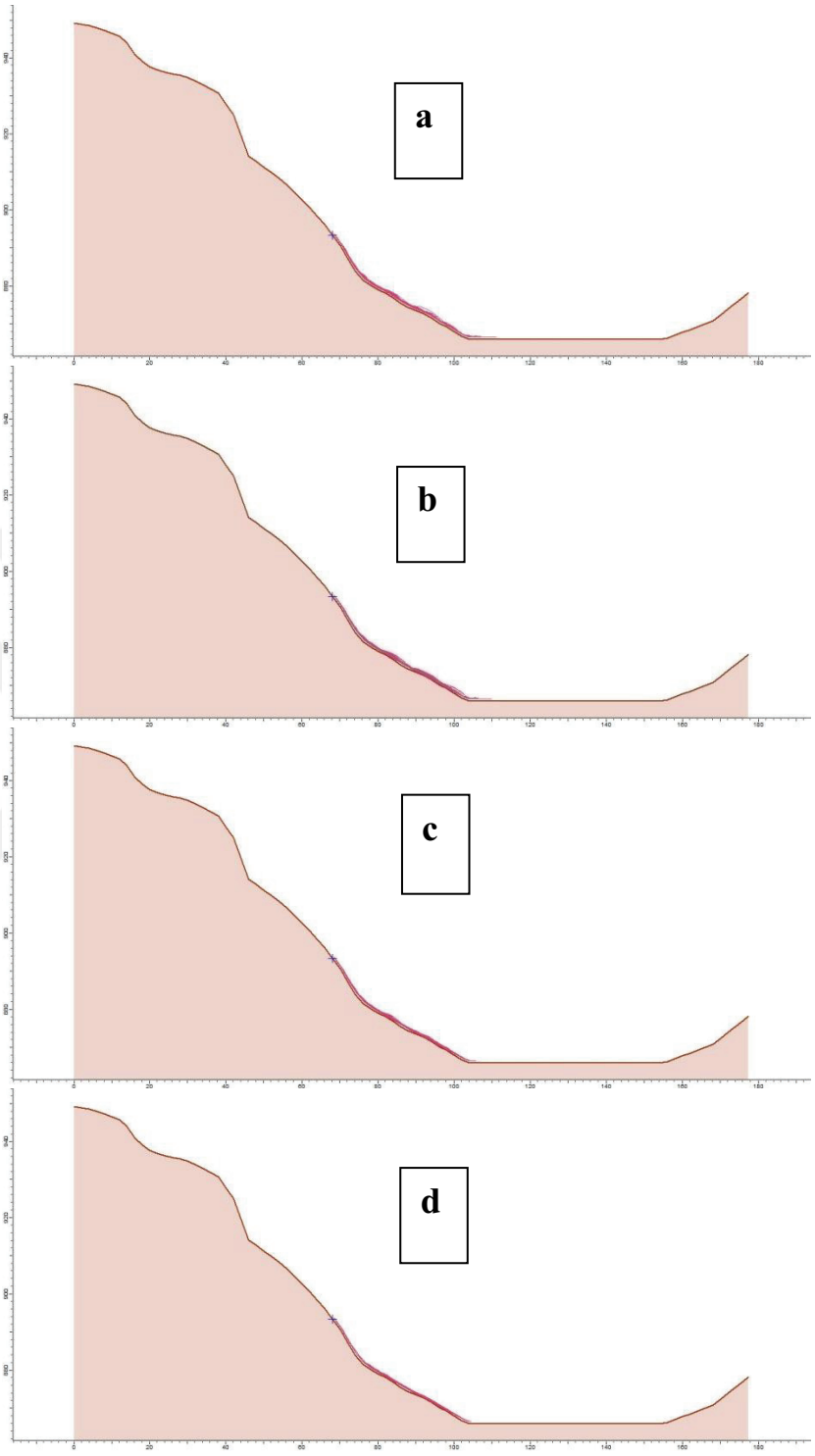

Figure 4.8 The result of the back analysis using different rolling resistance values of 0.4 (a), 0.65 (c), 0.9(c) and 1.31 (d).

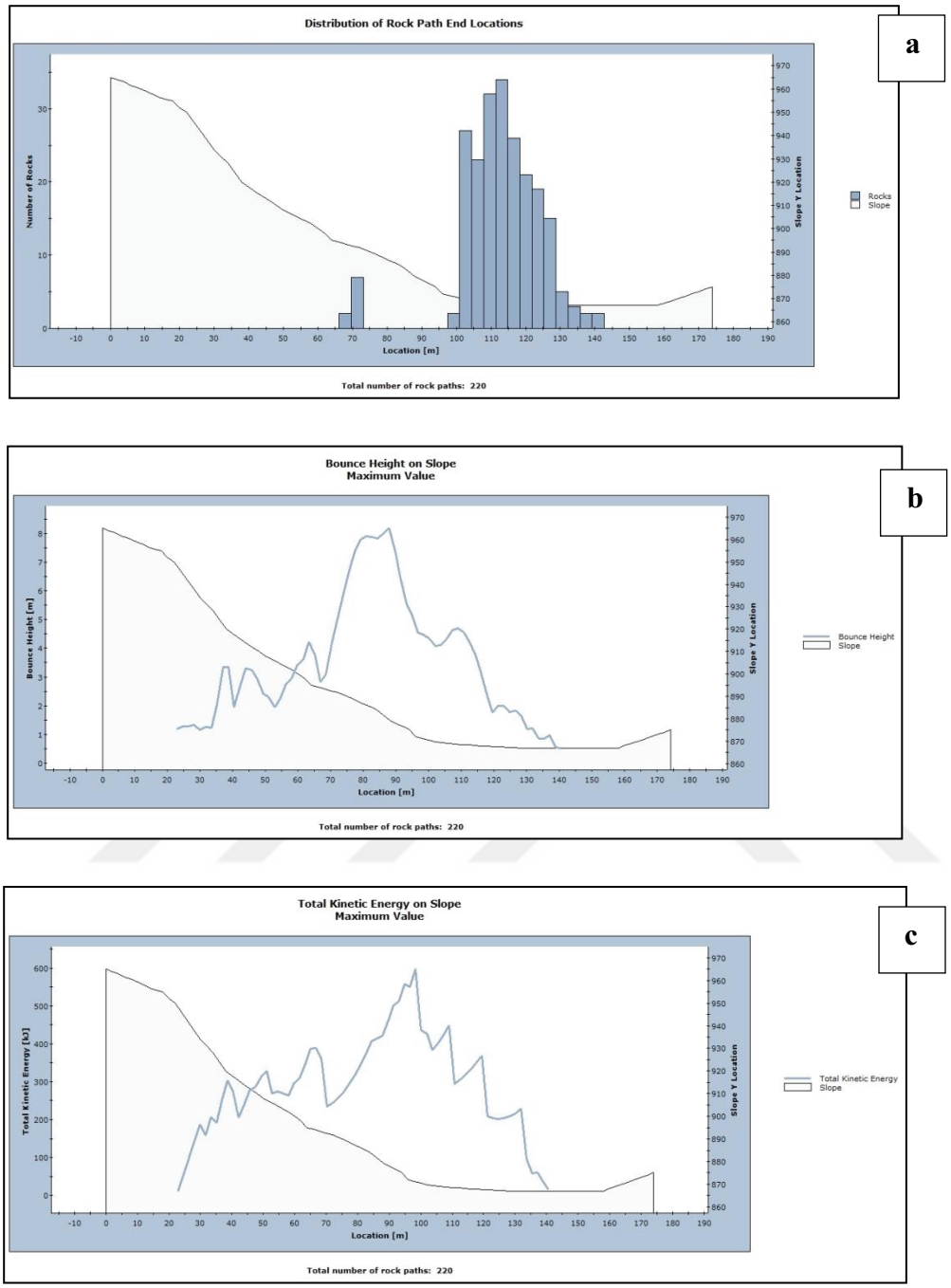

Figure 4.9 Typical graphics of 2D analyses results; (a) End point location, (b) Bounce height, and (c) Total kinetic energy.

By using the furthest end points of each profile for each weight of the rocks, danger zones are drawn individually on the topographic map. The danger zones of each weight are shown in Figures 4.10 - 4.13.

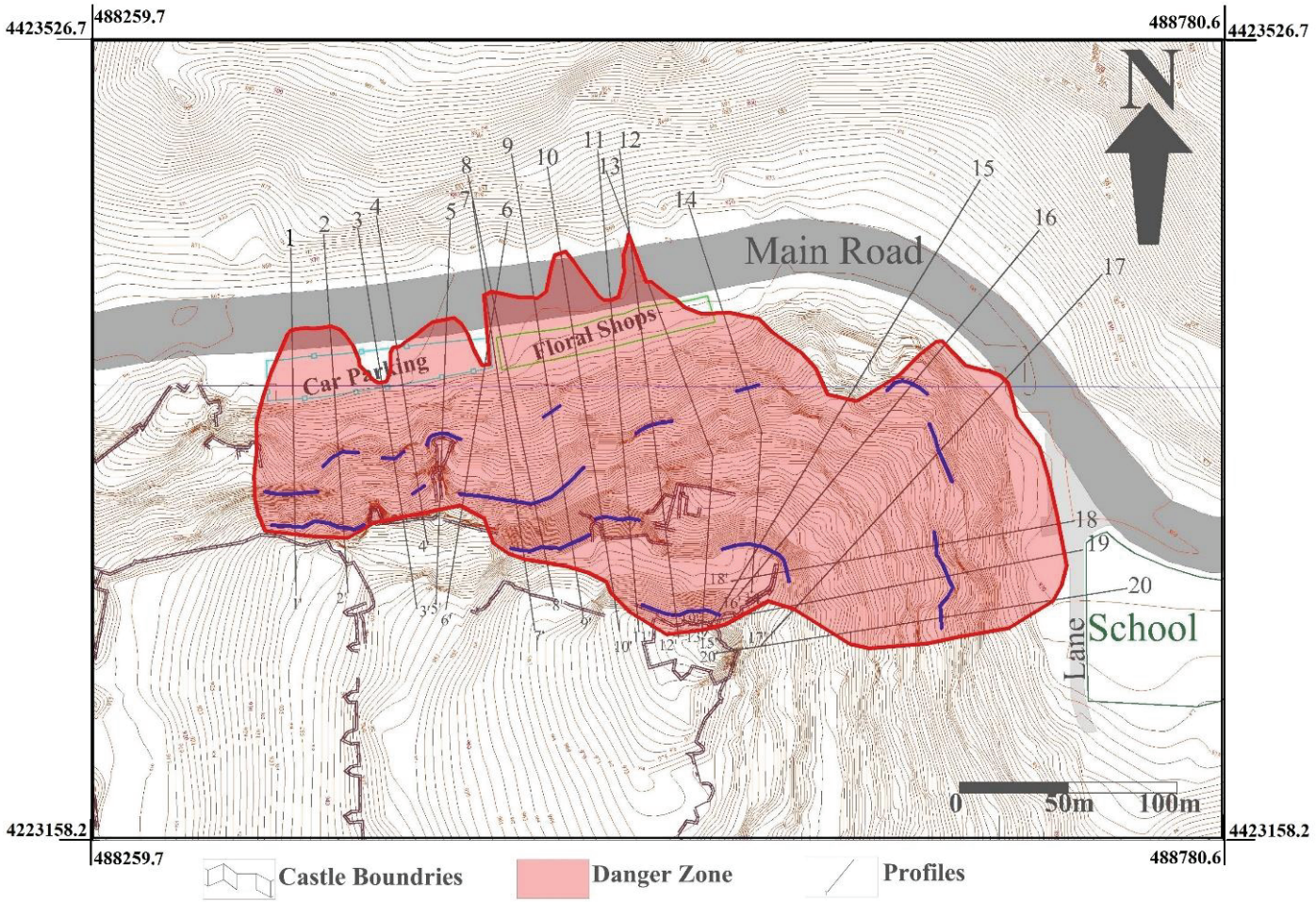

Figure 4.10 Danger zone estimated from the analyses with 250kg weights.

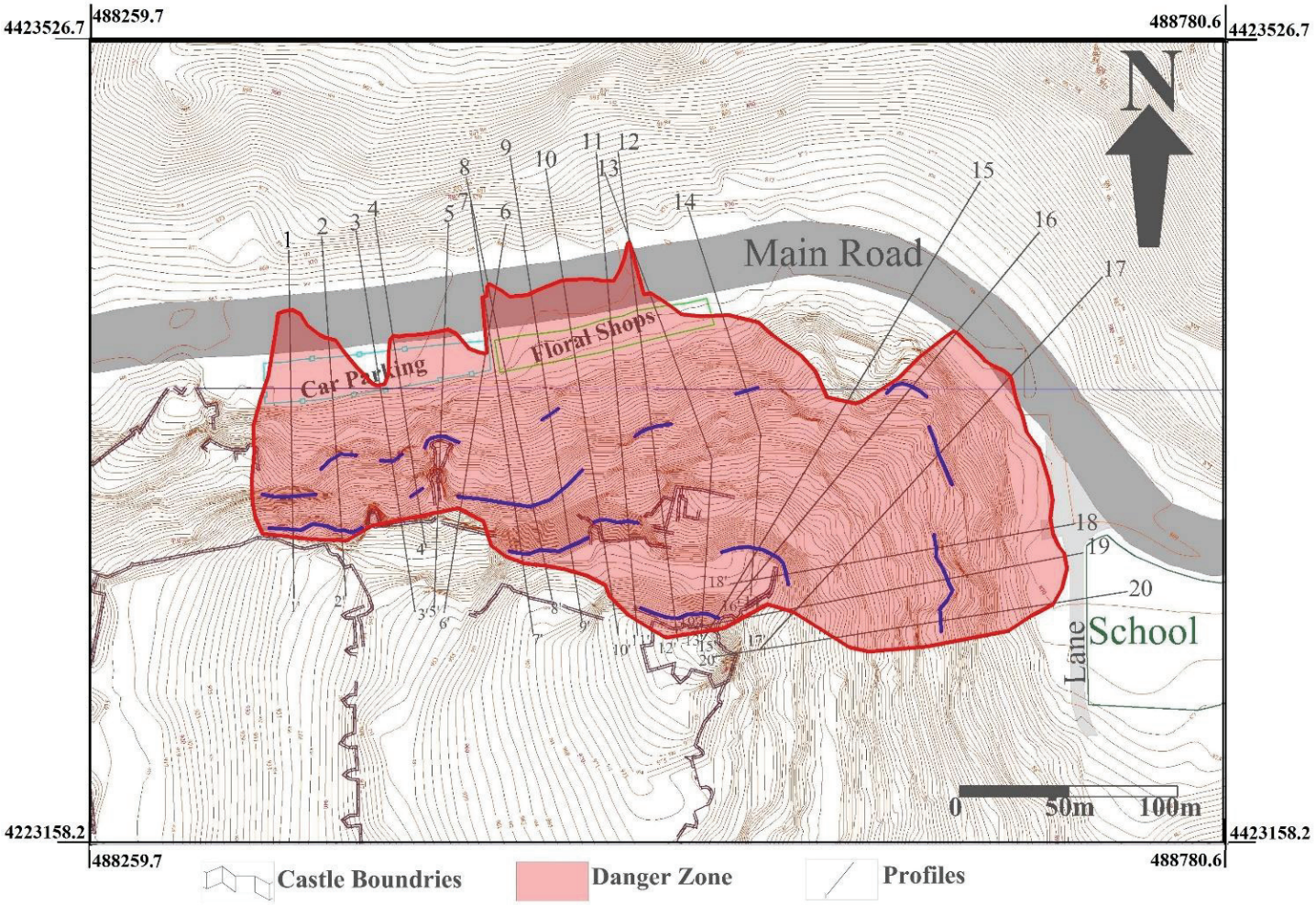

Figure 4.11 **Danger zone assessed from the analyses with 500kg weights of rocks.**

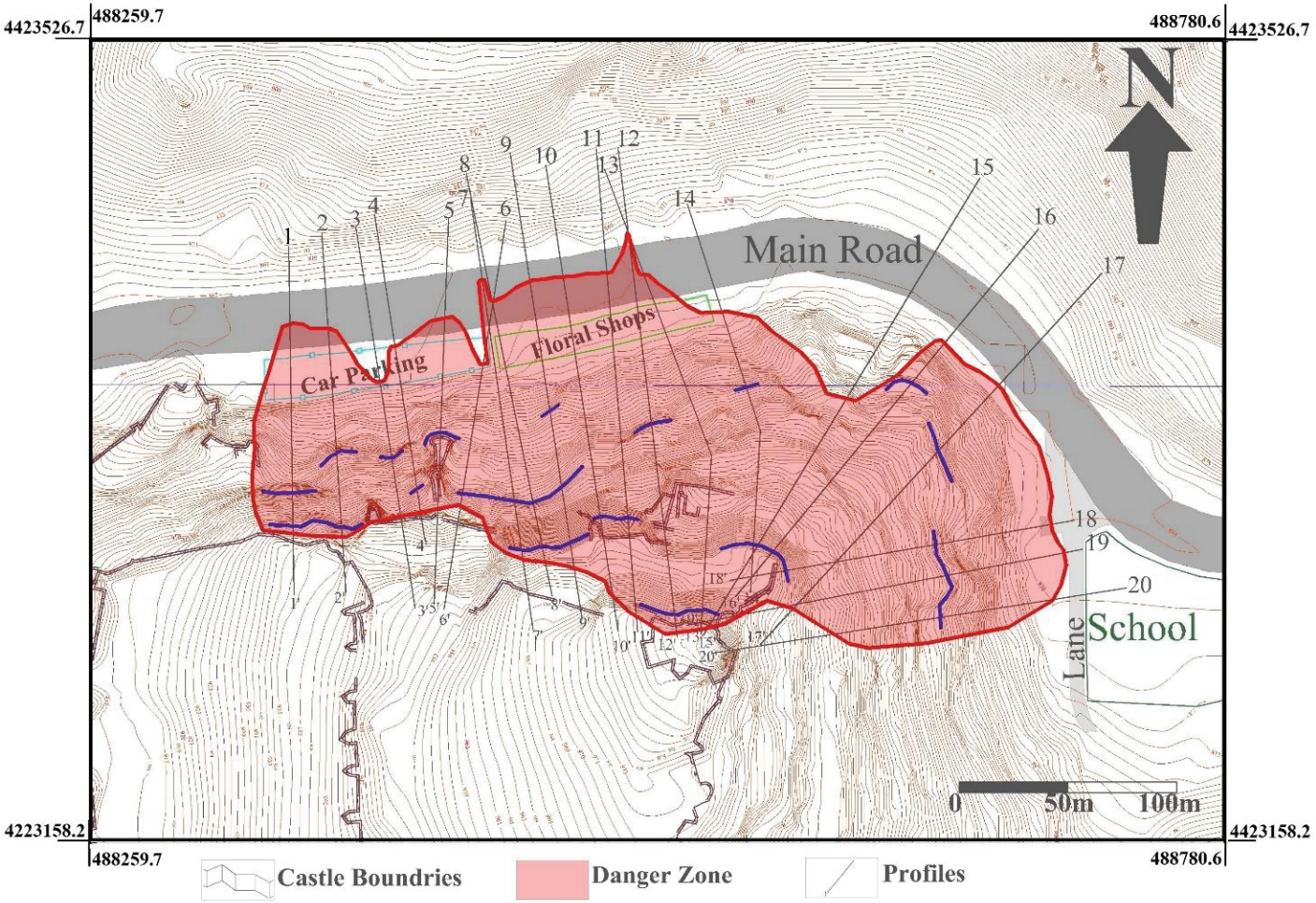

Figure 4.12 Danger zone evaluated from the analyses with the rocks of 750kg weights.

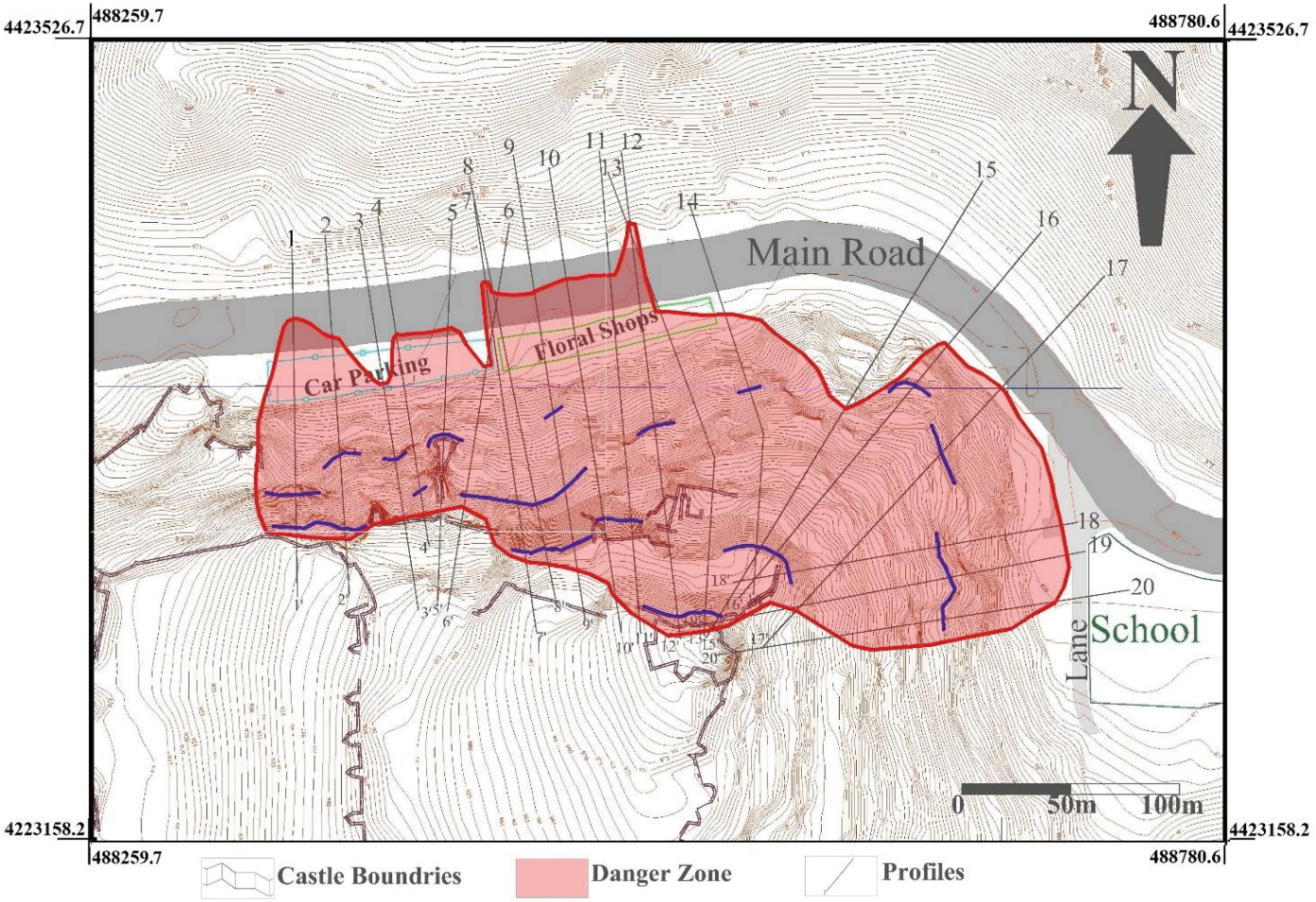

Figure 4.13 The danger zone estimated from the analyses with the rocks of 1800kg weights.

The map with all the danger zones illustrated in different colors is shown in Figure 4.14. The worst case is considered to be 1800kg weight rocks' danger zone since it has reached to the furthest point away from the hill. The resultant table of entire 2D analyses is attached in the Appendix B. From the results of the 2D analyses, the main road, car parking, floral shops and the small lane is under the threat of the rockfall. Therefore, protection measures are required. They are elaborated in Chapter 6 by taking the results into account.

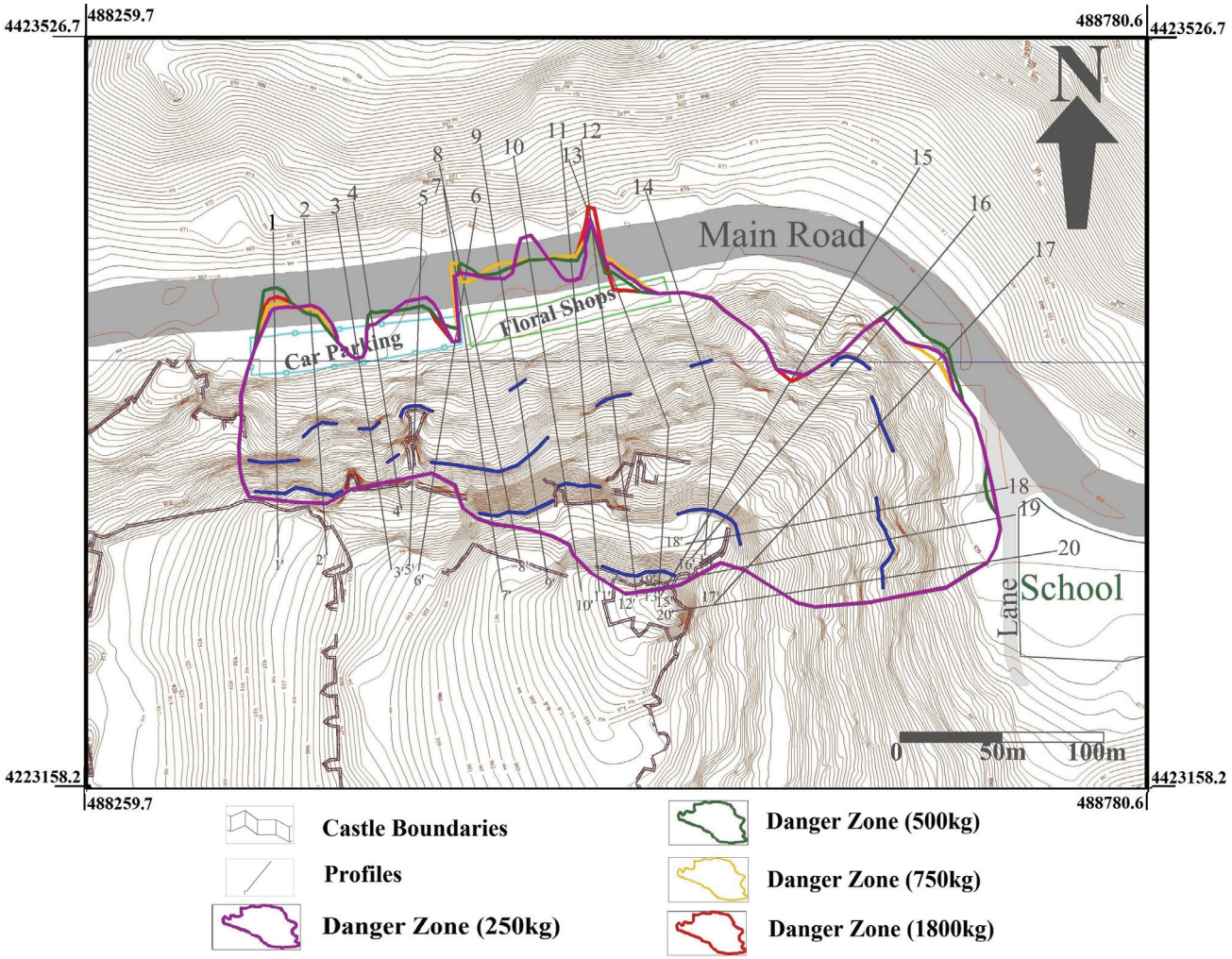

Figure 4.14 Danger zones assessed from the 2D analyses with the rocks of different weights.

4.3.2 3D Analysis

The ROTOMAP32 (Geo&soft, 2005) module was used for 3D rockfall analysis. ROTOMAP stimulates huge number of rockfalls and identifies the optimal areas for the installation of the protective structures, through the analysis of the distribution of the average and maximum kinetic energies (Scioldo, 1991).

The rockfall problem is quite complex because the apparently insignificant geometric and mechanical details determine the actual behavior of the boulders when rolling down a slope. The morphology and the path taken by the boulders interact nonlinearly.

In order to identify the areas where a rockfall can start and to distinguish the different surface types, a detailed topographic map and a geomorphologic data collection are needed for the program. The entry data must be a collection of sparse but uniformly distributed data set (X, Y, Z). Then, the program transforms the data into a regular grid which the entire model is run based on (Scioldo, 1991).

ROTOMAP can produce outputs of the topographic map, rockfall trajectories, kinetic energies, distribution of stop points and the vertical sections of each simulated fall.

The parameters used in the 3D analysis are given in Table 4.6. They were determined according to the field conditions.

Table 4.6 Parameters used in the 3D analysis.

PARAMETERS	VALUES
Flying limit angle (°)	9
Colliding limit angle (°)	9
Bouncing limit angle (°)	9
Number of starting points	20
Number of initial velocity	5
Minimum initial velocity (m/s)	0.5
Maximum initial velocity (m/s)	1.5
Number of initial directions	4
Maximum angular deviation (°)	40
Boulder mass (t)	1.98
Normal coefficient of restitution	0.46
Tangential coefficient of restitution	0.71
Friction coefficient of boulders	0.5

Flying limit angle: This is the parameter which determines when the boulders begin to fly after a bounce. The angle of the trajectory with the ground after an impact must be greater than the limit angle to initiate the flying of a boulder.

Colliding limit angle (°): This limit angle determines flying moment of the boulders over the slope. For starting a boulder to fly, increasing in the dip of slope must be greater than the limit angle.

Bouncing limit angle: This determines the impact time of the boulders with the ground and bounce. A boulder begins to bounce if the decrease of the slope dip is greater than the limit angle.

Number of starting points: The entry of individual points is not necessary, but rather lines of detachment, that can be arbitrarily placed below the top of the slope is required by the program. The number of starting points is the total number of starting

points aligned along one or more starting lines. The boulders are initiated from points aligned along those lines in the simulation of the program.

Number of initial velocities: The boulders are started from starting points with velocities ranging from minimum to maximum in the simulation based on the geometry of the unstable slopes. Therefore, the number of initial velocities is the number of starting velocities from each starting point.

Number of initial directions: A large number of initial directions around the dip direction is assigned in a given interval in the simulation. The multiplication of number of initial directions, number of initial velocities and number of starting points defines the total number of rockfalls.

Minimum and maximum initial velocities: This is the set of different initial velocities of the rock blocks.

Maximum angular deviation: This is the set of the maximum angles that the chosen starting directions around the dip direction deviated.

Boulders mass (t): The mass value of the boulders is necessary for proper plan of protection system.

The coefficients of restitution of normal and tangential energy, and friction coefficients of the rolling boulders are the geomechanical parameters applied in the model. Different sets of these coefficients with different colors are assigned to each unit if the rock is not homogenous. In this study, since andesite is the only rock existing in the area, only one set of the coefficients was entered (Figure 4.15).

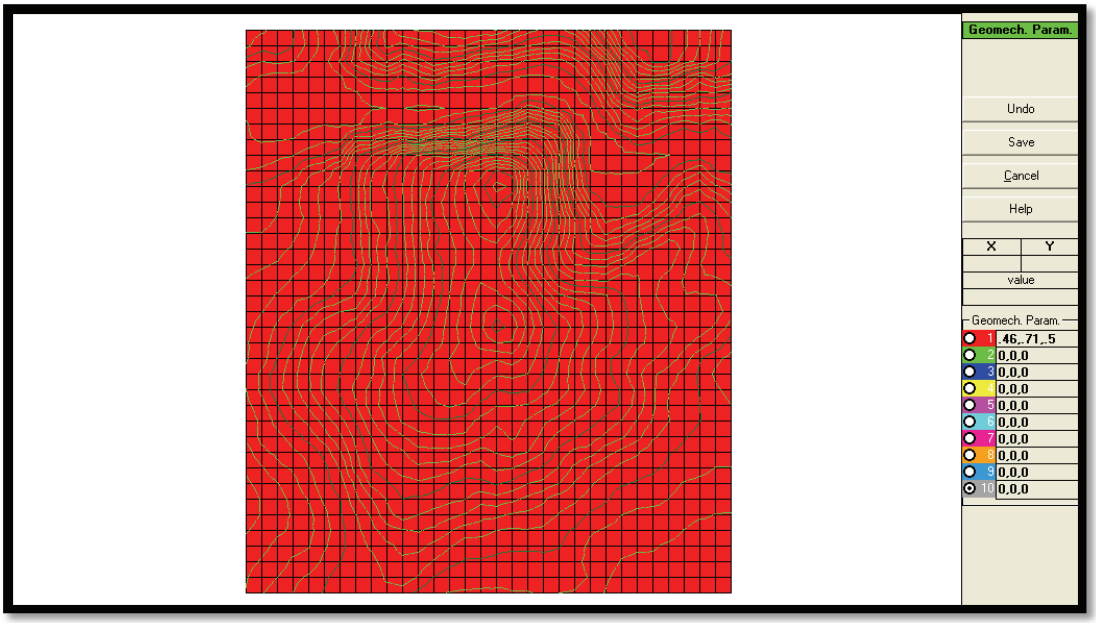

Figure 4.15 Study area assigned with single set of geotechnical parameters input with one color in the ROTOMAP software.

3D analysis evaluates the rockfall source areas as lines rather than location points. Therefore, the data of the source areas were prepared in 17 blue lines data as shown in Figure 4.7. After assigning all the parameters, the starting points were determined with these lines. Then, the model was run based on the input data in the software. The outputs of these results are given in Figures 4.16 - 4.18. In 3D analysis, the rockfall modes are rolling and bouncing. In the map showing rockfall path (Figure 4.16), the green parts of the lines mean the rolling distance, and the red parts are the bouncing distances of the rocks. The end of every single line is where the rock stop bouncing, and means the runout distance of the rocks. By connecting the ends of those lines, a danger zone for 3D analysis was obtained for the comparison of rockfall analyses, which is discussed in Chapter 5.

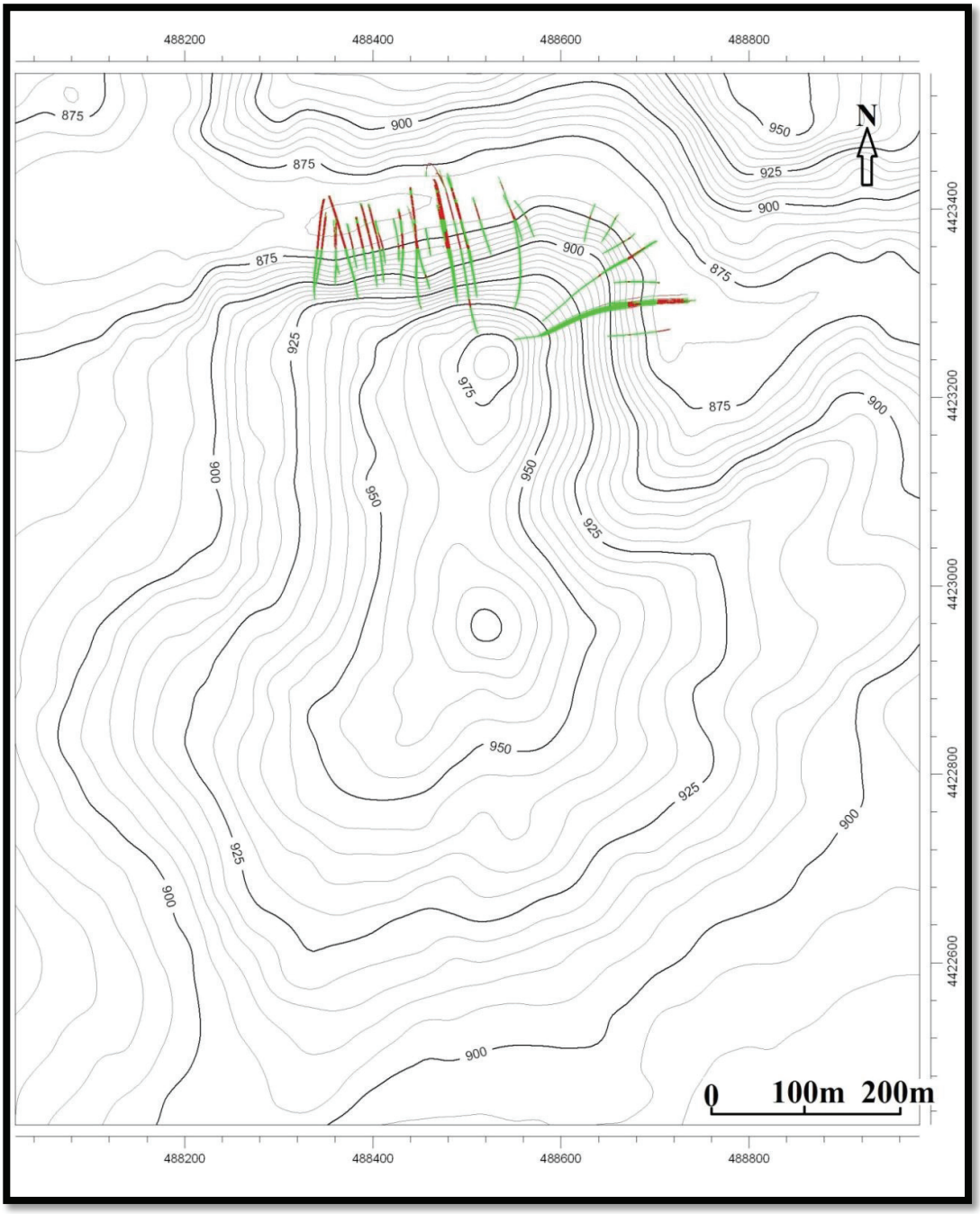

Figure 4.16 Map displaying the rockfall paths obtained from 3D analysis.

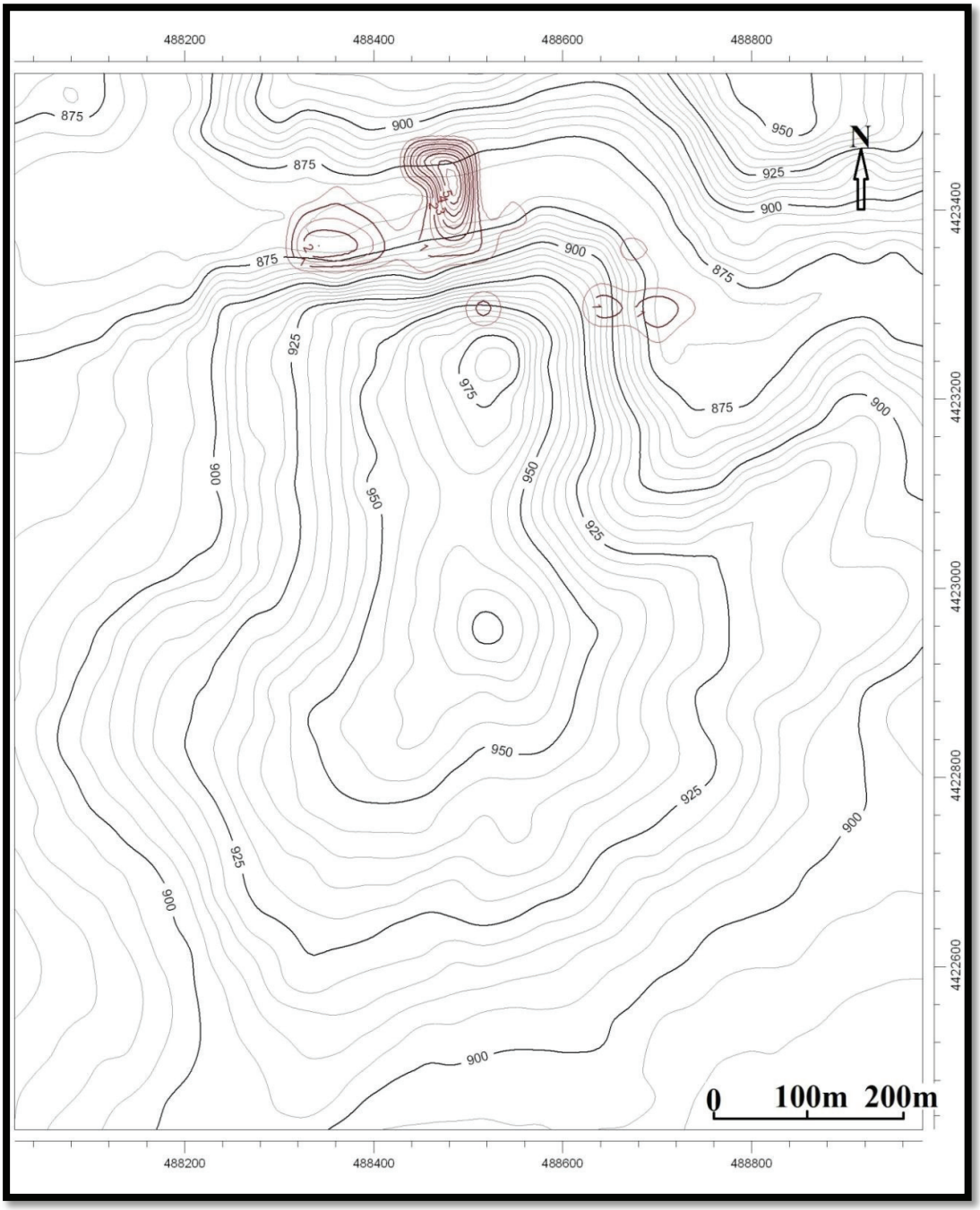

Figure 4.17 Map with bounce heights obtained from 3D analysis.

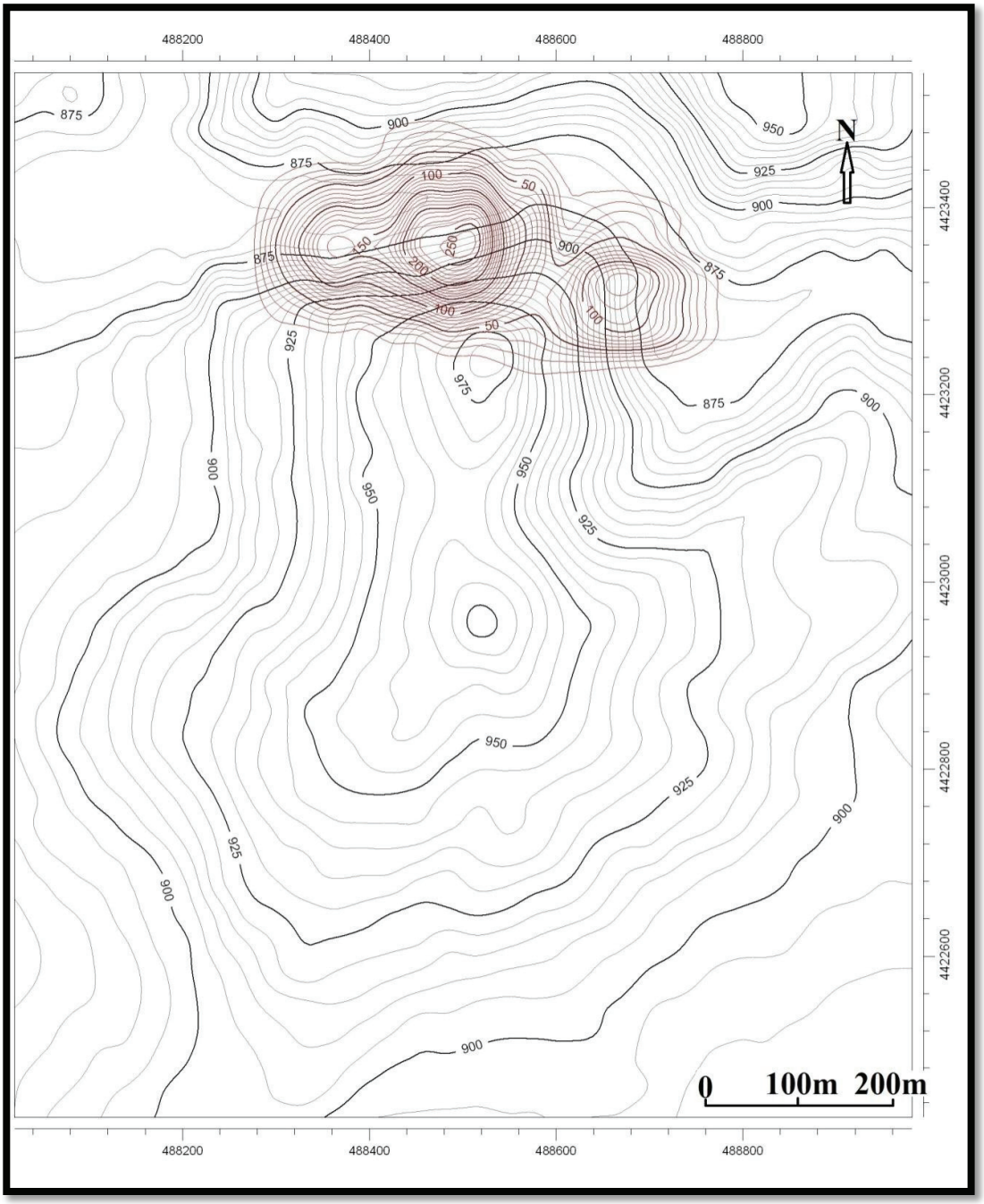

Figure 4.18 Map showing maximum kinetic energies acquired from 3D analysis.

CHAPTER 5

DISCUSSION AND REMEDIAL MEASURES

5.1 Field Study and Analyses of Rockfall

This main scope of this study is to analyze the potential rockfall hazard around the hill of a historical building, the Ankara Citadel. The Ankara Citadel is located on the very steep hill next to the main road in a populated area of Ankara. Highly fractured andesite is exposed at the slope of the study area. The andesite has flower layers and cooling joints almost perpendicular to the layering in different orientations. Some blocks of the andesite were already detached and many fallen andesite blocks were observed in the study area, with some reaching near the road and floral shops (Figures 1.2 and 3.22). Among the fallen blocks, the biggest one was observed to have the size of 160cm x 80 cm x 60 cm weighting nearly 1789.4kg.

During the field study, scanline surveys were performed to collect the discontinuity data of the andesite and the rockfall source area. Due to the very steep and high nature of the rocks, some parts of the andesite could not be accessed. The persistence of the joints developed in the andesite could be observed only when the outcrops are large enough.

In the field, the back analysis was considered to obtain the coefficients of restitution to be used for the rockfall analysis. However, due to the placement of the car parking and the floral shops, field tests by throwing rocks of different sizes for back analysis were not carried out. If the rocks were thrown from the top of the hill, it could hit the cars in the park (Figure 5.1). If the rocks were caught by the barrier and net structure

at the base, the desire results were not able to access. Therefore, it was decided to use the coefficients of restitution from a similar study. However, the rockfall study including the coefficients of restitution of the andesite, could not be found for Ankara Region. Hence, the values of Topal et al. (2007) were used because of the similar nature of the andesites exposed in Afyon Castle and Ankara Citadel.

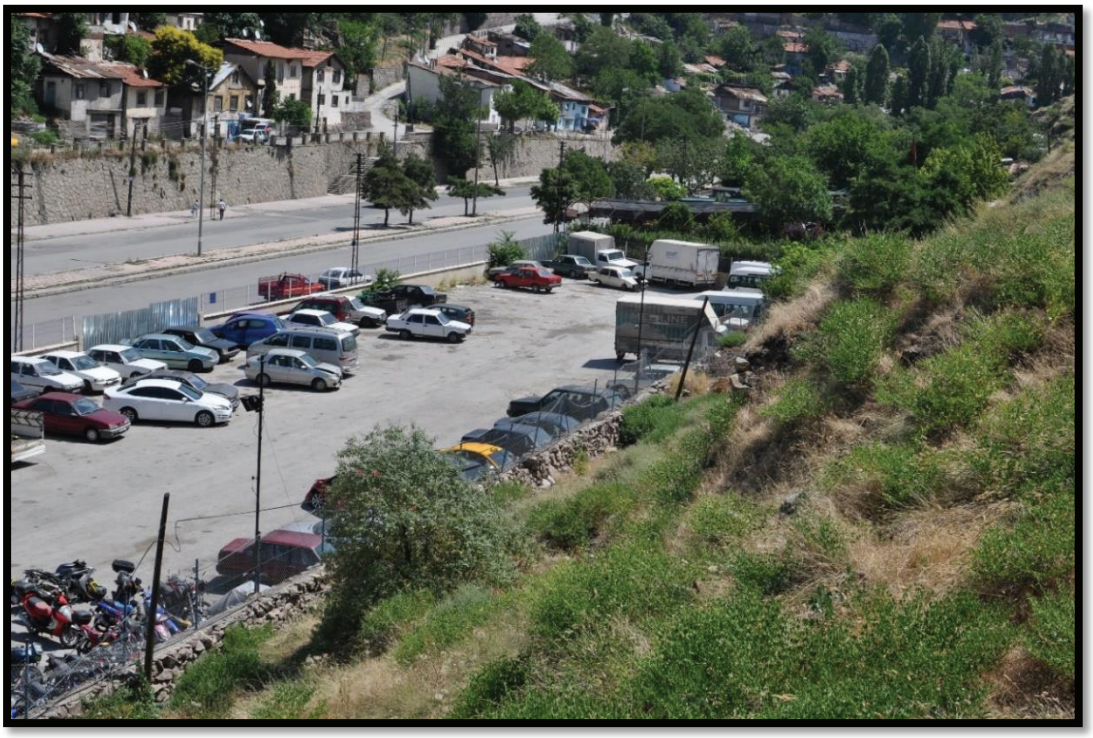

Figure 5.1 The position of car parking and the small barrier with net at the base of the slope.

Then, the slope stability analyses were carried out step by step. When performing the limit equilibrium analyses for the toppling, Roctopple 1.0 (Rocscience, 2015c) only allows the one spacing value for each analysis. Therefore, an average value of spacing was applied rather than evaluating all the spacing values for each stop.

Very low values of safety factors were obtained from static condition. However, the analysed blocks are still in place in the field. Therefore, the cohesion values were obtained for factor of safety value of 1 and internal friction angle of 30^{o} with Mohr-

Coulomb equation. The cohesion values of 30.8 kPa, 16 kPa, and 26.9 kPa were acquired for planar, wedge and toppling failure, respectively. The cohesion value was very close to 0 for the block samples from jointed samples examined laboratory and by using Barton-Bandis approach. But, especially in the andesites, the joints and the flow layers are firmly attached to each other during cooling process. Therefore, the cohesion values must be more than zero. Within the framework of the experiences from this study, the cohesions of the discontinuities of the andesites for the slopes around Ankara Citadel can be taken as 16 to 31kPa.

With these values, the factors of safety were calculated again with Mohr-Coulomb approach for planar, wedge and toppling failures. These safety factor values are tabulated in Table 5.1 and 5.2 for static and dynamic conditions, respectively.

Table 5.1 Safety factors for static condition by Mohr-Coulomb approach.

	Safety factors for static condition from Mohr-Coulomb equation		
Stops	Planar	Wedge	Toppling
1	1.412	1.274	2.938
2	2.420	2.026	1.870
3	2.678	4.790	3.539
4	1.659	2.579	3.008
	5.396	2.195	3.671
5	-	1.248	4.125
6	2.904	2.132	6.796
7	4.061	1.774	8.963
8	5.287	1.087	2.588
9	3.166	1.002	1.001
10	1.675	3.151	11.349
11	2.111	1.234	1.983
12	-	2.632	-
13	-	1.716	-
14	-	1.165	2.920
15	5.265	1.454	21.734
16	1.002	1.947	2.470
17	3.472	4.096	8.579
18	2.606	4.408	6.813
19	-	5.747	-
20	3.402	1.324	-
21	-	1.249	5.283

Table 5.1 Safety factors for dynamic condition by Mohr-Coulomb approach.

	Safety factors for dynamic condition from Mohr-Coulomb Equation		
Stops	Planar	Wedge	Toppling
1	1.297	1.223	2.499
2	2.359	1.968	1.747
3	2.535	4.549	3.068
4	1.582	2.454	2.691
	5.286	2.075	3.001
5	-	1.147	2.642
6	2.818	2.007	3.670
7	3.983	1.641	5.479
8	5.212	1.029	2.082
9	3.121	0.946	0.907
10	1.544	3.026	7.203
11	2.059	1.169	1.698
12	-	2.454	-
13	-	1.642	-
14	-	1.108	2.448
15	5.201	1.381	5.196
16	0.941	1.899	0.958
17	3.365	3.930	6.743
18	2.515	4.276	5.382
19	-	5.461	-
20	3.310	1.220	-
21	-	1.188	2.776

In the stage of 2D rockfall analyses, the different shapes of the rock were analyzed for every slope to observe the results, as a new feature provided by RocFall 5.013 (2015c). However, with the conditions of this study, the same results were given for different shapes. Therefore, only the hexagonal shape from the available range of the different shapes, were used to best represent the irregular nature of the blocks.

5.2 Comparison of the Rockfall Models

After completing the details of 2D and 3D rockfall analyses, their results are discussed at this stage. Figure 5.2 shows the comparison of danger zones acquired form 2D and 3D analyses illustrated in different colors.

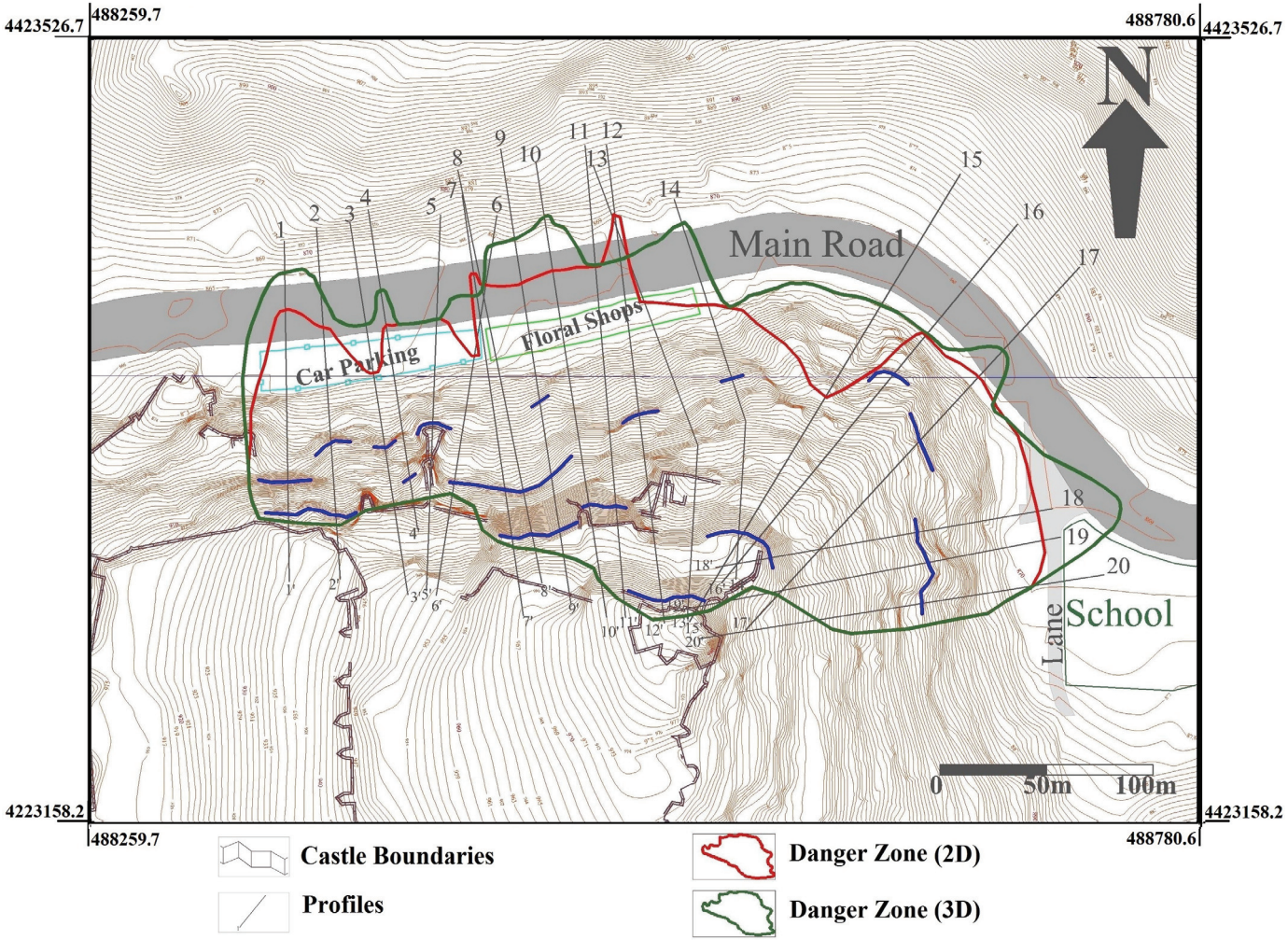

Figure 5.2 2D and 3D danger zones resulted from rockfall analysis for the blocks weighting 1800kg.

The runout distances obtained from the 3D analysis are further than that of the 2D analysis. There could be many factors causing this dissimilarity such as restriction in models, different algorithms utilized and parameters used in the software.

5.2.1 Restriction in the Rockfall Models

As it was mentioned in Chapter 2, 2D models have restriction like the lateral dispersion of the rockfall is not evaluated. The rocks are assumed to follow the straight line representing the mean slope gradient. However, in real case, the rocks may deviate from this straight line. In 3D analysis, there is no such restriction and the model takes the whole topographic data into consideration yielding the deviated rockfall path. In this aspect, 3D analysis seems to be more authentic than 2D analysis although the studies sections are so selected that they are more or less perpendicular to the topographic contour lines.

5.2.2 Algorithms Utilized on Softwares

Rocfall (2015c) utilizes the particle analysis for 2-dimensional analysis of rockfall. Particle analysis includes three sections such as the particle algorithm, the projectile algorithm, and the sliding algorithm. The particle algorithm is for assurance of the validation of the simulation parameters which are valid and setting up all of the initial conditions in preparation for the projectile and sliding algorithms. The rest of the simulation till the stopping point of the rock is in either the projectile algorithm or the sliding algorithm. Calculation of the rock's movement while in the air or bouncing on the slope is executed by the projectile algorithm. The sliding algorithm is applied to compute the rock's movement when the rock is on the slope (Stevens, 1998).

As for 3D analysis of ROTOMAP32 (Geo&soft, 2005), the facts about the algorithms used in the software cannot be assessed. However, the outcomes given by both analyses show that different algorithms were applied, giving different results.

5.2.3 Parameters Used in 2D and 3D Rockfall Analyses

Different sets of parameters were used in 2D and 3D rockfall analysis (Table 5.1). Only coefficients of restitution and friction were common parameters used in both

analyses. In the 3D rockfall analysis, only 1800kg weight of the blocks were used because it was the worst case in the 2D rockfall analyses. The rest of the parameters are applied differently in these softwares. 3D rockfall analyses had larger set of parameters. These parameter distinctions also result in the different runout distances.

Table 5.1 Parameters involved in 2D and 3D rockfall analysis.

Parameters in 2D analysis	**Parameters in 3D analysis**
Normal coefficient of restitution (Rn)	Flying limit angle (°)
Tangential coefficient of restitution (Rt)	Colliding limit angle (°)
Dynamic friction coefficient	Bouncing limit angle (°)
Rolling resistance	Number of starting points
Initial velocity (m/s)	Number of initial velocity
Number of throws	Minimum initial velocity (m/s)
Minimum velocity cut-off (m/s)	Maximum initial velocity (m/s)
Shape of the rocks thrown	Number of initial directions
	Maximum angular deviation (°)
	Boulder mass (t)
	Normal coefficient of restitution (Rn)
	Tangential coefficient of restitution (Rt)
	Friction coefficient of boulders

5.3 Comparision of Rockfall Source Areas

The rockfall source determined visually in the field in this study was compared with RSA (Rockfall Source Area) map around the Ankara Citadel and its vicinity produced by Aksoy and Ercanoglu (2006) (Figure 5.3). This RSA map was produced by rule-based fuzzy analysis integrated with the altitude difference, the number of discontinuities, the number of wedges and the number of potential slides. During their study, many rockfalls were observed around the Ankara Citadel. In the map (Figure 5.3), the blue diamond shapes show the rockfalls already observed in their

study. The dash line areas represent the possible rockfall source for those rockfalls determined by Aksoy and Ercanoglu (2006).

It is observed that most of the rockfall sources determined in this study area are in medium rockfall source area and partly in high rockfall source area according to Aksoy and Ercanoglu (2006). Nevertheless, the rockfall source area at the top of the hill near the inner circle, which was determined in this study, was not included in the RSA map. The runout distances from this rockfall source area reaches the furthest through profiles 12 and 13 in 2D rockfall analysis, and reaches out to the road in 3D rockfall analysis. However, the shortest runout distance is also from this rockfall source area through profile 15.

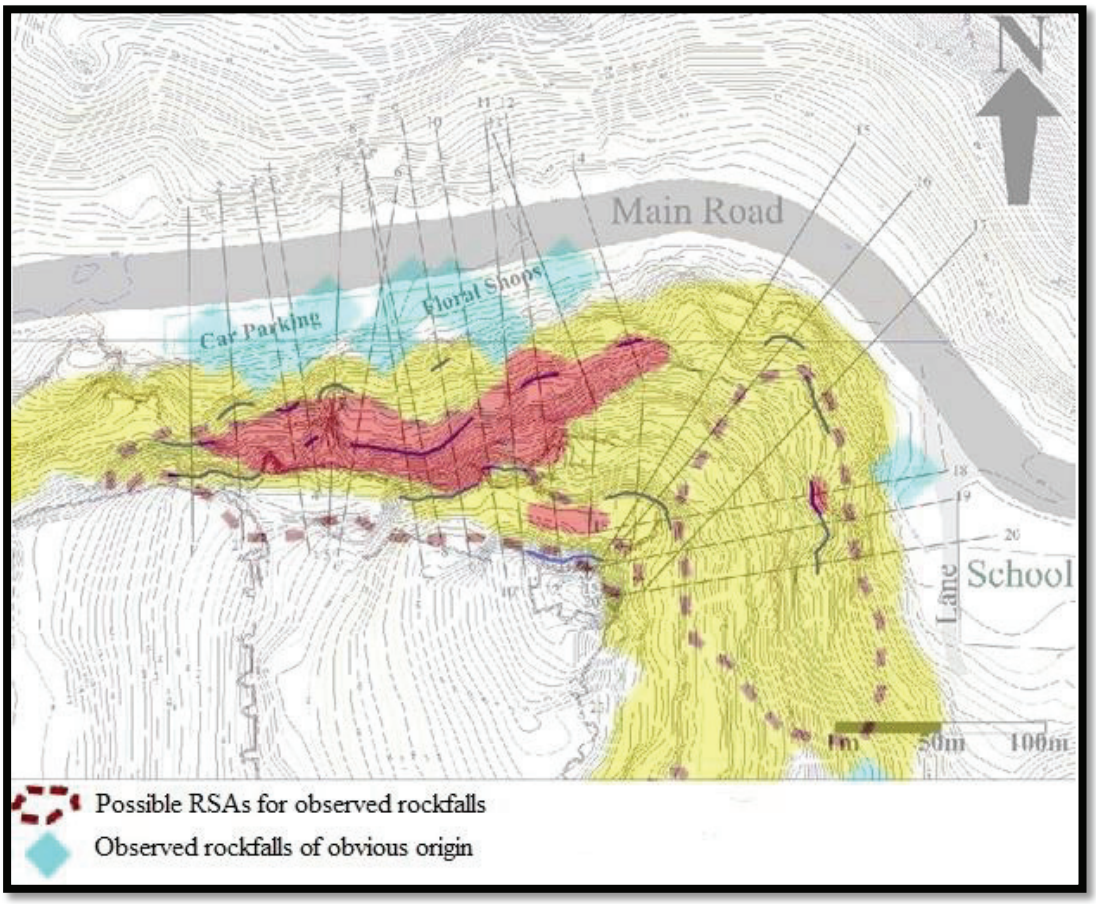

Figure 5.3 Possible RSA map around the Ankara Citadel and its vicinity generated by Aksoy and Ercanoglu (2006) illustrated on the study area. The yellow areas mean the medium rockfall source area, and red regions represent the high rockfall source

area according to RSA map. The dark blue lines represented the rockfall source area determined visually in this study.

Most of the rockfall source areas on the northern part of the hill are in the high rockfall source area according to RSA map. The furthest of runout distance is from one of this high rockfall source area in 3D rockfall analysis. The source on the eastern part of the hill is partly in the high and medium RSA, and gives the runout distances reaching to the road in 3D rockfall analysis. Although the leftmost part of the northern hill is in medium rockfall source in RSA map, that part was not considered in this study because there is outer castle wall surrounding it.

When considering the topographic map and observing in the field, some parts of the study area are nearly horizontal or the bottom of a local steep topography. Therefore, it is determined to be more realistic to take rock source areas determined visually in the field for this kind of rockfall analyses in this study.

5.4 Remedial Measures for Rockfall Danger

In this section, appropriate measures are suggested since there is a potential risk of rockfall in the study area. Since there are car parking and floral shops right at the bottom of the hill, construction of ditches is not feasible without disturbing the neighborhood and livelihood of people. Installations of rock bolts are not also feasible because the spacing values of the discontinuities of the andesite are generally very low. Too many bolts would be necessary to be installed, and also the design of the rock bolts' size would be difficult to determine due to unavailability of the persistence of the discontinuities into the andesite. As the first step of remediation, the andesite blocks that are already detached can be removed since those blocks may fall down anytime. Furthermore, loose blocks ready to fall down should be cleaned.

For the effective ways of protection, catch barriers are suggested to build on the slope to stop the blocks from reaching down the road. The impact energy and the fall trajectories are needed to determine the strength, the height and the location of the structure on the slope for the design of rockfall protection (Wyllie, 2015, Li et al,

2016). These design parameters are assessed from Rocfall 5.013 (2015c). In the software, based on these parameters given, the characteristics of the rock barriers were determined. The rockfalls were simulated by installing the barriers to observe the most appropriate barriers properties. As the result, barriers of various size ranging from 1m to 2.5m height with 15kJ to 250kJ capacities were chosen at different locations. The most appropriate catch barriers are suggested as shown in the map below (Figure 5.4). With the installations of these barriers, the rockfalls were simulated again and the danger zone is not affecting the infrastructures as shown in the Figure 5.4.

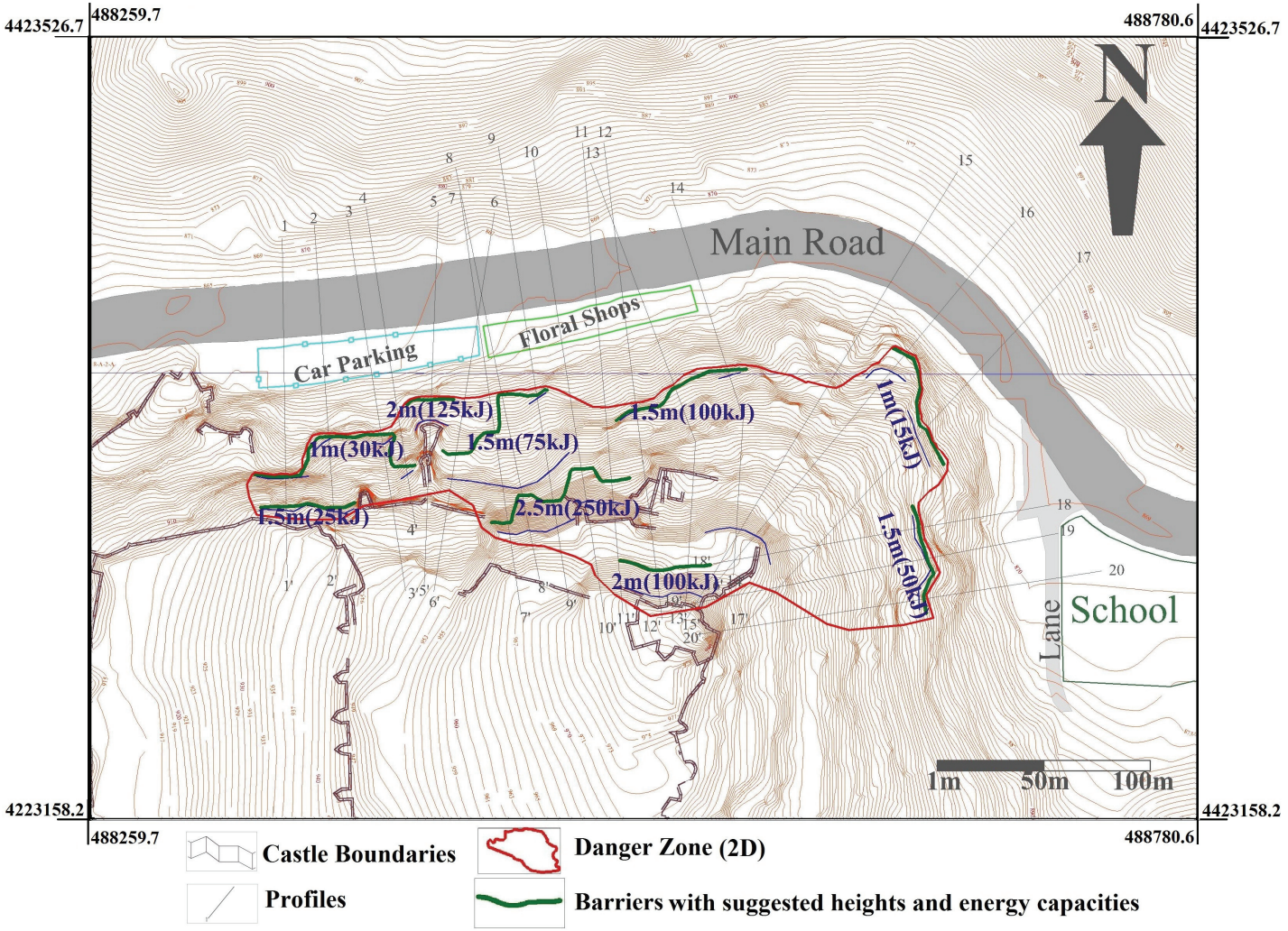

Figure 5.4 Design for installation of barriers on the slope to prevent rockfall damage in the study area.

CHAPTER 6

CONCLUSIONS AND RECOMMENDATIONS

This study manifests the analysis of rockfall on the northern and eastern part of the hill on which the Ankara Citadel is located.

The hill, on which the Ankara Citadel is located, is very steep reaching up to 986m. There are main road, floral shops, car parking and a school near the base of the hill. The geological unit exposed at the steep slope of the study area is highly fractured andesite. The andesite is generally pinkish grey in color and mostly slightly weathered. Detail scanline surveys carried out at 21 stops on the study area shows that many steeply dipping cooling joints developed in different directions perpendicular to the flow layers. The persistence values of the discontinuities are less than 5m but 15m of persistence was also observed locally. The spacing values ranges from 2 to 200cm concentrating mostly around 20 to 60cm. The apertures of the andesite are often tight, and have clay infillings close to the surface between the joints. The Schmidt hardness values vary between 25 and 41. The discontinuity surface of the andesite is undulating rough and JCS was determined as 3.55MPa. Many fallen rock blocks were observed in the field with some reaching near to the floral shops and main road, and the biggest andesite block's dimension is 160cm x 80 cm x 60 cm weighting nearly 1789.4kg.

According to the laboratory studies, the andesite has medium density, medium porosity and moderately strong UCS. The average water absorption by weight and volume of the andesite are 3.5% and 7.88%, respectively. The velocity of the andesite resulted from sonic velocity tests are in low to very low and medium to low

category. According to the direct shear tests along the saw-cut surfaces, the peak cohesion and internal friction angle are 32.81kPa and 28.1^{o}, the residual cohesion and internal friction angle are 4.21kPa and 23^{o}. The internal friction angle for peak values to be used in kinematic analysis was determined as 30^{o}.

As the result of kinematic analyses of each stop of the study area, the wedge failure is likely to happen at all the stops. The planar failure is expected to happen at all the stops except 5th, 12th, 13th, 14th, 19th and 21th stops. The toppling failure is probable to occur in most stops, excluding 12th,13th,19th and 20th stops. The safety factors of all failure types in static limit equilibrium analyses are very low under 1.0 except wedge failure of 3rd and 7th stop, and toppling failure of 10th stop. After conducting the dynamic limit equilibrium analyses by applying horizontal seismic ground acceleration of 0.05g, the safety factor values of the failures became lower than the static analyses.

2D rockfall analyses along 20 profiles, which were carried out with four different weights of the rocks such as 250kg, 500kg, 750kg and 1800kg revealed that the fallen rocks may reach to the main road, car parking, floral shops and the school. Comparison of 2D and 3D rockfall analyses showed that the runout distances of 3D analyses are further than those of 2D analyses. Different results were given by those two analyses due to rockfall models, algorithms used and the parameters input. However, based on the restriction of 2D analysis for the rockfall track, 3D results are accepted to be more authentic.

Since the neighborhood is not suitable to relocate, the removal of the detached and loosen andesite blocks is recommended. Since rockfall is an ongoing process, annual control is recommended on the study area. The removal of the fallen rocks and the loosed andesite blocks should be done periodically. Moreover, installations of the catch barriers on the slope with specified heights, energy capacities and locations are also suggested to protect the surroundings.

REFERENCES

Agliardi, F., Crosta, G.B. (2003). High Resolution Three-dimensional Numerical Modeling of Rockfalls. International Journal of Rock Mechanics and Mining Sciences, 40 (4), 455–471 pp.

Aksoy, H. and Ercanoglu, M. (2006). Determination of the Rockfall Source in an Urban Settlement Area by Using a Rule-Based Fuzzy Evaluation. Natural Hazards and Earth System Sciences, 6, 941–954 pp.

Akyürek, B., Duru, M., Sütçü, Y., Papak, I., Şaroğlu, F., Pehlivan, N., Gönenç, O., Granit, S., Yaşar, T. (1997). 1:100 000 Scaled Turkey Geological Map, Ankara - F15 plate, MTA press, Ankara. (in Turkish).

Altındağ Municipality. (2010). Topgraphic map and Ankara Citadel photograph. Ankara.

Anon. (1979). Classification of Rocks and Soils for Engineering Geological Mapping. Part 1. Rock and soil materials, Bulletin of the International Association Engineering Geology, 19, 364 - 371 pp.

Asteriou, P., Tsiambaos, G. (2016). Empirical Model for Predicting Rockfall Trajectory Direction. Rock Mechanic and Rock Engineering, 49, 927–941 pp.

Azzoni, A., Barbera, G.L. and Zaninetti, A. (1995). Analysis and Prediction of Rockfalls Using a Mathematical Model. International Journal of Rock Mechanics and Mining Science, 32, 709–24 pp.

Bozzolo, D. and Pamini, R. (1986). Simulation of Rock Falls Down a Valley Side. Acta Mechanica, 63, 113–30 pp.

Brawner, C. (1994). Rockfall Hazard Mitigation Methods. National Pooled Fund Study, Federal Highway Administration, Publication No. FHWA SA-93-085.

Bright hub engineering, retrieved on 2016 from http://www.brighthubengineering.com/structural-engineering/124326-responding-to-rock-fall-risk-on-public-roadways/#.

Budetta, P. and Santo, A. (1994) Morphostructural Evolution and Related Kinematics of Rockfalls in Campania (southern Italy): A Case Study. Engineering Geology, 36, 197–210 pp.

Chen, H., Chen, R.H., Huang, T. (1994). An Application of an Analytical Model to a Slope Subject to Rockfalls. Bulletin of the Association of Engineering Geologists, 31, 447–458 pp.

Copons, R., Vilaplana, J.M., Linares, R. (2009). Rockfall Travel Distance Analysis by Using Empirical Models (Sol`a d'Andorra la Vella, Central Pyrenees). Natural Hazards and Earth System Science, 9, 2107–2118 pp.

Day, R.W. (1997). Case Studies of Rockfall in Soft Versus Hard Rock. Environmental and Engineering Geoscience, 3(1), 133–40 pp.

Discover Central California, retrieved on 2016 from http://www.discover-central-california.com/rain-rocks-rock-shed.html#gallery[pageGallery]/0/.

Dorren, L.K.A. (2003). A Review of Rockfall Mechanics and Modelling Approaches. Progress in Physical Geography, 27 (1), 69–87 pp.

Dorren, L.K.A., Maier, B., Putters, U.S., Seijmonsbergen, A.C. (2004). Combining Field and Modelling Techniques to Assess Rockfall Dynamics on a Protection Forest Hillslope in the European Alps. Geomorphology, 57 (3–4), 151–167 pp.

Dorren, L.K.A. and Seijmonsbergen, A.C. (2003). Comparison of Three GIS-Based Models for Predicting Rockfall Runout Zones at a Regional Scale. Geomorphology. 56, 49–64 pp.

Deere, D.U., Miller, R.P. (1966). Engineering Classification and Index Properties for Intact Rocks. Technical Report Air Force Weapons Laboratory, New Mexico, No AFWL-67-144.

Ercanoğlu, M. and Aksoy, H. (2004). Potential Instability Map for Rock Slopes at Ankara Castle and Vicinity. Yerbilimleri (in Turkish), 29, 97–114 pp.

Erentöz, C. (1975). 1/15000 Scaled Turkey Geological Map, Ankara Region. MTA Press, (in Turkish).

Erol, O. (1961). Tectonic Development of Ankara Region. Bulletin of TJK, (in Turkish), 7, 57–85 pp.

Evans, S.G. and Hungr, O. (1993). The Assessment of Rockfall Hazard at the Base of Talus Slopes. Canadian Geotechnical Journal 30, 620–36 pp.

Federal Highway Administration (FHWA), U.S. Department of Transportation. (1993). Rockfall Hazard Rating System: Participant's Manual. FHWA SA-93-057. National Highway Institude.

Geo&Soft (2005). ROTOMAP32, 3D Rockfall Analysis, Torino, Italy.

Gokceoglu, C., Sonmez, H., and Ercanoglu, M. (2000). Discontinuity Controlled Probabilistic Rrisk Maps of the Altindag (settlement) Region in Turkey, Engineering Geology, 55, 277–296 pp.

Gökçe, O., Özden, Ş., Demir, A. (2008). Spatial and Statistical Distribution of Disaster in Turkey, Disaster Information Inventory, Department of Disaster Studies and Damage Assessment.

Guzzetti, F., Reichenbach, P., Ghigi, S. (2004). Rockfall Hazard and Risk Assessment Along a Transportation Corridor in the Nera Valley, Central Italy. Environmental Management. 34 (2), 191–208 pp.

Hegg, C. and Kienholz, H. (1995). Determining Paths of Gravity-Driven Slope Processes: the ‘Vector Tree Model’. In Carrara, A. and Guzetti, F., editors,

Geographic information systems in assessing natural hazards. Dordrecht: Kluwer Academic Publishers, 79–92 pp.

Heim, A. (1932). Bergsturz und Menschenleben. Beiblatt zur Vierteljahrschrift der Naturforschenden Gesellschaft in Zürich, 77, 218 pp.

Ischebeck Titan, retrieved on 2016 from http://www.ischebeck-titan.co.uk/products/drilldrain.html.

ISRM. (1981). Rock Characterization, Testing and Monitoring. International Society for Rock Mechanics Suggested Methods. Pergamon, Oxford, 211 pp.

Karacan, E. (1984). Geomechanical analysis of Ankara Andesite's Fractures and Joints. MSc Thesis, Hacetteppe University. 206 pp (In Turkish, Unpublished).

Kasapoğlu, K.E. (1980). Geo-Engineering Properties of the Ground in the City of Ankara, Thesis for Assoc. Prof., Hacettepe University (in Turkish, unpublished).

Kaya, Y., Topal, T. (2015). Evaluation of Rock Slope Stability for a Touristic Coastal Area Near Kusadasi, Aydin (Turkey). Environmental Earth Sciences, 74(5), 4187-4199 pp.

Keylock, C. and Domaas, U. (1999). Evaluation of Topographic Models of Rockfall Travel Distance for Use in Hazard Applications. Arctic, Antarctic, and Alpine Research, 31(3), 312–20 pp.

Krautblatter, M., Moser, M. (2009). A Nonlinear Model Coupling Rockfall and Rainfall Intensity Based on a Four Year Measurement in a High Alpine Rock wall (Reintal, German Alps). Natural Hazards and Earth System Sciences, 9, 1425-1432 pp.

Kirkby, M.J. and Statham, I. (1975). Surface Stone Movement and Scree Formation. Journal of Geology, 83, 349–62 pp.

Kobayashi, Y., Harp, E.L. and Kagawa, T. (1990). Simulation of Rockfalls Triggered by Earthquakes. Rock Mechanics and Rock Engineering, 23, 1–20 pp.

Lan, H., Martin, C.D., Lim, C.H. (2007). RockFall Analyst: A GIS Extension for Three-Dimensional and Spatially Distributed Rockfall Hazard Modeling. Computers & Geosciences, 33, 262–279 pp.

Lan, H., Martin, C.D., Zhou, C., Lim, C.H. (2010). Rockfall Hazard Analysis Using LiDAR and Spatial Modeling. Geomorphology, Volume 118, Issues 1–2, 15 May, 213–223 pp.

Li, L.P., Sun, S.Q., Li, S.C., Zhang, Q.Q., Hu, C., and Shi, S.S. (2016). Coefficient of Restitution and Kinetic Energy Loss of Rockfall Impacts. KSCE Journal of Civil Engineering, 20(6), 2297-2307 pp.

Lied, K. (1977). Rockfall Problems in Norway. ISMES Publication no. 90, Bergamo, 51–53. Coefficient of Restitution and Kinetic Energy Loss of Rockfall Impacts. KSCE Journal of Civil Engineering, 20 (6), 2297-2307 pp.

Ma, G., Matsuyama, H., Nishiyama, S., Ohnishi, Y. (2011). Practical Studies on Rockfall Simulation by DDA. Journal of Rock Mechanics and Geotechnical Engineering, 3 (1), 57–63 pp.

Maerz, N.H., Youssef, A.M., Pradhan, B. and Bulkhi, A. (2015). Remediation and Mitigation Strategies for Rock Fall Hazards Along the Highways of Fayfa Mountain, Jazan Region, Kingdom of Saudi Arabia. Arabian Journal of Geosciences, 8, 2633–2651 pp.

Marzorati, S., Luzi, L., Amicis, M.D. (2002). Rockfalls Induced by Earthquakes: A Statistical Approach. Journal, of Soil Dynamic and Earthquake Engineering, 22, 565–577 pp.

McCauley, M.L., Works, B.W., and Naramore, S.A. (1985). Rockfall Mitigation. Report FHWA/CA/TL-85/12. FHWA, U.S. Department of Transportation.

McNeil, B.E., Jasper, J.D., Luchsinger, D.A., Rainsmier, M.V. (2002). Implementation and Application of GIS at Timpanogos Cave National Monument, Utah. Journal of Cave and Karst Studies, 64 (1), 34–37 pp.

Meissl, G. (1998). Modellierung der Reichweite von Felsstürzen. Fallbeispeile zur GISgestützten Gefahrenbeurteilung aus dem Beierischen und Tiroler Alpenraum. Innsbrucker Geografischen Studien 28. Ph.D. Thesis, Universität Innsbruck, Innsbruck, 249 pp.

Munfakh, G., Wyllie, D., and Mah, C.W. (1998). Rock Slopes Reference Manual, Federal Highway Administration, Publication No. FHWA HI-99-007.

Müller, G. (1957). Geological, Hydrogeological and Civil Geologic Surveys on Kizilay-Kocattepe Region. MTA, Scientific Documentation Department, Compilation No: 2325, 5 pp (In Turkish, Unpublished).

Öncül, M.K. (1978). Relationship Between Size Slenderness Ratio, Strength and Stress-Strain for Cylindrical Specimens Loaded in Uniaxial and Triaxial Compression. MSc Thesis. Middle East Technical University. 148 pp (Unpublished).

Panoramio, http://www.panoramio.com/photo/25322855#, retrieved on 2016.

Pantelidis, L. (2009). Rock Slope Stability Assessment Through Rock Mass Classification Systems. International Journal of Rock Mechanics and Mining Sciences, Volume 46, No. 2, 315-325 pp.

Pantelidis, L. (2010). An Alternative Rock Mass Classification System for Rock Slopes. Bulletin of Engineering Geology and the Environment, Volume 69, No. 1, 29-39 pp.

Peng, B. (2000). Rockfall Trajectory Analysis - Parameter Determination and Application. Thesis for Master. University of Canterbury (Unpublished).

Pfeiffer, T.J., Bowen, T.D. (1989). Computer Simulation of Rockfalls. Bulletin of the Association of Engineering Geologists, 26 (1), 135– 146 pp.

Priest, S.D. (1993). Discontinuity Analysis for Rock Engineering. Chapman & Hall, London.

Prime Ministry Disaster & Emergency Management Authority (AFAD). (1996). Earthquake Zoning Map of Turkey. Earthquake Research Deapartment. Republic of

Turkey. Reterieved March 30, 2017 from http://www.deprem.gov.tr/en/Category/earthquake-zoning-map-96531.

Ritchie, A.M. (1963). Evaluation of Rockfall and Its Control. Highway Research Board Record, 17, 13–27 pp.

Rocscience (2015). Scientific Software, Statistical Analysis of Rockfalls, Version 5.013, Rocscience Inc., Canada.

Rocscience. (2015c). Dips Version 6, Graphical and Statistical Analysis of Orientation Data, Rocscience Inc., Canada.

Rocscience. (2015c). RocFall Version 5.013, Statistical Analysis of Slopes at risk for Rockfalls, Rocscience Inc., Canada.

Rocscience. (2015c). RocPlane Version 3, Planar Rock Slope Stability Analysis and Design, Rocscience Inc., Canada.

Rocscience. (2015c). RocTopple Version 1, Toppling Analysis for Rock Slopes, Rocscience Inc., Canada.

Rocscience. (2015c). Swedge Version 6, Stability of Surface Wedges in Rock Slopes, Rocscience Inc., Canada.

Saygılı, R. (2016). Ankara ili Haritası. Retrieved April 3rd, 2017 from http://cografyaharita.com/turkiye_mulki_idare_haritalari.html.

Scheidegger, A.E. (1975). Physical Aspects of Natural Catastrophes. Elsevier, Amsterdam.

Schumm, S.A., Chorley, R.J. (1964). The Fall of Endangering Rock. American Journal of Science, 262, 1041–54 pp.

Scioldo, G. (1991). ISOMAP and ROTOMAP, 3D Surface Modelling and Rockfall Analysis. Geo and Soft, Torino, 69 pp.

Skylinesteel, retrieved on 2016 from http://www.skylinesteel.com/globalnav/applications/storm-protection/slope-stabilization.

Spang, R.M., Sönser, T.H. (1995). Optimized Rockfall Protection by ROCKFALL. Proceedings of the 8th International Conference on Rock Mechanics, Tokyo, Volume 3, 1233-1242 pp.

Statham, I. (1976). A Scree Slope Rockfall Model. Earth Surface Processes, 1, 43–62 pp.

Stevens, W.D. (1998). RocFall: A Tool for Probabilistic Analysis, Design of Remedial Measures and Prediction of Rockfalls. Thesis for Master, University of Toronto, 38 pp (Published).

Teoman, M.B., Topal, T., Işık, N.S. (2004) Assessment of Slope Stability in Ankara Clay: A Case Study Along E90 Highway. Environmental Geology, 45(7), 963-977 pp.

The General Directory of State Hydraulic Works. (1957). South Ankara's Hydrological Survey's Report. Publication of General Directorate of Geotechnical Services and Groundwater Departments. 46 pp.

The General Directory of State Hydraulic Works. (1976). Hydrological Survey's Report of Mürted Plain. Publication of General Directorate of Geotechnical Services and Groundwater Departments. 49 pp.

Tokmak, M. (2005). Documentation and Examination of Historic Building Materials for the Purpose of Conservation: Case study, Part of the Walls at the Citadel of Ankara. MSc Thesis. Middle East Technical University (Unpublished).

Topal, T., Akin, M. K., Akin, M. (2012). Rockfall Hazard Analysis for an Historical Castle in Kastamonu (Turkey*).* Natural Hazards 62, 255–274 pp.

Topal, T., Akin, M., Özdan, U.A. (2007). Analysis and evaluation of rockfall hazard around Afyon Castle, Turkey. Environmental Geology, 53, 191-200 pp.

Toppe, R. (1987). Terrain Models – A Tool for Natural Hazard Mapping. In Salm, B. and Gubler, H., editors, Avalanche formation, movement and effects. IAHS Publication no. 162, 629–38 pp.

Turkish State Meteorological Services (TSMS). Retrieved Nov. 4, 2016 from http://www.mgm.gov.tr/veridegerlendirme/il-ve-ilceler-istatistik.aspx.

Turner, A.K. and Schuster, R.L. (1996). Landslides, Investigation and Mitigation. Transportation Research Board, National Research Council, Special Report 247, Washington, D.C., 673 pages.

Ulusay, R. (1975). Geo-engineering Properties of North-Central Part of Ankara. MSc Thesis, Hacettepe University. 81 pp (In Turkish, Unpublished).

van Dijke, J.J., van Westen, C.J. (1990). Rockfall Hazard, A Geomorphological Application of Neighbourhood Analysis with ILWIS. ITC Journal, 1, 40–44 pp.

Varnes, D.J. (1978) Slope Movement Types and Processes. In: Schuster RL, Krizek RJ (eds) Landslides: analysis and control. Special Report 176, Transportation and Road Research Board, National Academy of Science, Washington, DC, 11–33 pp.

Volkwein, A, Schellenberg, K., Labiouse, V., Agliardi, F., Berger, F., Bourrier, F., Dorren, L.K.A., Gerber, W., and Jaboyedoff, M. (2011). Rockfall Characterisation and Structural Protection – A Review. Natural Hazards and Earth System Sciences, 11, 2617–2651 pp.

Wasowski, J., Gaudio, V.D. (2000). Evaluating Seismically Induced Mass Movement Hazard in Caramanico Terme (Italy). Eng Geol 58, 291–311 pp.

Wick, E., Baumann, V., Jaboyedoff, M. (2010). Report on the Impact of the 27 February 2010 Earthquake (Chile, Mw 8.8) on Rockfalls in the Las Cuevas Valley, Argentina. Natural Hazards and Earth System Sciences, 10, 1989–1993 pp.

Wyllie, D.C. (2015). Rock fall engineering. CRC press, New York, 243 pages.

Wu, S.S. (1985). Rockfall Evaluation by Computer Simulation. Transportation Research Record, 1031, 1–5 pp.

Yalçın, E. (1988). Ankara City Water Needs and Examination of Options to Meet Them. MSc Thesis. Hacettepe University. 112 pp (In Turksih, Unpublished).

APPENDIX A

SUMMARY OF FIELD DATA FOR 21 STOPS

Table A1 Summary table of discontinuities data taken at 21 stops.

	Slope	Dominant set 1	Dominant set 2	Dominant set 3	Dominant set 4
Stops	Dip directions/Dip amounts in degrees				
1	310/80	295/22	060/73	133/71	294/79
2	315/82	382/5	041/87	107/83	298/76
3	325/56	325/8	210/85	135/75	146/69
4	277/61, 336/76	331/13	203/76	107/67	270/21
5	340/84	324/18	046/70	100/75	170/61
6	326/74	295/44	230/75	297/74	314/54
7	350/80	060/24	316/53	206/64	218/80
8	054/83	160/64	214/82	335/54	105/75
9	110/89	321/89	306-70	215/83	074/79
10	330/63	335/24	190/89	279/70	216/76
11	030/85	294/20	340/80	305/74	006/76
12	325/49	200/25	249/80	003/45	040/74
13	345/80	129/17	007/89	044/83	309/71
14	86/340	357/78	265/55	335/44	161/54
15	330/84	190/19	325/85	010/60	-
16	345/88	280/88	270/65	206/41	175/51
17	030/70	240/34	295/81	020/82	335/76
18	029/71	241/35	296/81	336/76	022/81
19	070/55	275/63	220/74	305/70	195/32
20	015/75	005/39	130/64	015/74	350/88
21	015/80	290/37	20/87	095/87	092/91

APPENDIX B

2D ROCKFALL ANALYSES'S RESULTS

Table B.1 The results of 2D rockfall analysis.

Profiles No	Weight (kg)	Runout Distance (m)	Kinetic Energy (kJ)	Max. Bounce Height (m)
	250	120.84	60.98	6.39
	500	130.78	119.71	7.20
	750	124.16	183.80	7.33
1-1'	1800	127.47	472.07	7.97
	250	100.80	23.58	2.01
	500	97.67	47.68	1.83
	750	100.98	78.23	1.78
1-1'.1	1800	100.80	185.48	1.99
	250	119.99	58.93	5.66
	500	113.59	117.53	4.86
	750	116.79	177.93	4.75
2-2'	1800	113.59	407.12	4.96
	250	81.59	3.11	0.33
	500	78.39	6.17	0.42
	750	91.19	14.62	0.58
2-2'.1	1800	91.19	31.97	0.78
	250	104.64	14.92	0.99
	500	104.67	32.94	1.11
	750	104.64	46.62	1.10
3-3'	1800	104.64	106.44	1.24

Table B.1 (Continued) The results of 2D rockfall analysis.

Profiles No	Weight (kg)	Runout Distance (m)	Kinetic Energy (kJ)	Max. Bounce Height (m)
	250	91.50	38.20	4.86
	500	94.50	79.31	4.76
	750	91.50	112.49	4.49
4-4'	1800	94.50	277.17	4.99
	250	125.50	33.15	4.64
	500	121.97	69.65	3.87
	750	125.50	102.87	4.17
5-5'	1800	121.97	241.10	4.79
	250	113.91	15.26	0.96
	500	124.76	50.25	2.15
	750	113.91	31.06	1.06
6-6'	1800	113.91	104.12	1.78
	250	121.76	11.33	0.72
	500	121.76	19.94	0.94
	750	121.76	31.36	0.85
7-7'	1800	121.76	67.30	1.03
	250	153.70	76.51	5.81
	500	153.70	174.13	7.19
	750	161.69	249.80	6.53
7-7'.1	1800	161.69	582.39	6.31
	250	108.90	14.36	0.98
	500	108.90	25.98	1.17
	750	108.90	51.16	1.16
8-8'	1800	108.90	84.11	1.29
	250	144.54	79.16	6.07
	500	148.50	164.35	6.65
	750	140.58	252.30	6.31
8-8'.1	1800	144.54	625.37	6.46

Table B.1 (Continued) The results of 2D rockfall analysis.

Profiles No	Weight (kg)	Runout Distance (m)	Kinetic Energy (kJ)	Max. Bounce Height (m)
	250	109.62	8.03	1.38
	500	109.62	23.54	1.40
	750	109.62	36.79	1.53
9-9'	1800	109.62	90.54	1.62
	250	113.10	20.62	1.82
	500	116.58	54.12	1.93
	750	120.06	74.43	2.19
9-9'.1	1800	120.06	198.01	2.04
	250	137.46	68.52	5.86
	500	140.94	170.29	9.01
	750	144.42	260.61	8.41
9-9'.2	1800	140.94	597.23	8.18
	250	175.53	78.17	10.42
	500	166.87	160.98	8.80
	750	166.87	245.50	8.66
10-10'	1800	166.87	509.66	11.18
	250	153.69	56.50	5.60
	500	162.60	153.31	8.50
	750	167.05	188.08	6.66
11-11'	1800	167.05	431.14	6.52
	250	156.20	33.84	2.50
	500	156.20	64.39	2.69
	750	156.20	108.95	3.34
12-12'	1800	156.20	229.02	2.95
	250	187.00	124.70	19.85
	500	182.60	240.73	17.97
	750	187.00	342.63	17.24
12-12'.1	1800	191.40	850.46	18.62

Table B.1 (Continued) The results of 2D rockfall analysis.

Profiles No	Weight (kg)	Runout Distance (m)	Kinetic Energy (kJ)	Max. Bounce Height (m)
	250	166.54	61.05	4.30
	500	162.09	123.29	2.57
	750	170.98	202.43	5.76
13-13'	1800	153.21	369.44	3.85
	250	130.75	22.55	1.37
	500	130.75	36.21	1.02
	750	130.75	54.40	1.04
14-14'	1800	130.75	132.96	1.14
	250	130.75	16.75	0.59
	500	130.75	33.40	0.68
	750	130.75	50.34	0.72
14-14'.1	1800	130.75	120.55	0.86
	250	37.16	18.88	0.98
	500	37.16	34.00	1.06
	750	37.16	55.20	1.14
15-15'	1800	37.16	121.04	1.41
	250	126.35	18.31	1.26
	500	126.35	34.15	1.12
	750	126.35	53.94	1.56
15-15'.1	1800	121.40	121.11	1.60
	250	90.20	17.76	1.44
	500	63.80	38.31	1.40
	750	85.80	50.85	1.30
16-16'	1800	63.80	116.45	1.49
	250	149.04	6.26	0.52
	500	157.68	23.57	1.20
	750	149.04	17.18	0.77
16-16'.1	1800	149.04	46.82	1.03

Table B.1 (Continued) The results of 2D rockfall analysis.

Profiles No	Weight (kg)	Runout Distance (m)	Kinetic Energy (kJ)	Max. Bounce Height (m)
	250	165.00	16.37	1.48
	500	169.40	31.63	1.48
	750	160.60	29.68	0.81
17-17'	1800	160.60	55.08	1.05
	250	69.13	18.23	1.07
	500	85.21	36.22	1.37
	750	107.72	57.82	1.16
18-18'	1800	143.09	151.77	1.38
	250	152.74	31.22	2.80
	500	149.52	55.61	2.47
	750	149.52	80.35	2.26
18-18'.1	1800	152.74	231.17	2.97
	250	172.14	29.32	1.96
	500	175.85	64.09	2.55
	750	175.85	94.06	2.10
19-19'	1800	175.85	215.89	2.10
	250	159.68	19.33	1.92
	500	155.83	34.31	1.45
	750	155.83	56.38	1.36
20-20'	1800	155.83	143.53	1.61